Assessment of uncertainties in simulated European precipitation

Ronald van Haren

Thesis committee

Promotor
Prof. Dr W. Hazeleger
Professor of Climate Dynamics
Wageningen University

Co-promotor
Dr G.J. van Oldenborgh
Senior scientist, Royal Netherlands Meteorological Institute (KNMI),
De Bilt

Other members
Dr E. Hawkins, University of Reading, UK
Prof. Dr B.J.J.M. van den Hurk, Utrecht University
Prof. Dr R. Uijlenhoet, Wageningen University
Dr R. Vautard, National Centre for Scientic Research (LSCE), Gif-
sur-Yvette, France

This research was conducted under the auspices of the SENSE
Research School

Assessment of uncertainties in simulated European precipitation

Ronald van Haren

Abstract

The research presented in this thesis is aimed to understanding the changes and the simulation of precipitation in Europe. A correct representation of simulated (trends in) European precipitation is important to have confidence in projections of future changes therein. These projections are relevant for different hydrological applications. Among others, simulated changes of summer drying are often accompanied by an enhanced increase in air temperatures [*Zampieri et al.*, 2009]. This can be expected to have large impacts on society and ecosystems, affecting, for example, water resources, agriculture and fire risk [*Rowell*, 2009]. Projections of changes in extreme precipitation are critical for estimates of future discharge extremes of large river basins, and changes in frequency of major flooding events [e.g. *Kew et al.*, 2010].

The subjects that are studied in this thesis are divided in three parts: (1) evaluation of 20th century European precipitation trends; (2) effect of general circulation model (GCM) spatial resolution on simulated western European winter precipitation in the current climate; and (3) effect of GCM spatial resolution on simulated future summer drying in central and southern Europe.

In the first part of the thesis (chapters 2 and 3) an investigation of (extreme) precipitation trends in multi-model ensembles including both global and regional climate models is performed. The results show that these models fail to reproduce the observed trends over (parts of) the past century. In many regions the model

spread does not cover the trend in the observations: the models significantly underestimate the observed trend. A misrepresentation of large scale atmospheric circulation changes in climate models is found to be responsible for the underestimation of winter precipitation trends in Europe over the past century. Additionally, the underestimation of trends in winter precipitation extremes in the Rhine basin is directly related to this as well. In summer a misrepresentation of sea surface temperature (SST) trends is responsible for the underestimation of summer precipitation trends along the coastal regions of western Europe.

The second part (chapter 4) investigates the effect of GCM spatial resolution on modeled precipitation over Europe using an atmosphere-only GCM at two resolutions (EC-Earth, ~25 km and ~112 km horizontal resolution). The results show that the high resolution model gives a more accurate representation of northern and central European winter precipitation. The medium resolution model has a larger positive bias in precipitation in most of the northern half of Europe. Storm tracks are better simulated in the high resolution model, providing for a more accurate horizontal moisture transport and precipitation. A decomposition of the precipitation difference between the medium- and high resolution model in a part related and a part unrelated to a difference in the distribution of vertical atmospheric velocity confirms that the reduced precipitation in the high resolution model is likely the result of a reduced moisture transport at this resolution: the precipitation difference in this area in unrelated to a difference in the distribution of vertical atmospheric velocity. In areas with orography the change in vertical velocity distribution is more important.

Using the same atmosphere-only model, the third part (chapter 5) of this thesis investigates the influence of GCM spatial resolution on the simulated future summer drying of central Europe. High resolution models have a more realistic representation of circulation in the current climate and could provide more confidence on future projections of circulation forced drying. The results show that the high resolution model is characterized by a stronger drying in spring and summer, mainly forced by circulation changes. The initial spring drying intensifies the summer drying by a positive soil moisture feedback. The results are confirmed by finding analogs of the difference between the high and medium-resolution model circulation in the natural variability in another ensemble of climate

model simulations. In current climate, these show the same precipitation difference pattern resulting from the summer circulation difference. In future climate the spring circulation plays a key role as well. It is concluded that the reduction of circulation biases due to increased resolution gives higher confidence in the strong drying trend projected for central Europe by the high-resolution version of the model.

Samenvatting

Klimaatsimulaties van het huidige, en toekomstige klimaat worden gemaakt met behulp van klimaatmodellen. Het onderzoek in voorliggend proefschrift heeft als oogmerk om een beter begrip te verkrijgen van neerslag en neerslagtrends in deze simulaties. Om vertrouwen te krijgen in de klimaatprojecties voor de toekomst met dezelfde klimaatmodellen, is het van essentieel belang dat (1) de waargenomen trends in kilmaatsimulaties op de juiste wijze gereproduceerd worden; en (2) deze trends goed begrepen worden. Projecties van toekomstige neerslagtrends worden gebruikt in verschillende hydrologische toepassingen. Een droger klimaat in de zomer gaat vaak samen met een sterkere opwarming. Het is dan ook de verwachting dat dit grote gevolgen zal hebben voor de maatschappij en verschillende ecosystemen, met invloed op bijvoorbeeld watervoorraden, landbouw en brandrisico. Projecties van trends in extreme neerslag zijn bijvoorbeeld relevant voor projecties van rivierafvoer en veranderingen in frequentie van overstromingen.

De onderwerpen die worden bestudeerd in dit proefschrift, zijn verdeeld in drie delen: (1) evaluatie van trends in Europese neerslag in de vorige eeuw; (2) effect van de ruimtelijke resolutie van een mondiaal klimaatmodel (GCM) op gesimuleerde West-Europese winter neerslag in het huidige klimaat; en (3) effect van de ruimtelijke resolutie van een mondiaal klimaatmodel op gesimuleerde, toekomstige uitdroging in Midden- en Zuid-Europa.

Het eerste gedeelte van dit proefschrift (hoofdstukken 2 en 3) evalueert de trends in (extreme) neerslag door gebruik te maken

van ensembles bestaande uit mondiale en regionale klimaatmodellen. Uit deze evaluatie blijkt dat modellen de neerslagtrends voor grote delen van Europa structureel onderschatten: de waargenomen trends in winterneerslag zijn vaak groter dan de gesimuleerde trends in de modellen. Oorzaak van deze onderschatting is een misrepresentatie van de trends in grootschalige atmosferische circulatie. Tevens blijkt de onderschatting van de trends van grootschalige atmosferische circulatie ook verantwoordelijk te zijn voor het onderschatten van trends in extreme winterneerslag in het stroomgebied van de Rijn. In de zomer speelt de onderschatting van trends in oppervlakte zeewatertemperaturen een belangrijke rol in het onderschatten van de toename in neerslag langs de Europese westkust in de afgelopen eeuw.

Het tweede gedeelte van dit proefschift (hoofdstuk 4) bestudeert het effect van de ruimtelijke resolutie van een mondiaal klimaatmodel op de gesimuleerde neerslag in Europa. Hierbij is gebruik gemaakt van een ongekoppeld atmosfeermodel (AGCM), gedraaid op twee modelresoluties (EC-Earth, ~25 km and ~112 km horizontale resolutie). De resultaten tonen aan dat het hoge resolutiemodel de winterneerslag in Noord-, en Centraal-Europa beter representeert. Synoptische systemen worden beter gesimuleerd in het hoge resolutiemodel, wat zorgt voor een betere representatie van horizontaal vochttransport en neerslag. Een decompositie van het neerslagverschil tussen de twee modelresoluties (in een gedeelte gerelateerd, en een gedeelte ongerelateerd aan het verschil in distributie van verticale atmosferische snelheid), bevestigt dat de neerslagreductie in het hoge resolutiemodel waarschijnlijk het resultaat is van een afname van horizontaal vochttransport: het neerslag verschil is niet gerelateerd aan het verschil in distributie van verticale atmosferische snelheid. In gebieden met orografie blijkt het verschil in distributie van verticale atmosferische snelheid wel relevant.

Door gebruik te maken van hetzelfde atmosfeermodel, onderzoekt het derde gedeelte van dit proefschrift (hoofdstuk 5) het effect van ruimtelijke resolutie van een mondiaal klimaatmodel op het droger worden van het toekomstige klimaat van Centraal-Europe in klimaatsimulaties. Hoge resolutiemodellen hebben een betere representatie van atmosferische circulatie in het huidige klimaat. Deze modellen zouden daardoor meer vertrouwen kunnen geven in circulatie geforceerde uitdroging in klimaatprojecties voor de toekomst. De resultaten laten zien dat het hoge resolutiemodel

gekarakteriseerd wordt door een grotere uitdroging in het voorjaar en in de zomer, voornamelijk geforceerd door veranderingen in atmosferische circulatie. De initiële uitdroging in het voorjaar versterkt de uitdroging in de zomer middels een positieve feedback van bodemvocht. Deze resultaten worden bevestigd middels analogen van het verschil in atmosferische circulatie tussen de twee modelresoluties in de natuurlijke variabiliteit van een ander klimaatmodelensemble. Dit laat in het huidige klimaat hetzelfde neerslagverschil zien, resulterend uit het circulatieverschil in de zomer. In het toekomstig klimaat speelt het circulatieverschil in het voorjaar ook een belangrijke rol. Er wordt geconcludeerd dat de afname van de systematische fout in atmosferische circulatie door de toename in resolutie meer vertrouwen geeft in het sterkere uitdrogingssignaal in de projectie voor Centraal-Europa in het hoge resolutie model.

Contents

Introduction

1.1 Climate change

1.1.1 Historical changes

The Earth's climate has changed throughout history. The last 430,000 year, which have been reconstructed, are characterized by 100,000 year cycles of glacial advance and retreat. The start of the Holocene around 7000 years ago, the latest of these interglacial periods, marked the start of the modern climate era - and of human civilization [*IPCC*, 2007, chapter 6]. Most of these climate changes are attributed to changes in orbital forcing, very small variations in incoming solar radiation due to variations in Earth's orbital parameters as well as changes in its axial tilt. Variations on shorter timescales are attributable to e.g. changes in solar solar forcing, volcanic eruptions, and internal variability of the climate system itself [*IPCC*, 2013, chapter 5].

In recent times, human influence started to play a more and more important role in determining the Earth's climate. Human activity has caused a variety of changes in the composition of the atmosphere and the land surface (forcing agents). Greenhouse gases, as well as atmospheric aerosols, increased since the start of the industrial era, some of which are entirely of anthropogenic origin. Human activity has also caused changes in land cover and surface

albedo [*IPCC*, 2013, chapter 8]. Forcing agents change the Earth's radiation balance, of which the part that is caused by human activity is called anthropogenic forcing. The largest contributor to anthropogenic forcing is the increase in atmospheric concentration of carbon dioxide since 1750. Anthropogenic forcing has led to an uptake of energy by the climate system, resulting in changes in Earth's climate: a widespread change is detected in temperature observations of the surface, free atmosphere and ocean. Consistent changes in other parts of the climate system strengthens the evidence that greenhouse gas forcing is the dominant cause of warming during the past several decades [*IPCC*, 2007, chapter 9].

The water-holding capacity of the atmosphere in a warmer climate increases according to the Clausius-Clapeyron (C-C) relationship. The C-C relationship dictates an increase in water-holding capacity of 7% for each 1ºC increase in temperature. Changes in humidity are evident in observations. Over oceans, the increases are consistent with C-C expectations, with a constant relative humidity, while increases are somewhat lower over land, especially where water availability is limited [*Trenberth et al.*, 2011]. The increase in humidity has also an effect on precipitation, although also other factors, such as changes in large scale atmospheric circulation, play a role. Over the second half of the past century, significant drying (due to changes in precipitation, evaporation or both) has occurred in many parts of Africa, especially in the Sahel and eastern Africa, eastern Asia, eastern Australia, the Mediterranean and partly in northeastern Brazil. Wetting trends are found in eastern North America, parts of South America, and Scandinavia [*Greve et al.*, 2014].

1.1.2   Projections

Projections of future climate change have a broad range of possible outcomes. In the first place because they depend on uncertain future emissions of greenhouse gases and aerosols, secondly because of our incomplete understanding of the climate system and imperfect models used to make these projections. Nevertheless, major advances have been made in science over the years, resulting in increased confidence in recent reports from the Intergovernmental Panel on Climate Change (IPCC) that assesses the advances in science. Some of the projected changes affecting the climate in Europe

are summarized as follows in the latest IPCC report [*IPCC*, 2013, projections with at least 90% probability[1]]:

- Global mean temperatures will continue to rise over the 21st century if greenhouse gas emissions continue unabated. The temperature change will not be regionally uniform.

- Mean sea level pressure is projected to decrease in high latitudes and increase in the mid-latitudes as global temperatures rise.

- Global mean precipitation will increase with increased global mean temperatures. Changes in average precipitation will exhibit substantial spatial variation.

- Arctic sea ice cover is expected to continue shrinking and thinning year-round in the course of the 21st century and Northern Hemisphere snow cover will reduce in spring and summer as global mean surface temperatures rise.

- The ocean will warm and the Atlantic Meridional Overturning Circulation (AMOC) will weaken over the 21st century.

Some general features of the water cycle are projected to change in response to a warming climate: ice and snow will melt more rapidly, the atmosphere will hold more water vapor, and surface water evaporation will increase. In response, precipitation is expected to change as well. Projected changes simulate in general an increase in precipitation in parts of the tropics and high latitudes, whereas large areas of the subtropics could have decreases. These changes are governed by changes in atmospheric water vapor and changes in atmospheric circulation [*IPCC*, 2013, chapter 12].

1.2 Understanding the climate system

1.2.1 History of climate modeling

1.2.1.1 Conceptual models

The first person to argue the existence of a greenhouse effect and human influence on the climate was Joseph Fourier (1768–1830). In the early 1800s, Fourier [*Fourier*, 1827, a reprint of his 1824

---

[1]likelihood of occurrence, IPCC AR5 uses the term 'very likely'

article] hypothesized that by retaining heat, the atmosphere keeps the Earth's surface temperature far higher than it would otherwise be. Fourier also described the principle of radiative equilibrium, which states that the Earth maintains a balance between the energy it receives from the sun and the energy it re-radiates into space.

In 1859 John Tyndall (1820–1893) had successfully set up an experiment to prove the ideas introduced by Fourier. Tyndall demonstrated that a group of polyatomic gases – a group later collectively named greenhouse gases – possessed distinct and differential radiative properties with regard to infrared radiation. His work suggested the possibility that by altering concentrations of these gases in the atmosphere, human activities could alter the temperature regulation of the planet [*Hulme*, 2009].

1.2.1.2   Energy balance models

Early mathematical models approached the climate problem by calculating the radiation balance between incoming solar energy and outgoing long wave radiation. At the end of the 19th century, Svante Arrhenius (1959–1927) developed a energy balance model (EBM), the first of its kind, to estimate how much the heat retained by carbon dioxide (CO_2) and water vapor contributes to Earth's surface temperature [*Arrhenius*, 1896]. He calculated that a doubling of atmospheric CO_2 would raise the global average temperature by 5-6 degrees Celsius [*Edwards*, 2011].

Energy balance models estimate the global radiative temperature from an analysis of the energy budget of the Earth, incorporating factors such as solar radiation, albedo, absorption and thermal radiation. In their simplest form, they do not include any explicit spatial dimension (zero-dimensional, Earth is a point mass). Energy balance models can be extended in one dimension (latitudinal dependency), or two dimension (account for both latitudinal and longitudinal energy flows) [*Goosse et al.*, 2014]. A second type of mathematical climate model, the radiative convective model, focuses on vertical transfers of energy in the atmosphere. A third type is the two-dimensional statistical-dynamical model, employed primarily to study the circulatory cells [*Edwards*, 2011].

1.2.1.3 Numerical weather prediction & radiative convective models

In the beginning of the 20th century, soon after the first generation of mathematical models (Arrhenius, 1896) that tried to describe the Earth's climate, major advances were made in atmospheric physics [*Edwards*, 2010]. Soon after, in 1904, Vilhelm Bjerknes (1862–1951) presented the first description of the necessary physics for modeling the atmosphere [*Trenberth*, 1992]. Bjerknes argued that numerical weather forecasting should be considered an initial value problem and could be solved by integrating the governing equations, what are now known as the primitive equations of motion and state, in time [*Bjerknes*, 1954, an English translation of his 1904 article]. He identified seven independent equations available to compute the change in the state: the three components of the equation of motion (Newton's Second Law); the equation of continuity expressing conservation of mass; the equation of state that ties together pressure, temperature, and density; an equations on conservation of energy (first law of thermodynamics); and the second law of thermodynamics [*Grønøs*, 2013]. Bjerknes made an error in including the second law of thermodynamics in his set of equations (he should instead have specified a continuity equation for water substance) [*Lynch*, 2014], an error that was later corrected by Richardson. However, numerical techniques capable of approximate solutions to Bjerknes' equations did not yet exist.

In 1922, Lewis Fry Richardson (1881–1953) developed the first numerical weather prediction system based on simplified versions of Bjerknes's equations [*Richardson*, 1922]. Richardson's idea was to divide an area into grid cells, each with its own measured set of parameters, such as air pressure and temperature, for a given hour. He would then use the grid to find finite difference solutions to the differential equations [*Weart*, 2010]. Due to the huge amount of calculations involved Richardson did not imagine it as a weather forecast technique. His own attempt to calculate the weather for an eight-hour period took him six weeks and ended in failure [*Edwards*, 2000].

Useful mathematical methods for minimizing numerical instabilities in massively iterative calculations emerged only after the introduction of digital computers in the 1940s. After World War II, weather prediction was one of the first major applications of digital computers [*Edwards*, 2011]. Richardson's equations were used as a

starting point to develop the first weather forecast. In 1950 the first two-dimensional weather simulation was completed, covering North America with 270 points about 700 km apart. The time step was 3 hours [*Weart*, 2010]. Although results were far from perfect, they justified further work [*Edwards*, 2000].

The early forecast models were all regional or continental in scale [*Edwards*, 2000]. By 1955 Norman Phillips (born 1923) had completed a two-layer, hemispheric, quasi-geostrophic computer model of the general circulation. Despite the primitive nature, Phillip's model is now often regarded as the first working general circulation model (GCM) [*Edwards*, 2011]. Scientists concerned with extending numerical prediction schemes to encompass hemispheric or global domains were also studying the radiative and thermal equilibrium of the Earth-atmosphere system. It was these studies that resulted in the design of radiative-convective (RC) models, the first one of which was published in 1961 by Syukuro Manabe (born 1931) [*McGuffie, K. and Henderson-Sellers, A.*, 2014]. RC models are one-dimensional models that model the temperature profile of the atmosphere by considering radiative and convective energy transport up through the atmosphere.

The development of the NWP models discussed in this section, continued in two directions. On the one hand into present day-state-of-the-art weather models, which are capable of predicting the weather for up to a week or more in advance. On the other hand into general circulation models (GCMs). These are discussed in the next section.

1.2.2   General circulation models

GCMs were developed from the NWP models discussed in the previous section. Both models share the same equations of motion, but the purpose is to numerically simulate changes in climate as a result of slow changes in some boundary conditions (such as solar constant) or physical parameters (such as greenhouse gas concentration) [*Abbaspour et al.*, 2009]. NWP models are used to predict the weather up to 2 weeks in the future, whereas GCMs run much longer to derive information about the statistics of the climate. Current generation GCMs, also named Earth System Models, have typically more components compared to NWP models, as they try to simulate all aspects of the Earth system.

One of the pioneers in GCM development is Manabe. Manabe had joined Geophysical Fluid Dynamics Laboratory (GFDL) General Circulation Modeling Program in 1959 to work on GCM development. By 1965, Smagorinsky (GFDL director), Manabe, and their collaborators had completed a nine-level, hemispheric primitive equation GCM [*Edwards*, 2010]. In 1969, Kirk Bryan at GFDL developed the ocean model that has become the basis for most ocean GCMs [*McGuffie, K. and Henderson-Sellers, A.*, 2014]. The group at GFDL was also among the first to perform carbon-dioxide doubling experiments with GCMs [*Manabe*, 1970, 1971], to couple atmospheric GCMs with ocean models [*Manabe and Bryan*, 1969], and to perform very long runs of GCMs under carbon-dioxide doubling [*Manabe and Stouffer*, 1994].

In general terms, a climate model (here referred to as a general circulation model) is a mathematical representation of the climate system based on the physical, chemical and biological properties of its components, their interactions and feedback processes, and accounting for all or some of its known processes (IPCC, definition). The mathematical system that describes the climate system is so complex that it can only be solved numerically, requiring large amounts of computer time. As computing power increases, longer simulations with a higher resolution become affordable, providing more regional details than the previous generation of models [*Goosse et al.*, 2014].

The climate system includes many small scale processes such as turbulence in the atmospheric and oceanic boundary layers, the interaction of the circulation with small scale topography features, thunderstorms, cloud microphysics, etc. Due to the limited resolutions of even the highest resolution climate models, many of these processes are not resolved adequately by the model grid and must therefore be parameterized [*IPCC*, 2007, chapter 8]. Furthermore, many processes are not sufficiently known to be explicitly modeled and are therefore also parameterized in climate models. Because these parameterizations reproduce only the first order effects and are usually not valid for all possible conditions, they are often a large source of considerable uncertainty in models [*Goosse et al.*, 2014]. Even if parameterized unresolved scales only describe a small fraction of the total variance of the system, neglecting their variability can, in some circumstances, lead to gross errors in the climatology of the dominant scales [*Palmer*, 2001]. *Palmer* [2001] suggests

that some of the remaining errors in weather and climate prediction models may have their origin in the neglect of subgrid-scale variability, and that such variability should be parameterized by non-local dynamically based stochastic parameterization schemes.

Many climate models have been developed by independent research institutes to perform climate projections. However, many parameterizations are shared among climate models. As a results to the total number of independent models is far less than the total number of models. Climate models are used to simulate and understand the climate change response to changes in concentrations of greenhouse gases and aerosols. In addition, climate models are often used to to perform sensitivity experiments. These experiments provide insight in the role of a single process or element on the system.

1.2.3   Regional downscaling

The typical horizontal resolution (defined as horizontal grid spacing) for current GCMs is roughly 1 to 2 degrees for the atmospheric component and around 1 degree for the ocean [*IPCC*, 2013, chapter 9]. Results from GCMs are the primary source of information for assessments of the future impacts of climate change. For some types of impact assessment (e.g. risk of drought and flooding on large catchments) the output of a coarse resolution GCM may be sufficient, but in many cases information on a much finer spatial scale is needed (e.g. if the climate model output is used to drive a hydrological model), implying the need to "downscale" the GCM output [*Murphy*, 1999].

In addition to prevailing large-scale conditions, local climate is influenced by regional aspects, such as local orography, land-sea contrast, and small-scale atmospheric features such as convective cells, which are often not well represented in coarse resolution GCMs [*Feser et al.*, 2011]. Any viable downscaling technique must take these regional forcings into account [*Murphy*, 1999]. Different approaches to perform downscaling of coarse resolution GCM output: statistical and dynamical.

Statistical downscaling uses statistical relationships between observed small- and large-scale variables to derive climate at the regional scale from global climate model results [*Feser et al.*, 2011]. The assumption underlying the statistical approach is that there is a statistical link between a set of large-scale "predictor" variables

(e.g. temperature, humidity, wind, geopotential height) and a local-scale "predictand" [*Eden and Widmann*, 2013].

Dynamical downscaling can be described as embedding a high resolution regional climate model (RCM) within a coarse resolution GCM (see figure 1.1). The common approach employs a continuous integration of RCMs where GCM data are used to provide initial conditions (ICs), lateral boundary conditions (LBCs), sea surface temperatures (SSTs), and initial land surface conditions. It is well known that GCMs are not perfect and all simulations suffer from biases to some extent. The downscaled RCM simulation is strongly influenced by the skill of the driving GCM. The dynamical downscaling approach brings GCM biases into RCMs through the LBCs of the RCM and degrades the downscaled simulation [*Xu and Yang*, 2012]. In practice, the RCMs add useful information to the GCM output due to more their more detailed coastlines and mountains, and due to their better representation of convective precipitation.
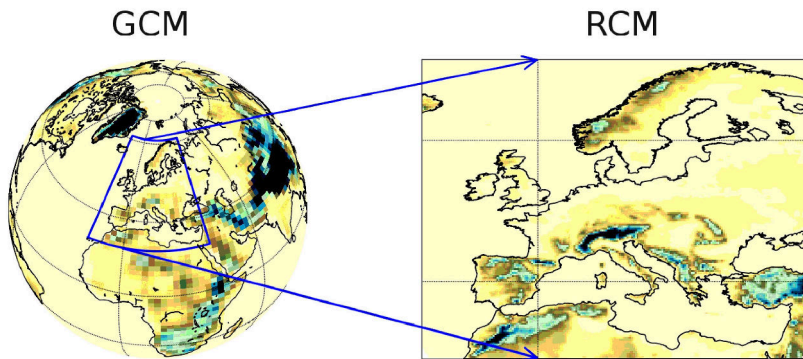
FIGURE 1.1: Schematic of dynamical downscaling

1.3 Evaluation of climate model output

1.3.1 Uncertainties in climate projections

A wide range of studies have shown the impact of new radiative forcing conditions on the climate, affecting many variables [*Hegerl and Zwiers*, 2011]. Studies on climate change are typically done using climate models. Climate model based simulations produce a wide range of possible climate change projections [*Cox and Stephenson*,

2007], partly because uncertainties in constructing and applying climate models are manifold [*Tebaldi and Knutti*, 2007], and partly because of uncertain future forcing. Therefore, a thorough assessment of climate models is needed to judge the value of simulated climate scenarios and their uncertainties. *Räisänen* [2007] divides the question on the reliability of climate change simulations into two parts: (i) how well do models agree with each other, and (ii) does the variation between model results give a good estimate of uncertainty?

Different classifications of uncertainties in climate projections are used in the literature. *Cox and Stephenson* [2007] group the uncertainties into initial condition uncertainty, emission scenario uncertainty and process/parameter uncertainty. A slightly different classification is used in for example *Hawkins and Sutton* [2009, 2011] and *Murphy et al.* [2009], where the uncertainties are grouped into model uncertainty, scenario uncertainty and internal or natural climate variability. Internal variability is the natural unforced fluctuation of the climate. Scenario uncertainty is caused by the missing information about future emissions. Model uncertainty stems from our incomplete understanding of Earth System processes and their imperfect representation, or parameterization, in models [*Murphy et al.*, 2009].

The relative importance of the three types of uncertainty, model uncertainty, scenario uncertainty and internal variability, varies with parameter, region, forecast lead time and with spatial and temporal averaging scale [*Hawkins and Sutton*, 2009]. Using the model spread as representation for model uncertainty, and thus neglecting epistemological uncertainty (ignorance), the dominant sources of uncertainty up to a few decades ahead are model uncertainty and internal variability. For lead times longer than a few decades the dominant sources of uncertainty are scenario uncertainty and model uncertainty. The importance of internal variability in general increases at smaller spatial scales and shorter time scales [*Hawkins and Sutton*, 2009].

The focus in this thesis is mainly on the performance of climate models in performing long-term climate change projections. Therefore, the relevant types of uncertainty are therefore model uncertainty and scenario uncertainty. Written from a climate model perspective, this thesis considers the model uncertainty.

Information on climate and future climate change is used in decision making and climate adaptation. Uncertainty in climate projections plays an important role in, for example, the chosen adaptation strategy and its design. What the best adaptation strategy is, is very context dependent and depends for example on the types of uncertainty that dominate, the time horizons that need to be taken into account, the robustness of the strategy to a range of climate change scenarios and the flexibility of the chosen adaptation strategy.

1.3.2 Validation of climate models

Validation of climate models is, for several reasons, a challenging task [*Räisänen*, 2007]. There are many aspects of climate models that should be compared to the real world. Examples include, among others, (changes in) the mean state of the climate and extremes, and processes like monsoons, blockings, etc. In addition, climate models should realistically represent observed trends and natural variability. This comparison is further complicated by lack of and errors in observations. Another problem is that climate models are, to a certain extent, tuned to reproduce the current state of the climate.

Because of the many difficulties in comparing model results to the real world, ranking models based on performance is not an easy task. A model may outperform other models for certain climate parameters, but not for others. Combining models generally increases the skill, reliability and consistency of model forecasts [*Tebaldi and Knutti*, 2007], indicating that part of the errors are random [*Knutti*, 2008]. Controversial results exist regarding the best way to combine model results [*Tebaldi and Knutti*, 2007], but naive averaging is unlikely the best option [*Knutti*, 2008].

Several studies have focused on the ranking and weighing of models within an ensemble to come to a best possible prediction of future climate change. One such method is the Reliability Ensemble Average (REA) method by *Giorgi and Mearns* [2002]. The REA method uses two reliability criteria to weigh the quality of individual models within an ensemble. The first criteria is based on the ability of each model to reproduce elements of present-day climate (model performance criterion). The second criterion is based on the convergence of the model simulations of elements of the future climate (convergence criterion). Greater convergence implies

higher reliability of robust signals that are little sensitive to the differences among models. Although the REA method was introduced by *Giorgi and Mearns* [2002] as a reasonable quantification of heuristic criteria, there exists a formal statistical model that can justify the REA method as the optimal procedure [*Tebaldi et al.*, 2005]. Nevertheless, one could argue that outliers are in fact very relevant and provide valuable information on the size of uncertainties. That is, unless it can be shown that they are caused by a misrepresentation of a physical process.

Because climate models are, to a certain extent, tuned to reproduce the current state of the climate, outliers in simulations of future climate are not necessarily the ones that perform worse in simulations of present-day climate [*Giorgi and Mearns*, 2002]. Understanding what makes the projections of two models agree or disagree, evaluating models on key processes, developing metrics that demonstrably relate to projections, and searching for emerging constraints in the system on the basis of observations may be ways forward [*Knutti et al.*, 2010]. In emerging constraints, relationships are derived between currently observable quantities and the GCM response to changes in forcing [*Caldwell et al.*, 2014; *Xie et al.*, 2014]. With this technique, statistical relationships between future and historical model runs in multi-model ensembles are exploited to make more constrained projections [*Bracegirdle and Stephenson*, 2013].

Various techniques exist to quantify uncertainties of different origin. Model uncertainty is handled by analyzing multi-model ensembles, perturbed parameter experiments or stochastic parameterizations. Natural variability, due to the chaotic nature of the atmosphere and low-frequency variability in climate, is handled by analyzing large ensembles of one model. Scenario uncertainty is dealt with by analyzing a range of emission scenarios of greenhouse gasses and aerosols. Initial condition uncertainty is of interest when addressing near-future (decadal) predictions, starting from observed initial states. Regional and local downscaling uncertainty involves the use of regional climate modeling archives and high resolution (several km) non-hydrostatic models. There are other sources of uncertainty that may be relevant when applying the model data to the real world, e.g., calibration uncertainty [*Ho et al.*, 2011].

1.4 Representation of precipitation in climate models

Precipitation is one of the most important climate variables. The largest impact of future climate changes on the society will likely come from changes in precipitation patterns and variability. Precipitation changes affect, among others, water resources, agriculture, fire risk and flooding. However, it is still a big challenge for climate models to realistically simulate the (changes in) regional patterns, temporal variations, and correct combination of frequency and intensity of precipitation. The difficulty arises from the complexity of the precipitation processes in the atmosphere that include cloud microphysics, cumulus convection, planetary boundary layer processes, large-scale circulations, and many others. Errors in simulated precipitation fields often indicate deficiencies in the representation of these physical processes in the model. It is therefore important to analyze precipitation for model evaluation and development [*Dai*, 2006].

Figure 1.2 shows the ensemble mean bias of the Coupled Model Intercomparison Project Phase 5 (CMIP5) climate model ensemble with respect to observed precipitation from the Global Precipitation Climatology Centre [GPCC v6, *Becker et al.*, 2013] dataset for boreal winter (a) and summer (b). CMIP5 models simulate on average too much precipitation (wet bias) in much of the northern hemisphere, both in summer and winter. Wet biases are also found in Australia (winter), southern half of Africa (winter) and the western coast of South America (both seasons). Dry biases are found in the central part of South America (both seasons) and India (summer). Note that these biases are only valid under the assumption that the GPCC dataset provides a correct representation of actual precipitation over the past century.

In addition to biases in mean precipitation, previous studies have shown a tendency for climate model ensembles to underestimate precipitation trends as well [*Wentz et al.*, 2007; *Zhang et al.*, 2007; *Bhend and von Storch*, 2008]. Over Europe, local weather variations are to a large extent determined by changes in circulation [*Osborn et al.*, 1999; *Turnpenny et al.*, 2002; *van Oldenborgh and van Ulden*, 2003; *van Ulden and van Oldenborgh*, 2006], but also changes in sea surface temperature (SST) are known to be responsible for precipitation variations on different spatial scales [*Rowell*, 2003; *van*

(A) boreal winter
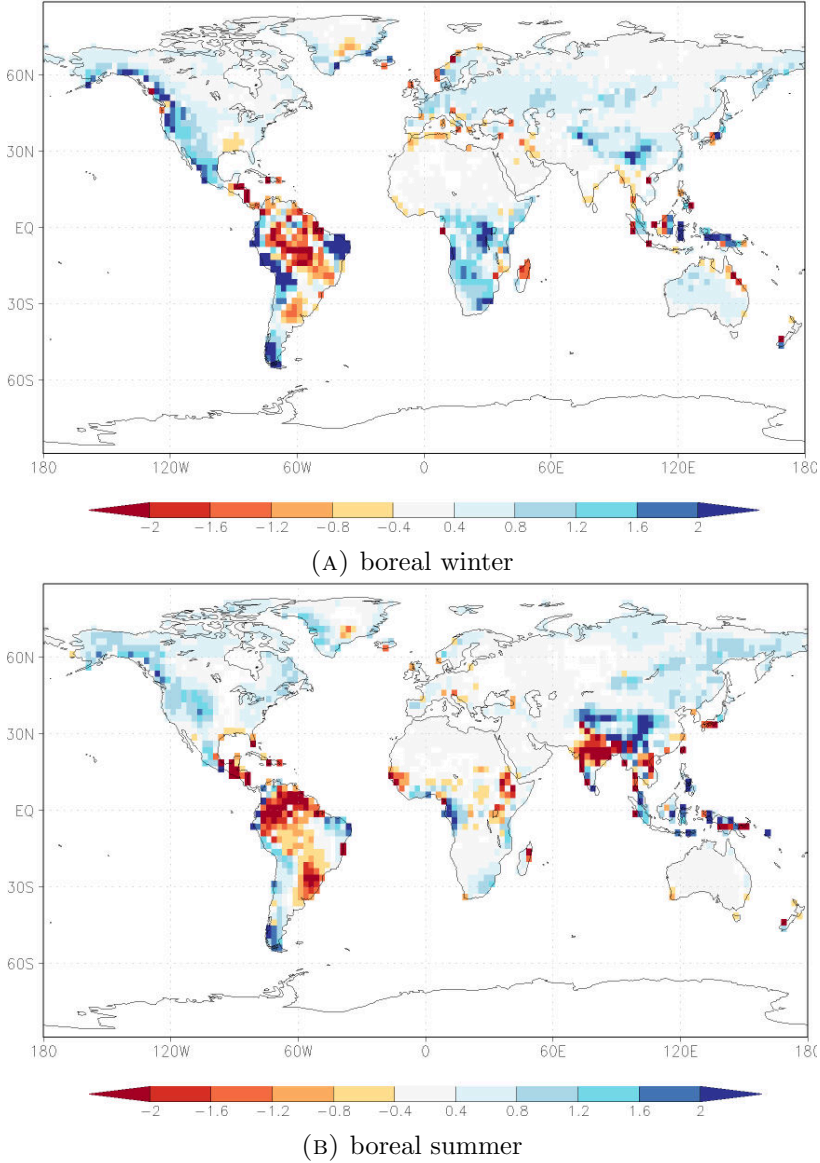

(B) boreal summer

FIGURE 1.2: CMIP5 mean precipitation bias [mm/day] with respect to GPCC observations for the period 1901-2010 for (a) boreal winter (October–March) and (b) summer (April–September). Areas with p>10% are masked (Figure obtained from the KNMI Climate Explorer, climexp.knmi.nl).

Ulden and van Oldenborgh, 2006; *Kjellström and Ruosteenoja*, 2007; *Lenderink et al.*, 2009]. Modeled trends in atmospheric circulation [*Osborn*, 2004; *van Oldenborgh et al.*, 2009a] and SST [*van Oldenborgh et al.*, 2009a; *Ashfaq et al.*, 2010] contain large biases and could be responsible for the underestimation of precipitation trends.

1.5   Research questions & thesis outline

Many climate models have been developed by independent research institutes. Although all of these models are developed to describe the climate system, all of these models respond (slightly) different to a common forcing. Partly because of internal variability in the climate system, but foremost because of different implementations of physical processes and parameterizations thereof. By combining model output from different models, independent errors are averaged out, while errors common to all or multiple models remain. Further progress in the quality of climate change projections requires the identification and understanding of these common errors: i.e., a thorough climate model assessment is needed. In this thesis an assessment is performed for one parameter and one region: European precipitation.

A correct representation of simulated (trends in) European precipitation is important to have confidence in projections of future changes therein. These projections are relevant for different hydrological applications. Among others, simulated changes of summer drying are often accompanied by an enhanced increase in air temperatures [*Zampieri et al.*, 2009], and can be expected to have large impacts on society and ecosystems, affecting, for example,water resources, agriculture and fire risk [*Rowell*, 2009]. Projections of changes in extreme precipitation are critical for estimates of future discharge extremes of large river basins and changes in frequency of major flooding events [e.g. *Kew et al.*, 2010].

These considerations lead to the following research questions, which will be addressed in this thesis:

- **Evaluation of 20th century European precipitation trends (chapters 2 & 3)**
  In chapter 2 an evaluation of European summer and winter precipitation trends over the past century is performed. Chapter 3 discusses the performance of climate models in simulating trends in extreme winter precipitation over the Rhine river

basin. In these chapters the following research questions are
answered:

Q1 Can the current generation climate models realistically
represent observed trends over the past century?

Q2 What are the underlying physical mechanisms responsi-
ble for biases in simulated trends?

- **Effect of GCM spatial resolution on simulated western
European winter precipitation in the current climate
(chapter 4)**
Chapter 4 investigates the effect of GCM spatial resolution
on simulated western European winter precipitation in the
current climate. The following research question is answered
in this chapter:

Q3 Do climate models have sufficient spatial resolution to
accurately represent synoptic systems that are associated
with European winter precipitation?

- **Effect of GCM spatial resolution on simulated future
summer drying in central and southern Europe (chap-
ter 5)**
Chapter 5 investigates the influence of GCM spatial resolu-
tion on simulations of future central European summer dry-
ing. The following research questions are answered in this
chapter:

Q4 Does the increased AGCM spatial resolution change the
future climate change projected circulation forced sum-
mer drying over central and southern European?

Q5 Is there a link between resolution dependent projected
future spring circulation change, drying of the soil in
spring, and soil moisture feedback in summer?

Finally, a synthesis of the research is provided in chapter 6. Main
conclusions from the previous chapters and answers to the research
questions are provided. Chapter 6 ends with an outlook.

CHAPTER 2

Evaluation of European precipitation trends[1]

Chapter Abstract

Clear precipitation trends have been observed in Europe over the past century. In winter, precipitation has increased in north-western Europe. In summer, there has been an increase along many coasts in the same area. Over the second half of the past century precipitation also decreased in southern Europe in winter.

An investigation of precipitation trends in two multi-model ensembles including both global and regional climate models shows that these models fail to reproduce the observed trends. In many regions the model spread does not cover the trend in the observations.

In contrast, regional climate model (RCM) experiments with observed boundary conditions reproduce the observed precipitation trends much better. The observed trends are largely compatible with the range of uncertainties spanned by the ensemble, indicating that the boundary conditions of RCMs are responsible for large parts of the trend biases. We find that the main factor in setting the trend in winter is atmospheric circulation, for summer sea surface temperature (SST) is important in setting precipitation trends

---

along the North Sea and Atlantic coasts. The causes of the large trends in atmospheric circulation and summer SST are not known. For SST there may be a connection with the well-known ocean circulation biases in low-resolution ocean models. A quantitative understanding of the causes of these trends is needed so that climate model based projections of future climate can be corrected for these precipitation trend biases.

2.1   Introduction

A wide range of studies have shown that increases in atmospheric CO_2 concentrations and other greenhouse gasses influence the climate, affecting many variables [*Hegerl and Zwiers*, 2011]. Projections of future climate based on these studies are uncertain [e.g. *Déqué et al.*, 2007; *Räisänen*, 2007; *Hawkins and Sutton*, 2009; *Knutti et al.*, 2009]. To have confidence in future climate projections, a correct representation of trends in the past is necessary (but not sufficient). In this paper we consider the uncertainty in one variable and one region: European precipitation trends.

Simulations of present and future climate are typically done using climate models. Climate models are a mathematical representation of the climate system and should in principle give a physics-based response to increased CO_2 concentrations and changes in other forcings. However, projections also depend on uncertain parameterizations of unresolved processes that are used in climate models, uncertainty about land use and the magnitude of forcings due to aerosol and black carbon emissions. Part of this uncertainty is described by the spread of multi-model and perturbed physics ensembles. In this paper we investigate whether the ensemble spread indeed covers the observed precipitation trends in Europe.

Previous studies have shown a tendency for climate model ensembles to underestimate precipitation trends [*Wentz et al.*, 2007; *Zhang et al.*, 2007; *Bhend and von Storch*, 2008]. Over Europe, local weather variations are to a large extent determined by changes in circulation [*Osborn et al.*, 1999; *Turnpenny et al.*, 2002; *van Oldenborgh and van Ulden*, 2003; *van Ulden and van Oldenborgh*, 2006], but also changes in sea surface temperature (SST) are known to be responsible for precipitation variations on different spatial scales [*Rowell*, 2003; *van Ulden and van Oldenborgh*, 2006; *Kjellström and*

Ruosteenoja, 2007; *Lenderink et al.*, 2009]. Modeled trends in atmospheric circulation [*Osborn*, 2004; *van Oldenborgh et al.*, 2009a] and SST [*van Oldenborgh et al.*, 2009a; *Ashfaq et al.*, 2010] contain large biases and could be responsible for the underestimation of precipitation trends.

We evaluate modeled precipitation trends in a few different climate model ensembles. First we compare observed precipitation trends with trends from the CMIP3 ensemble of climate model experiments [*Meehl et al.*, 2007], an ensemble composed of Global Circulation Models (GCMs). Searching for causes of the difference in trends, we discuss trend differences between the CMIP3 ensemble and an ensemble of regional climate models (RCMs). RCMs are a dynamical downscaling tool and provide more details on local conditions such as surface conditions, topography, coastlines and soil moisture that could affect modeled precipitation. RCMs are constrained by the lateral boundaries, and it is therefore relatively straightforward to prescribe circulation. For GCMs this is much more difficult [*van der Schrier and Barkmeijer*, 2007]. Also SST is commonly prescribed in RCM simulations. We use this property to compare the RCM results with the results of a similar set of RCMs forced by prescribed quasi-observed circulation and SST. This allows for a separation between errors in lateral boundary conditions and internal model errors [*Hudson and Jones*, 2002]. Trend biases that exist in both RCM ensembles are ascribed to model errors, whereas trend biases only found in the GCM driven RCM ensemble are ascribed to errors in the boundary conditions, large scale atmospheric circulation and SST. Finally, we try to separate these two factors using a statistical analysis.

2.2 Data and preprocessing

2.2.1 Trend definition

We use the common definition of a trend in this paper, regression against time. Previous studies have shown that the magnitude of regional climate changes increases quasi-linearly with changes in the global mean temperature [*Räisänen*, 2007; *Alexander and Arblaster*, 2009], a definition adopted in e.g. *van Oldenborgh et al.* [2009a]. Although the latter definition may physically be better justified, it did not significantly increase the signal-to-noise ratio, nor did it

affect any of the conclusions. We therefore adopted the former, more common, approach in this paper. As a result the trend is highly dependent on the chosen time interval: because global warming has not been linear with time, the trends over the last century are smaller than over the last 50 years.

We consider precipitation trends separately for the summer (April – September) and winter (October – March) half year. This increases the signal to noise ratio compared to a three monthly definition of the summer and winter period. In order to compare wet and dry regions in a single figure, we use relative precipitation trends in this paper. The relative precipitation trend is related to the absolute precipitation trend by

$$P'(x,y) = \frac{P'_{abs}(x,y)}{\overline{P(x,y)}} \qquad (2.1)$$

where $P'_{abs}(x,y)$ is the absolute precipitation trend and $\overline{P(x,y)}$ is the mean seasonal (summer/winter) precipitation over the period that the trend is computed. Relative precipitation trends are further referred to as precipitation trends, or just trends.

2.2.2 Observations

We use four observational datasets in this study to evaluate the model results. First the low (2.5º) resolution gridded precipitation dataset of the Global Precipitation Climatology Centre [*Schneider et al.*, 2010, GPCC v5 (1901 – 2009)] is used for comparison with the results derived from a large multi-model GCM ensemble. Later the state-of-the-art gridded high (0.5º) resolution precipitation fields of the European ENSEMBLES project [*Haylock et al.*, 2008, E-OBS v5.0 (1951 - 2011)] is used to verify the results derived from RCM ensembles. We also used the precipitation dataset from the Climate Research Unit [*Mitchell and Jones*, 2005, CRU TS3.10 (1901 - 2009)], as well as the high resolution GPCC v5 dataset (0.5º), to verify the quality of the observational datasets.

It is well known that observations are affected by many sources of error. Errors stem from sources of uncertainty in the observational data and their analysis, from measurement, recording and representativity errors to data quality, homogeneity and interpolation errors [*Haylock et al.*, 2008]. *Haylock et al.* [2008] claim that the typical interpolation error is much larger than the expected magnitude of

other sources of uncertainty. To investigate the uncertainty we compare the three observational sets as well as the ERA-40 re-analysis. This is done for the common time period where all datasets and model results have data (1961 – 2000, figure 2.1). We also show the absolute summer and winter precipitation trends in figure 2.2.

The summer precipitation trend found for the ERA-40 dataset differs largely from the trends found for the observational datasets. Largest deviations are mainly found for central Europe, but also for other European regions in the summer half year. The relatively small amount of wind-induced undercatch (difference between the actual amount of precipitation and the amount measured by a precipitation gauge) during the summer and the high number of measurement stations in this area make it likely that the observational datasets give a better representation of the actual trend. We will therefore not consider the ERA-40 precipitation trends any further in this paper.

As a measure of uncertainty we compute for each grid point the standard deviation between the trend fields of the different observational datasets (panels (e,j) of figure 2.1) according to

$$\sigma = \sqrt{\frac{1}{N} \sum_{i=1}^{N} \left(P'(x,y)_i - \mu \right)^2},$$

$$\text{with} \quad \mu = \frac{1}{N} \sum_{i=1}^{N} P'(x,y)_i$$

(2.2)

in which $P'(x,y)_i$ are the relative precipitation trends as given by panels (b–d) and (g–i) of figure 1 and N is the number of observational datasets. Note that this samples only part of the uncertainty as the datasets are based on a subset of the same station data. Inhomogeneities in the underlying station data propagate into all observational datasets. Inhomogeneities could be caused by e.g. a drop in ratio of snow to liquid rainfall [*Hundecha and Bárdossy*, 2005] or changes in measuring arrangements.

We find considerable differences between the observational datasets over Greece, Finland, the former Soviet Union and the Iberian peninsula (both seasons) and France and the Scandinavian peninsula (winter half year). Differences on smaller spatial scales are found in many other areas. We will only consider model ensemble

trend biases larger than the difference between the different observational datasets.

2.2.3   Model ensembles

We use three multi-model ensembles in this study: one composed of GCMs and two composed of RCMs. The GCM composed ensemble used is the Coupled Model Intercomparison Project phase 3 [*Meehl et al.*, 2007, CMIP3] multi-model ensemble from the World Climate Research Programme (WCRP). The CMIP3 dataset consists of 23 models (left column of figure 2.3) at varying spatial resolution, typically in the order of 200 km. For the period before 2000 we use the climate of the 20th century runs (20c3m). For the period after 2000 we use the SRES A1b scenario runs, but it should be noted that the other SRES emission scenarios are almost identical for the short period after 2000 that is used in this study.

For the ensembles composed of RCMs we use those provided by Research Theme 2b (RT2b) and Research Theme 3 (RT3) from the European ENSEMBLES project [*van der Linden and Mitchell*, 2009], interpolated on a regular 0.5º longitude-latitude grid. The main difference between the two RCM ensembles is the forcing at the boundaries; the regional models are fed at their boundaries with fields containing temperature, humidity, horizontal winds and surface pressure. The fields are commonly provided each 6 hours from the GCMs (RT2b) or ERA-40 (RT3), and are linearly interpolated in time. The boundary relaxation zone in the regional models is typically 8-16 grid points wide, and relaxation is done with a short time scale (in the order of the typical time step of the model) at the outer relaxation zone and a longer time scale at the inner relaxation zone. The exact way this is done varies between the models. SSTs are prescribed from the GCMs or ERA-40.

An overview of the models used in this analysis from the RT2b ensemble is given in the right column of figure 2.3. Most model data used in the two ensembles is available at a 25 km spatial resolution. Exceptions are the MIROC3.2hires forced RACMO (KNMI) model in the RT2b ensemble and the CLM (GKSS) model in the RT3 ensemble that are only available at a 50 km resolution. Models that were excluded in this analysis were either not available for the complete 1951-2009 time period or for the complete European domain. The models used from the RT3 ensemble are mostly the same as those used from the RT2b ensemble. However, we re-added
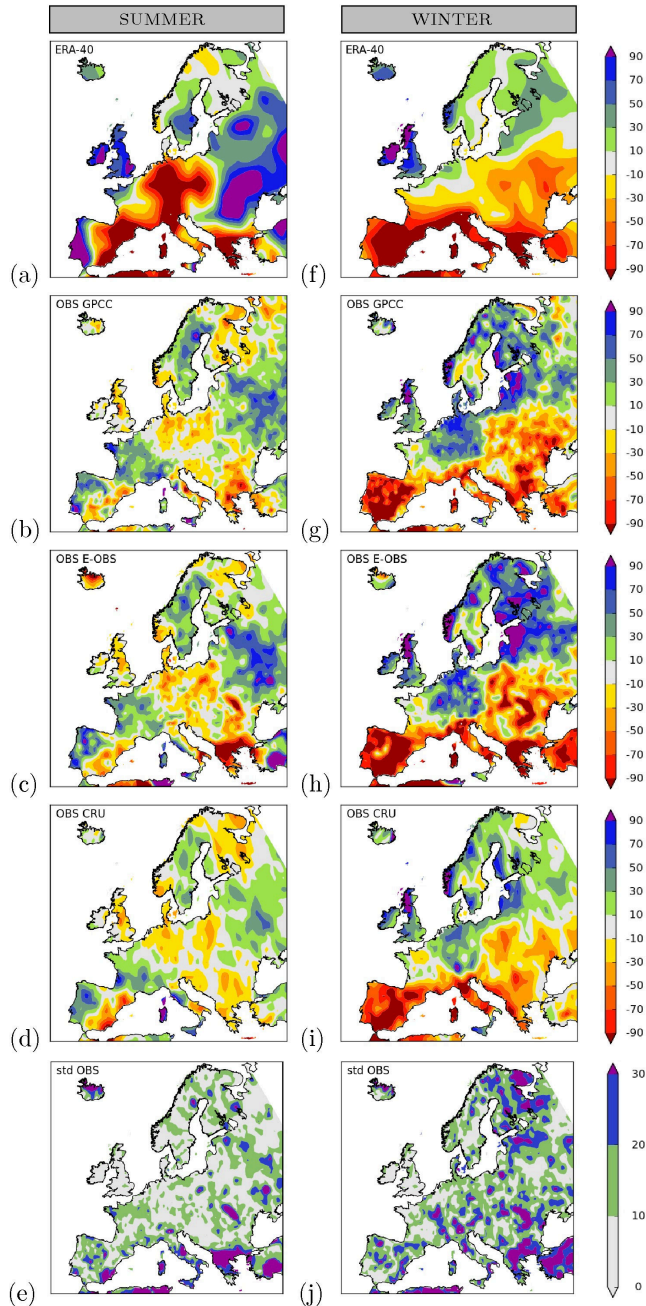
FIGURE 2.1: Comparison of ERA-40 and observed precipitation trends over 1961-2000, defined as the regression against time. Relative trends in (a) ERA-40, (b) GPCC, (c) E-OBS, and (d) CRU summer precipitation [%/Century]; (e) Standard deviation between GPCC, CRU and E-OBS trends summer (f–j) Same but for winter precipitation.
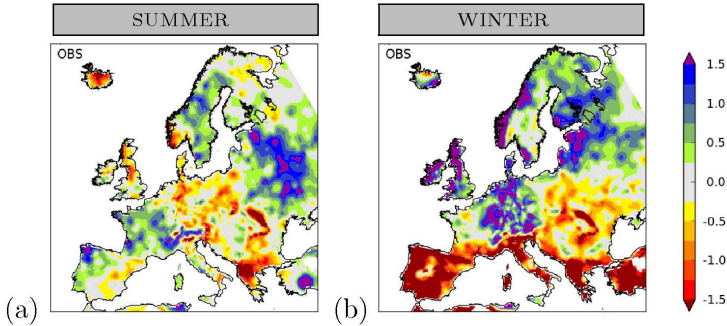
FIGURE 2.2: E-OBS absolute precipitation trend [mm/day/Century] over 1961–2000 for the summer (a) and winter half years (b).

the CLM (GKSS) model that we removed from the RT2b ensemble because it was not available for the complete time period. We also excluded the PROMES (UCLM) model from the RT3 ensemble because the spatial noise in the computed trend was found to be unrealistic.

2.3 GCM/RCM trends vs observations

2.3.1 GCM simulations

Precipitation trends for the GCM and GCM forced RCM multi-model ensembles are computed as regression against time. In order to be least affected by natural variability we used the largest common period for the model ensembles and the observations, yielding 1901 - 2009 for the GCM ensemble and the GPCC precipitation data, and 1951 - 2009 for the GCM forced RCM ensemble and the E-OBS precipitation data. The results for the GCM forced RCM ensemble are also shown for the shorter 1961 - 2000 period, the common period shared with the ERA-40 forced RCM ensemble.

The comparison between each multi-model ensemble and the observational data is twofold. First the trend of the ensemble mean is compared to the trend in the observational data. Next we verify if the observational trends fall within the bandwidth of natural variability combined with model uncertainty as parameterized by the spread of the multi-model ensemble. This is indicated by the fraction of the model ensemble members with a trend larger than the observed one.

GCM   **RCM/GCM (institute)**

BCCR-BCM2.0	HIRHAM (DMI)
	HIRHAM (Met.No)
	RCA3 (SMHI)
CGCM3.1(T47)	CRCM (Ouranos)
CNRM-CM3	Aladin (CNRM)
	HIRHAM (DMI)
	HIRHAM (DMI)
	RACMO (KNMI)
	RCA3 (C4I)
ECHAM5/MPI-OM	RCA3 (SMHI)
	RegCM3 (ICTP)
	REMO (MPI)
MIROC3.2(hires)	RACMO (KNMI)
	low sensitivity → HadRM3Q3 (HC)
	→ RCA3 (SMHI)
	HadRM3Q0 (HC)
UKMO-HadCM3	stand. sensitivity → HIRHAM (Met.No)
	→ PROMES (UCLM)
	high sensitivity → HadRM3Q16 (HC)
	→ RCA3 (C4I)

CCSM3
CGCM3.1(T63)
CSIRO-Mk3.0
CSIRO-Mk3.5
ECHO-G
GFDL-CM2.0
GFDL-CM2.1
GISS-AOM
GISS-EM
GISS-ER
INGV-SXG
INM-CM3.0
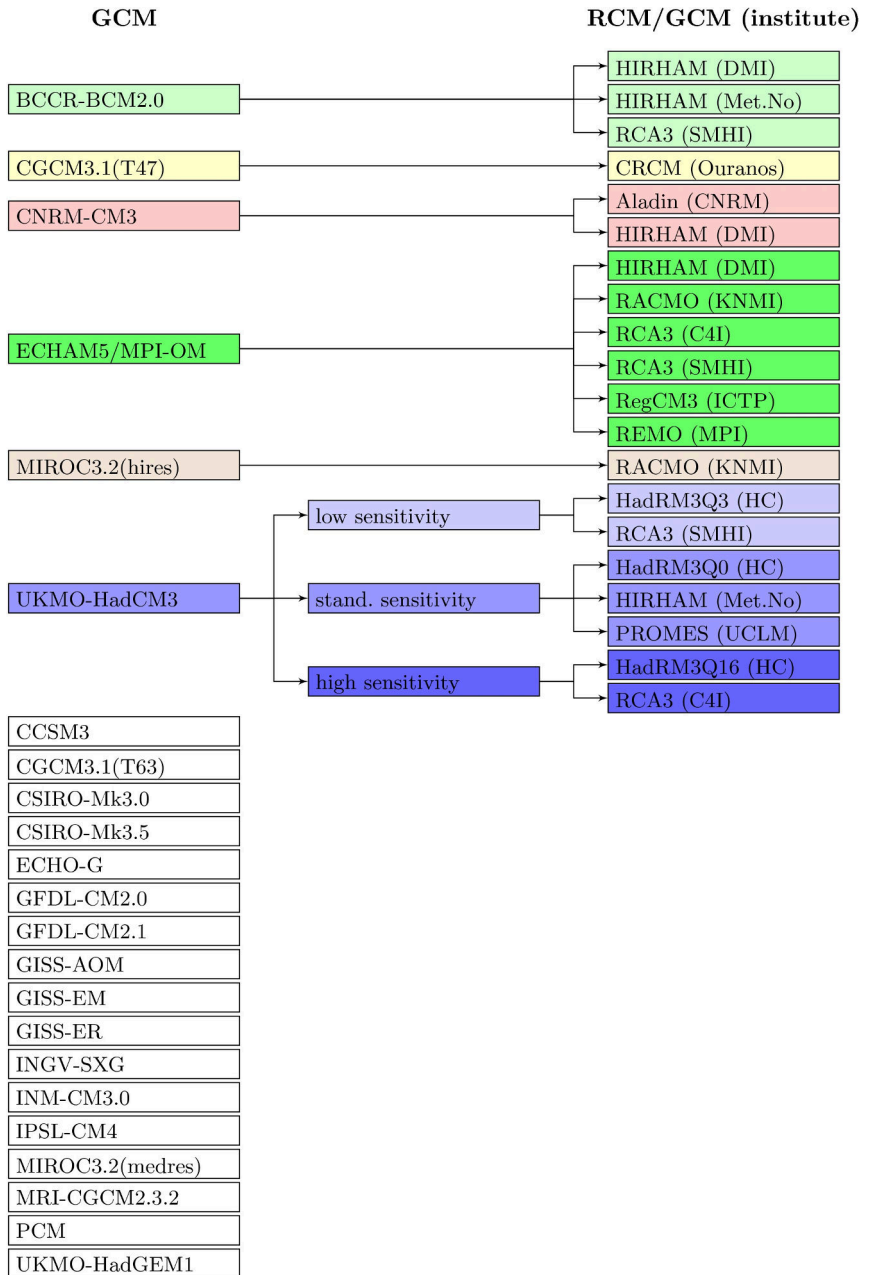IPSL-CM4
MIROC3.2(medres)
MRI-CGCM2.3.2
PCM
UKMO-HadGEM1

FIGURE 2.3: Overview of GCMs and GCM forced RCMs used in the analysis.

Figure 2.4 shows the results for the GCM ensemble and the GPCC observational dataset. Whereas the observations show clear positive trends in northern Europe (both seasons) and part of western Europe (both seasons), these are much smaller in the GCM ensemble. Panels (d,i) of figure 2.4 show that the model spread in these areas does not cover the observations. Similar results are obtained when using the CRU observational dataset at a resolution of 2.5°.

As an aggregated statistic we computed the Talagrand diagram or rank histogram over the land area of Europe and show them in panels (e,j) of figure 2.4. At every grid point the N ensemble members are ranked from lowest to highest, representing N+1 possible bins in which the observations could fall (including the extremes). For every grid point the bin in which the observed trend falls is identified and recorded and the histogram is built up over all area-weighted grid points. For a *reliable* ensemble the histogram would be flat. If the model ensemble has a trend bias, a larger part of the area lies at one end of the ensemble spread, i.e., that end of the histogram will curve up. Because of large uncertainties in the observations in especially Greece and Finland (panels (e,j) of figure 2.1) we only considered the area west of these two countries (west of 20° longitude). Different observational estimates are used to compute the histograms to give some indication of uncertainties in the observations. In figure 2.4 the blue and red lines curve up at the low fractions indicating a bias towards less wetting and more drying trends in the models compared to the observations.

The next question is whether the bias is significant, i.e., whether it is unlikely to be a fluctuation in the distribution of model spread and natural variability. The strong correlation between neighboring grid points is a major issue when conducting significance tests. We therefore take the correlation as represented in the RCMs into account when constructing the significance intervals for each bin in the Talagrand diagrams. All bins have a common scale by design; between 0 and 1. To compute significance intervals around the flat line we compute the same histogram considering each model in turn to be the 'truth' [*Annan and Hargreaves*, 2010]. The confidence interval, depicted as the gray bars in panels (e,j) of figure 2.4, is constructed as the distance between 0 (the minimum) and the second highest ranked member for each bin. This gives, under the assumption that the members are equally distributed over the N+1

inter-point intervals of the empirical distribution function (including the two beyond the minimum and maximum sample values), a confidence interval of around 90% (1-sided test).

We find that the bias in reproducing wetting trends is significant at the 90% confidence level, both in the summer and winter half years. The bias in reproducing drying trends in the winter is not significant. From this we conclude that the problem appears to be a bias in the trends and not in the width of the ensemble: the low and high ranks are not symmetric but the trend in the observations is systematically larger than the trend in the models. This shows that the trend in the observations does not fall within the bandwidth of natural variability combined with model uncertainty as parameterized by the spread of the multi-model ensemble.

2.3.2 RCM simulations

To investigate whether the observed trend biases are due to the coarse resolution of GCMs, we considered a large multi-model RCM ensemble forced by boundary conditions derived from GCM simulations (RCM/GCM). Figure 2.5 shows the results for the RCM/GCM ensemble for the period 1951-2009. Figure 2.6 shows the same but for the period 1961-2000. The available time periods for the RCM/GCM ensemble are considerably shorter compared to the GCM ensemble. As a result the observed trends, and trend mismatches with the model ensemble, are harder to detect against the background of natural variability. Nevertheless, the modeled trends again show large biases.

For the considered time periods the observations show in the winter half year wetting trends in northern Europe and drying trends in southern Europe. Wetting trends are also observed in part of western Europe (winter half year) and northern Europe (summer half year). With the exception of slightly positive trends in parts of northern Europe (both seasons) and a small negative trend in southern Europe for the 1961-2000 period only, the GCM forced RCM ensemble fails to reproduce any of these. In fact, when considered over the same time period, the GCM ensemble shows, with the exception of details, mainly in coastal and mountainous regions, similar seasonal average trends as the GCM forced RCM ensemble (not shown).

The difference between the observed trends and modeled trends is significant in most of these areas. This is visualized in panels (d,h)

FIGURE 2.4: Comparison of observed and GCM precipitation trends over 1901-2009, defined as the regression against time. (a) Relative trends in observed (GPCC) summer precipitation [%/Century]. (b) Mean relative trends of summer precipitation of the GCM ensemble [%/Century] (c) Bias of the GCM ensemble trend compared to the observed trend [%/Century] (d) Fraction of the GCM ensemble with trend larger than the observed one [-]. (e) Talagrand diagram (f–j) Same for winter precipitation.
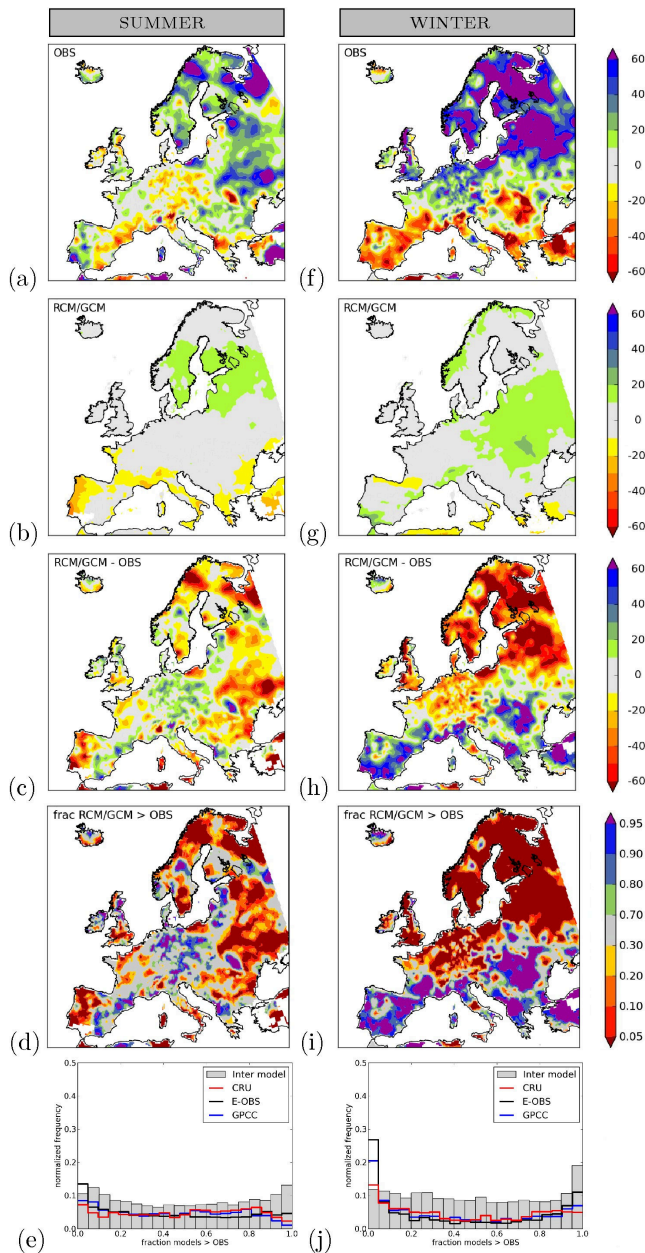
FIGURE 2.5: Comparison of observed and GCM forced RCM precipitation trends over 1951-2009, defined as the regression against time. (a) Relative trends in observed (E-OBS) summer precipitation [%/Century]. (b) Mean relative trends of summer precipitation of the GCM forced RCM ensemble [%/Century] (c) Bias of the GCM forced RCM ensemble trend compared to the observed trend [%/Century] (d) Fraction of the GCM forced RCM ensemble with trend larger than the observed one [-]. (e) Talagrand diagram (f–j) Same for winter precipitation.
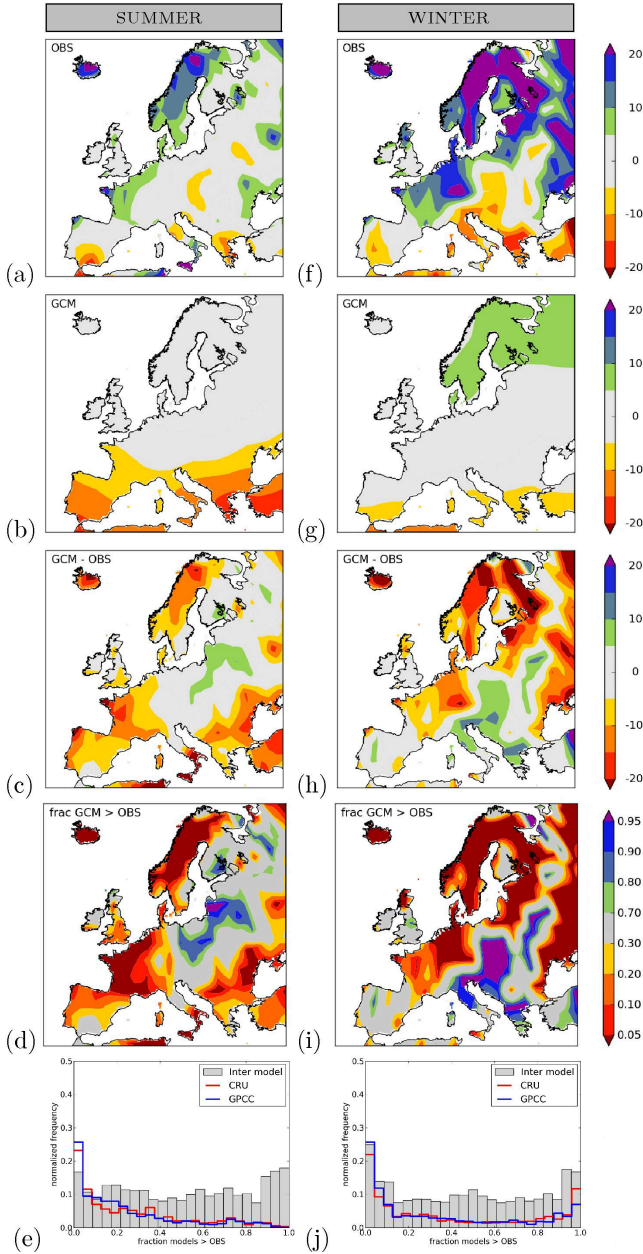
FIGURE 2.6: Comparison of observed and GCM forced RCM precipitation trends over 1961-2000, defined as the regression against time. (a) Relative trends in observed (E-OBS) summer precipitation [%/Century]. (b) Mean relative trends of summer precipitation of the GCM forced RCM ensemble [%/Century] (c) Bias of the GCM forced RCM ensemble trend compared to the observed trend [%/Century] (d) Fraction of the GCM forced RCM ensemble with trend larger than the observed one [-]. (e) Talagrand diagram (f–j) Same for winter precipitation.
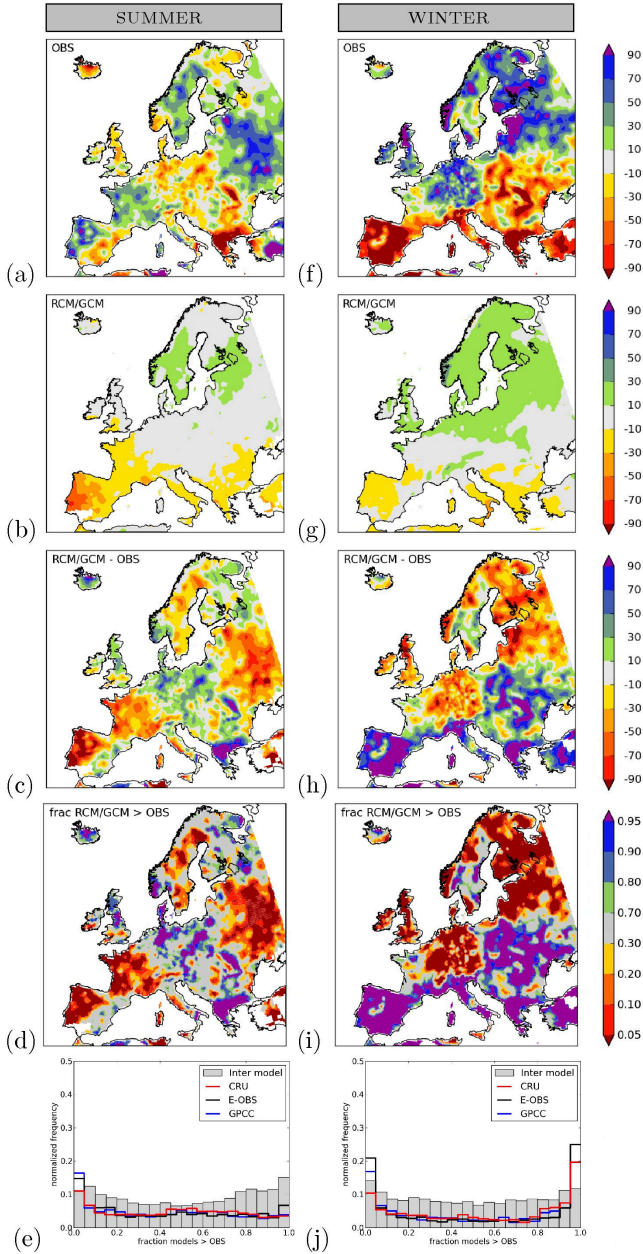
FIGURE 2.7: Inter-annual standard deviation over 1901-2009 (detrended). (a) Observations (GPCC) summer half year [mm/-day] (b) GCM ensemble summer half year [mm/day] (c-d) Same for winter half year.

of figures 2.5 and 2.6, where we show the fraction of the GCM forced RCM ensemble with a trend larger than the observed one. Note that for the GPCC observational dataset a similar spatial trend pattern is found, but often with a somewhat smaller magnitude. This is even more so for the CRU observational dataset. Especially the amount of low fractions in and around Finland differs greatly between the different observational datasets. The high fractions in southern Europe are more robust and are largely shared among the different observational datasets. Panels (e,j) show Talagrand diagrams for the different seasons for the area west of 20º longitude, where the approximately 90% confidence interval is indicated by the gray bars. The rank histogram curls up at the low fractions in the winter half year for all observational datasets. In the summer half year they show that the models severely underestimate the observed increase in summer precipitation. This is despite the increased natural variability due to the shorter timespan considered for the GCM forced RCM ensemble.
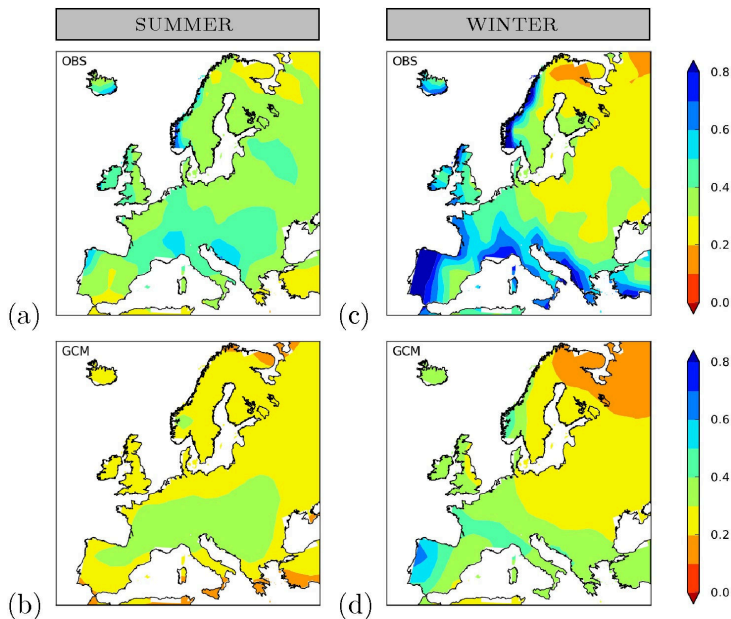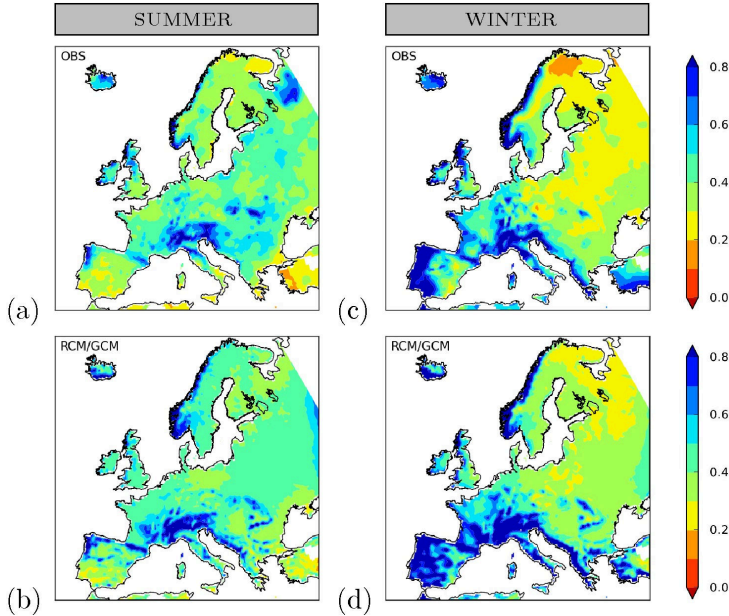
FIGURE 2.8: Inter-annual standard deviation over 1951-2009 (detrended). (a) Observations (E-OBS) summer half year [mm/-day] (b) GCM forced RCM ensemble summer half year [mm/day] (c-d) Same for winter half year.

One possible reason for the low reliability of the models would be that they underestimate the natural variability of precipitation and therefore the uncertainty in the trend. We estimated the natural variability from the same simulations as the fluctuations around the linear trend. As the autocorrelation from year to year is very small in Europe (except in southeastern Spain in winter and northern Iceland all year), and AMO teleconnections to precipitation in Europe negligible [*van Oldenborgh et al.*, 2009b, Fig. 3d], these 60 years should give a good estimate of the fluctuations. We find that the GCMs indeed underestimate the natural variability in the precipitation trends (figure 2.7), but the RCMs rather overestimate the natural variability (figure 2.8). Note that the mean precipitation in the RCMs is, for most regions, larger than observed (not shown), slightly affecting the modeled relative precipitation trends. As a result the relative standard deviation with respect to the trend in the RCMs is smaller than in the observations. Nevertheless, we find that for absolute trends the modeled trends still fall outside

the model spread for most regions and the overall conclusions are not affected by this.

It is unlikely that the trend biases are largely caused by either the coarse resolution of GCMs or natural variability. Because high resolution RCMs in itself are no solution for the trend biases, the remaining possibilities are that they are caused by RCM boundary conditions, large scale circulation and SST, or by local model errors present in both the RCMs and GCMs.

2.4 RCM simulations forced by re-analysis data

To investigate the cause of the observed trend biases in large multi-model GCM and RCM ensembles we compare the results of regional climate models with boundary conditions derived from GCMs (RT2b) with the results of a similar set of RCMs forced by quasi-observed boundary conditions (RT3). This separates the errors caused by incorrect boundary conditions from internal model errors in the RCMs [*Hudson and Jones*, 2002].

Figure 2.9 shows the results for the ERA-40 forced RCM ensemble and the E-OBS observational dataset. In general terms, the ERA-40 forced RCM ensemble reproduces much better the observed precipitation trends in both seasons than the GCM forced RCM ensemble. Wetting trends in much of northern Europe (both seasons) and in western and southwestern Europe (summer half year), as well as drying trends in southeastern (summer half year) and southern (winter half year) Europe are mostly reproduced. The Talagrand diagrams in panels (e,j) of figure 2.9, calculated for the area west of 20º longitude, indicate that in the summer half year the ERA-40 forced ensemble often overestimates the observed trend. In the winter half year the relative large amount of low ranks is observed for some observational datasets is largely from the Alpine region and other mountainous regions, where also the observations are uncertain.

The boundary conditions are prescribed in the ERA-40 forced RCM ensemble and are the same among the different models. Therefore, the model uncertainty in this ensemble is smaller compared to the GCM forced RCM ensemble, often resulting in a smaller spread
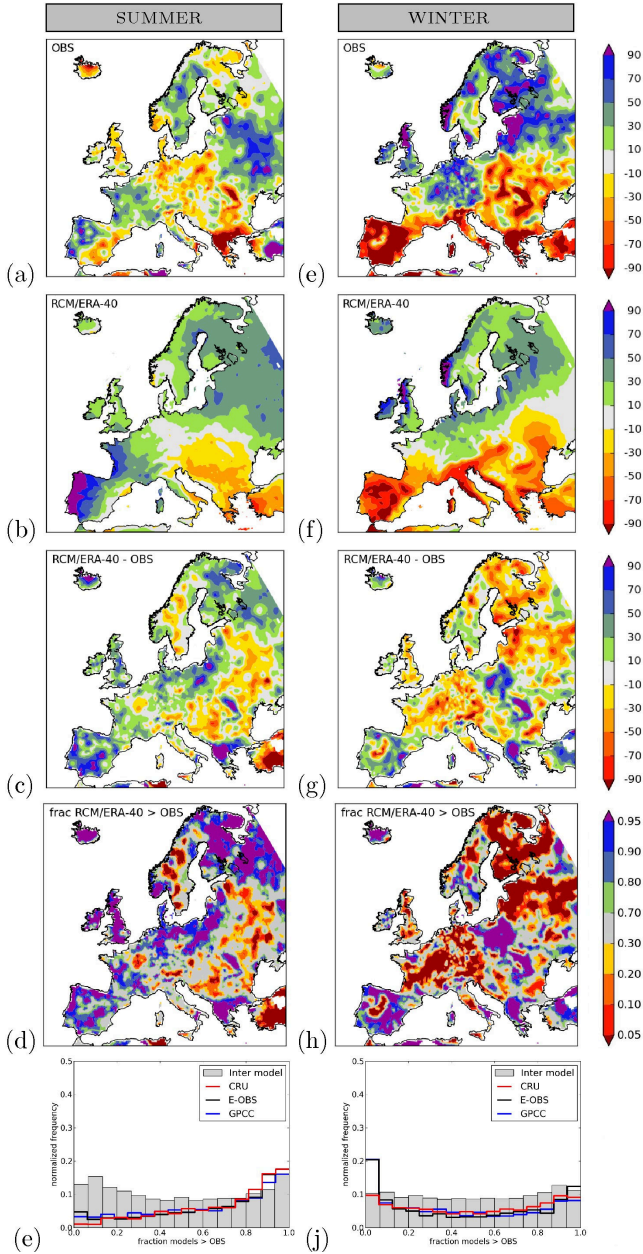
FIGURE 2.9: Comparison of observed and ERA-40 forced RCM precipitation trends over 1961-2000, defined as the regression against time. (a) Relative trends in observed (E-OBS) summer precipitation [%/Century]. (b) Mean relative trends of summer precipitation of the ERA-40 forced RCM ensemble [%/Century] (c) Bias of the ERA-40 forced RCM ensemble trend compared to the observed trend [%/Century] (d) Fraction of the ERA-40 forced RCM ensemble with trend larger than the observed one [-]. (e) Talagrand diagram (f–j) Same for winter precipitation.

between the different models in the ensemble. However, the Talagrand diagram in the winter half year is flatter than in figure 2.6 despite the smaller spread of the ensemble.

2.5 Simulated trends of regional climate change

Observational errors may be an important factor determining the magnitude of the observed trend on small spatial scales. Here, we will therefore look at the regional trends when aggregated over intermediate large areas. The discrepancies between modeled and observed precipitation trends are illustrated by the histograms of figure 2.11 and 2.12 for respectively the summer and winter half year. These show the position of the observations within the model spread for the PRUDENCE regions (see figure 2.10, after *Christensen and Christensen* [2007]). The mean trend is calculated as the trend of the average precipitation within the selected region. For illustration purposes we only consider a few specific regions and periods in the remainder of this section.

FIGURE 2.10: PRUDENCE regions, after *Christensen and Christensen* [2007]. (1) British Isles; (2) Iberia Peninsula; (3) France; (4) Mid-Europe; (5) Scandinavia; (6) Alps; (7) Mediterranean; (8) Eastern Europe.
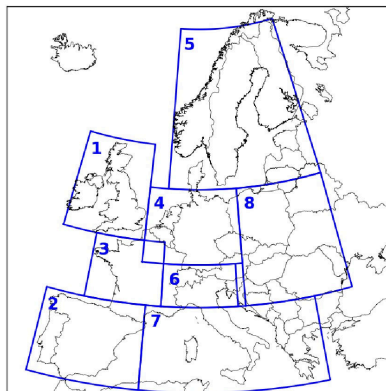
To illustrate that trend biases in the RCM boundary conditions do not affect modeled precipitation trends in all regions equally, we show in panels (g,o) of figure 2.12 the mean relative precipitation trend for the Mid-European region for the winter half year. The means of the precipitation trends of the GCM forced and ERA-40 forced RCM ensembles are similar but the spread of the model ensemble is reduced due to the prescribed boundary conditions. Therefore, the influence of SST and atmospheric circulation trend errors on the mean precipitation trend of the ensemble in the winter half year for this region is small. Common model errors in climate models could be an explanation for the trend bias in this region, but the large spread between the different observational datasets make it difficult to determine if there indeed is a discrepancy between modeled and observed trends.

Next we show two regions where the ERA-40 forced RCM ensemble performs better compared to the GCM forced RCM ensemble. In panels (d,l) of figure 2.11 the mean relative precipitation trend for the France region is shown for the summer half year. Whereas the mean of the GCM forced RCM ensemble shows a large negative trend bias, the mean of the ERA-40 forced RCM ensemble shows a (smaller) positive trend bias. In Panels (e,m) of figure 2.12 the mean relative precipitation trend for the Iberian Peninsula in the winter half year is shown. Whereas the ensemble spread does not cover the observations for the GCM forced RCM ensemble, it does for the ERA-40 forced RCM ensemble.

Finally we show with the British Isles for the summer half year (panels (b,j) of figure 2.11) a region where the trend in the observations falls within the GCM forced RCM ensemble, but is smaller than the trend in the ERA-40 forced RCM ensemble. The trend bias in local processes is hidden in the larger spread of the GCM forced RCM ensemble and can have in an opposite trend bias in the GCMs. By effectively reducing the spread of the ensemble by prescribing SST and large-scale circulation, this trend bias has become visible in panel (j) of figure 2.11, where the observed trend is not compatible with the ensemble spread. The better performance of the GCM forced RCM ensemble (in panel (b) of figure 2.11 the observed trend falls within the much wider ensemble of trends) is therefore caused by the larger spread and compensating errors in the RCMs.

It appears that prescribing realistic atmospheric flow conditions

and realistic SST improves our ability to model observed trends in precipitation. Therefore, we hypothesize that the mismatch between the observations and the GCM simulations and the GCM driven RCM simulations is to a large extent due to a misrepresentation of SST and atmospheric circulation. In the next section we will investigate this further.

2.6 Influence of atmospheric circulation and sea surface temperature

Changes in SST and atmospheric circulation influence regional and local precipitation through convergence, evaporation and transport of moisture. Hence, in this section we investigate the influence of both large-scale circulation and SST trend biases on the precipitation trend biases in the GCM forced RCM ensemble. Changes in trend biases between the GCM forced RCM ensemble and the ERA-40 forced RCM ensemble are found in many regions. Dry trend biases in coastal regions of the North Atlantic and the North Sea are often replaced by smaller wet trend biases when realistic boundary conditions are applied. In north and south Europe the large underestimation of the trend in winter precipitation is much reduced. In Central Europe the lack of changes between the two ensembles indicate that the trends do not strongly depend on SST and circulation trend biases.

In the winter half year (most noticeably in January – March) there has been a shift towards a more westerly circulation over Europe north of the Alps (figure 2.13). This change is underrepresented in climate models [*Osborn*, 2004; *van Oldenborgh et al.*, 2009a]. Westerlies carry moist air from the Atlantic Ocean to the continent [*van Ulden and van Oldenborgh*, 2006], and thereby influence the amount of precipitation. To investigate the effects of trends in the atmospheric circulation, monthly mean precipitation anomalies are approximated by a simple model that isolates the linear effect of circulation anomalies [*van Ulden and van Oldenborgh*, 2006; *van Oldenborgh et al.*, 2009a]. These effects include the influence of mean geostrophic wind anomalies $G'_{\text{west}}(x, y, t)$, $G'_{\text{south}}(x, y, t)$ and vorticity anomalies $G'_{\text{vorticity}}(x, y, t)$. The other terms are the time t, and the remaining noise $\eta(x, y, t)$:

$$P'(x, y, t) = P'_{\text{circ}}(x, y, t) + P'_{\text{noncirc}}(x, y, t) \qquad (2.3)$$
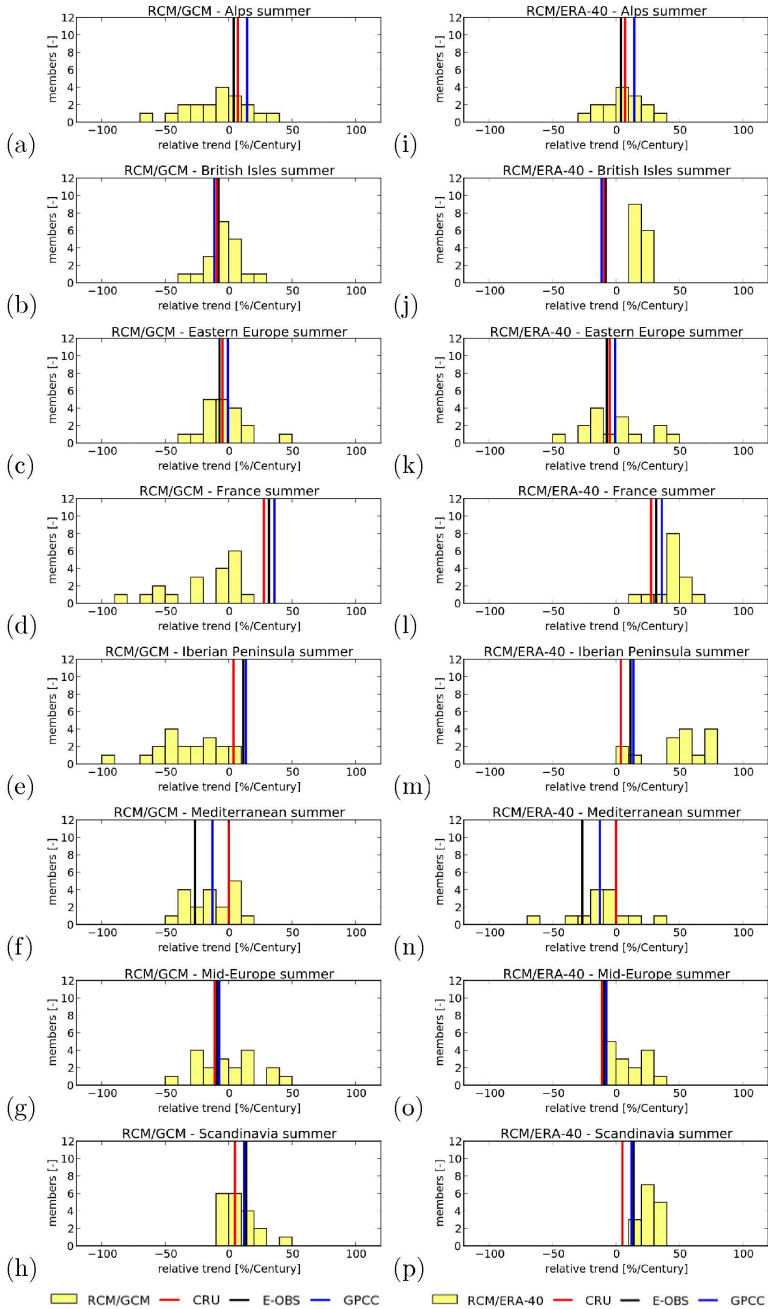
FIGURE 2.11: Distribution of mean relative precipitation trend per region over 1961-2000 for the summer half year [%/Century].
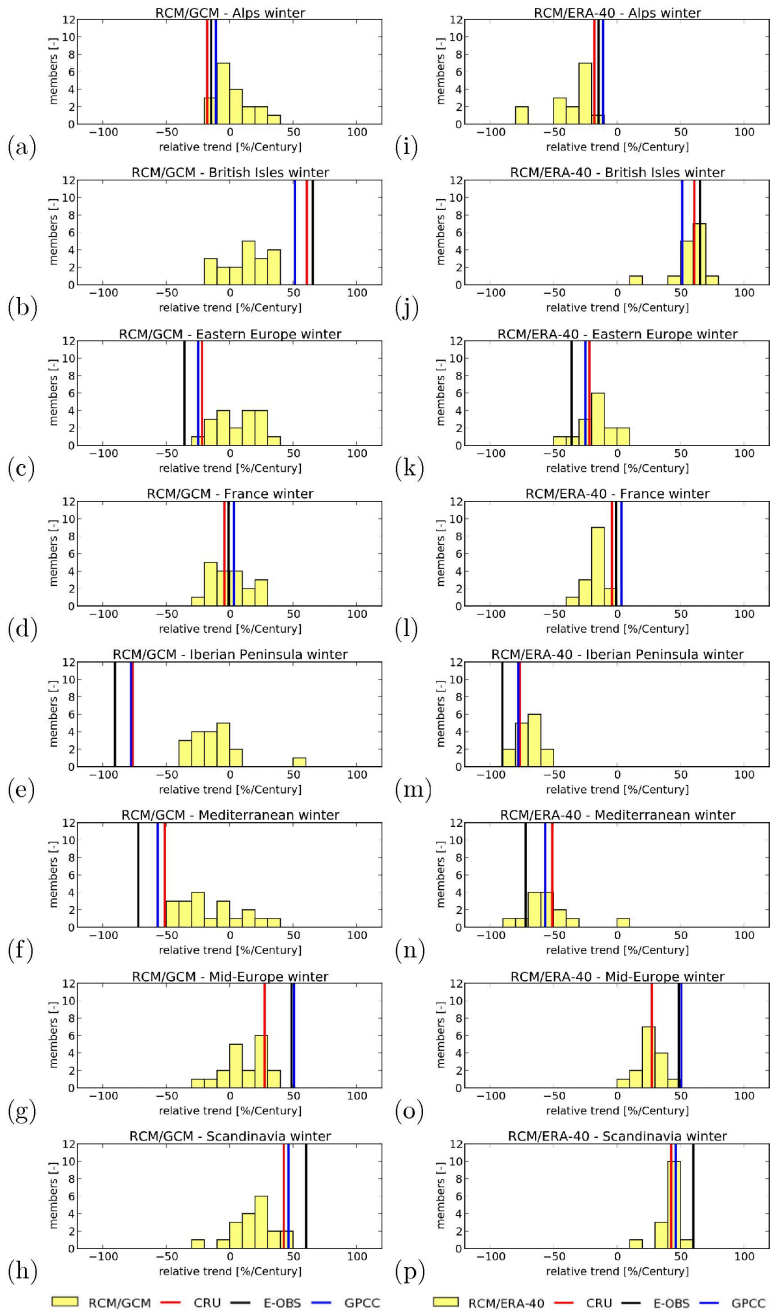
FIGURE 2.12: Distribution of mean relative precipitation trend per region over 1961-2000 for the winter half year [%/Century].

$$P'_{\text{circ}}(x,y,t) = B_W G'_{\text{west}}(x,y,t) + B_S G'_{\text{south}}(x,y,t)$$
$$+ B_V G'_{\text{vorticity}}(x,y,t) \tag{2.4}$$

$$P'_{\text{noncirc}}(x,y,t) = At + \eta(x,y,t) \tag{2.5}$$

The geostrophic wind anomalies $G'_{\text{west}}(x,y,t)$, $G'_{\text{south}}(x,y,t)$ and vorticity anomalies $G'_{\text{vorticity}}(x,y,t)$ are computed from the monthly ERA-40 reanalysis sea-level pressure data and the coefficients B_W, B_S, B_V and A are fitted over 1961-2000 for each calendar month.

Atmospheric circulation induced precipitation changes show up as trends in P'_{circ}. Panels (a,d) of figure 2.14 show the circulation induced precipitation trend estimated by the regression model for respectively the summer and winter half year. Panels (b,e) show the circulation independent trend and panels (c,f) the total precipitation trend.
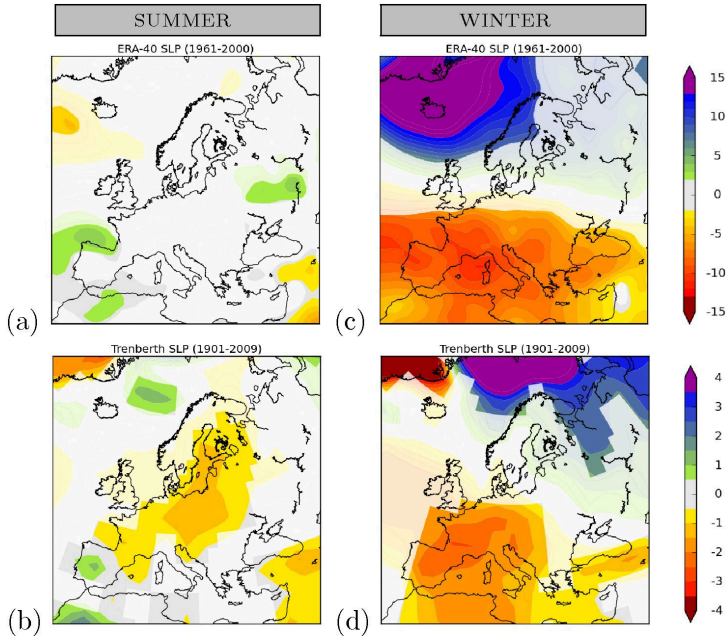
FIGURE 2.13: Sea-level pressure trend (p < 10%) [hPa/Century]. (a) ERA-40 for 1961-2000 in the summer half year (b) Trenberth for 1901-2009 in the summer half year (c–d) Same but for winter.

Most of the trend in summer precipitation is, within the linear approximation of a statistical decomposition, independent of circulation (figure 2.14b). Trends are mostly observed along the coast of
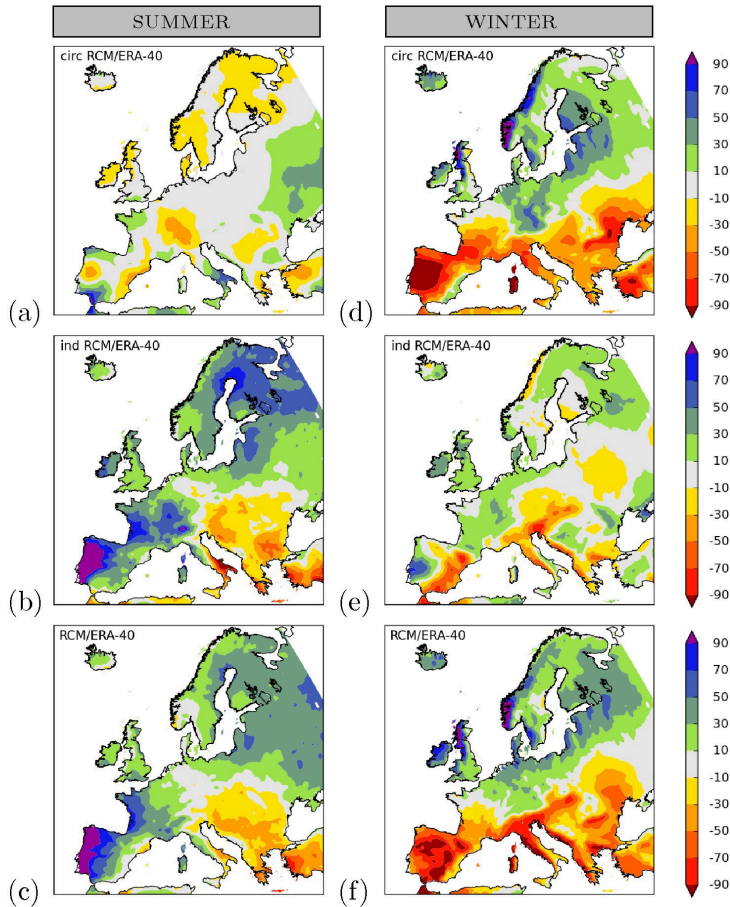
FIGURE 2.14: Precipitation trends ERA-40 forced RCM ensemble (1961-2000). (a) Circulation dependent in the summer half year [%/Century] (b) Circulation independent in the summer half year [%/Century] (c) Total in the summer half year [%/Century] (d–f) Same but for winter precipitation.

the North Atlantic Ocean, the North Sea and the Baltic Sea. Because most of the trends are observed in coastal areas and are not in the GCM forced RCM ensemble, this points to a large influence of SST trend biases in the summer half year in these regions.

The oceans and seas around Europe are major sources of precipitation above Europe. Differences in SST changes affect the precipitation over Europe [*Rowell*, 2003; *van Ulden and van Oldenborgh*, 2006; *Kjellström and Ruosteenoja*, 2007; *Lenderink et al.*, 2009]. The modeled SST trends contain indeed biases: the GCM forced

RCM ensemble underestimates the SST trends (figure 2.15) along the Atlantic coast and other coastal areas (if represented at all). This leads to a lower evaporation trend (not shown) and a reduced trend in coastal precipitation, even in the high-resolution RCMs. Possible explanations for the wrong SST trends in the models are a lack of resolution in the ocean component of the climate models, which causes a misrepresentation of the North Atlantic Current in the models [*van Oldenborgh et al.*, 2009a; *Ashfaq et al.*, 2010] and problems resolving smaller, shallow seas like the North Sea [*Lenderink et al.*, 2009].

For most regions, a large part of the precipitation trend in the winter half year is explained by the circulation dependent part of the model (figure 2.14d). An increase in westerly circulation (figure 2.13) has resulted in an increase in precipitation in the northern part of Europe, and a decrease in the southern part of Europe [*Rummukainen et al.*, 2004]. Between 1960 - 2000 this may be partly related to a non-significant positive trend in the NAO [*Bhend and von Storch*, 2008], but for the other considered time periods no positive NAO trend is observed. The trend is due to a different pattern, a pressure difference between the Mediterranean and Scandinavia rather than Iceland and the Azores [*van Oldenborgh et al.*, 2009a]. The continental pressure dipole has a significant trend over all considered time periods and explains more of the variance of precipitation over most of Europe (the Ukraine is the only clear exception). In central and northern Europe and in Italy, the Mediterranean-Scandinavia pressure difference explains more variance of precipitation than the NAO, making it more suitable for analysis of precipitation trends as well (figure 2.16). Therefore, circulation trend biases are, under the same assumption of linearity, responsible for a large part of the underestimation of precipitation trends in northern and southern Europe in the winter half year.

Note that this analysis assumes that the effects of SST and large-scale circulation trends on the precipitation trends add linearly to the total trends. Non-linear effects are not represented and may affect the conclusions.

2.7   Conclusions

A combination of GCMs and RCMs is often used to construct scenarios of future climate conditions. Here, the modeled precipitation
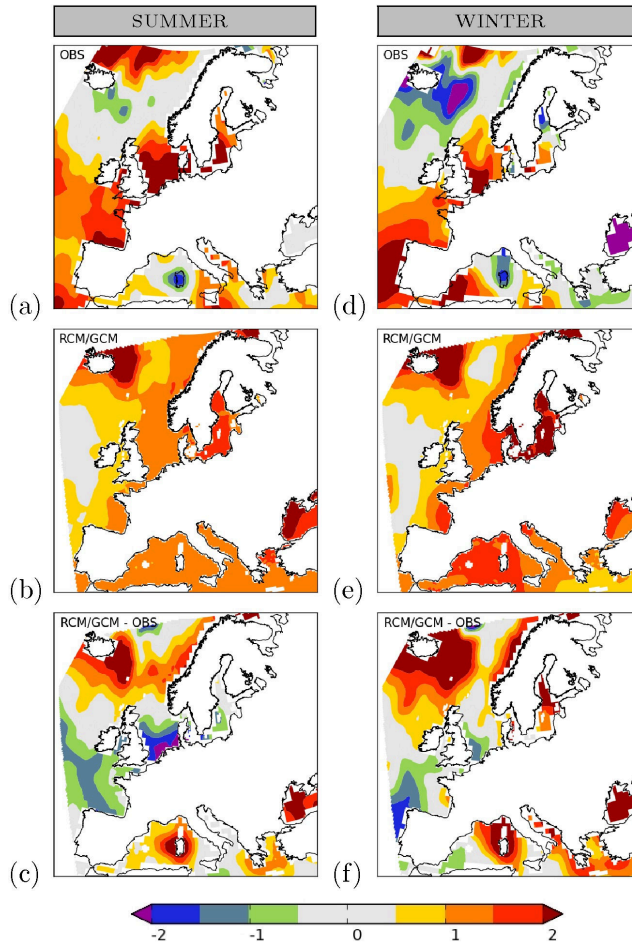
FIGURE 2.15: Observed and modeled trends in SST over 1961-2000 [K/Century]. (a) Observed HadISST summer half year (b) RCM/GCM ensemble summer half year (c) Bias of the RCM/GCM ensemble compared to the observed trend (d-f) same but for winter half year.

trends and uncertainties over (parts of) the last century are compared to observations for a large multi-model ensemble composed of GCMs, an ensemble of RCMs forced at its boundaries by results derived from GCMs and a RCM ensemble forced by realistic, quasi-observed, boundary conditions. Such trends are relevant in, for instance, hydrological applications. A correct representation of the trend in the past is a necessary (but not sufficient) condition for confidence in future projections.
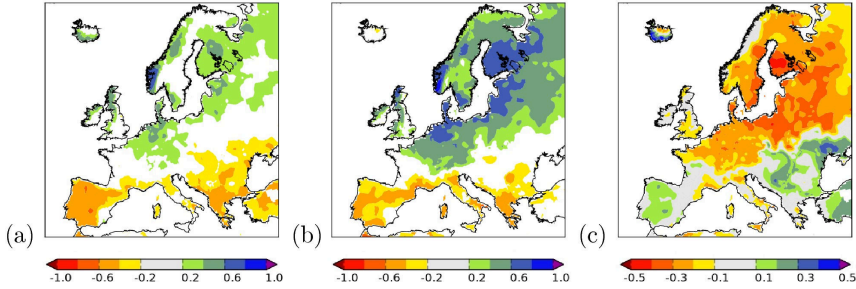
FIGURE 2.16: Correlations of the NAO (a) and Mediterranean-Scandinavia pressure dipole (b) with local winter precipitation in Europe over 1951-2009 (p < 10%). (c) Difference in absolute correlation.

We find that modeled precipitation in GCM and GCM forced RCM ensembles contain large trend biases that fall often outside the spread of the ensemble members. A multi-model RCM ensemble forced by realistic, quasi-observed boundary conditions reproduces the observed trend much better and is largely compatible with the range of uncertainties spanned by the members of the ERA-40 forced RCM ensemble. We conclude that the boundary conditions of RCMs are responsible for large parts of the trend biases found in GCM and RCM ensembles, but are not able to explain all trend biases. The underestimation of precipitation trends in GCM forced RCM ensembles in the summer half year is mainly limited to the coastal regions and is, within the linear approximation of a statistical decomposition, largely caused by SST trend biases in the boundary conditions. The underestimation of precipitation trends in the winter half year that are observed in both northern and southern Europe are, under the same assumption of linearity, for a large part caused by circulation trend biases as present in the GCMs [*van Oldenborgh et al.*, 2009a]. This is not due to a positive trend in the NAO [*Bhend and von Storch*, 2008], but due to a pressure difference between the Mediterranean and Scandinavia [*van Oldenborgh et al.*, 2009a]. Remaining trend biases are likely caused by a combination of model errors in the RCMs, including land cover schemes, and errors in the observations.

To conclude, modeled atmospheric circulation and SST trends over the past century are significantly different from the observed

ones. These mismatches are responsible for a large part of the misrepresentation of precipitation trends in climate models. The causes of the large trends in atmospheric circulation and summer SST are not known. For SST there may be a connection with the well-known ocean circulation biases in low-resolution ocean models. Because it is not clear (yet) whether the trend biases in SST and large scale circulation are due to greenhouse warming, their importance for future climate projections need to be determined. Therefore, a quantitative understanding of the causes of these trends is needed so that climate model based projections of future climate can be corrected for these trend biases.

Acknowledgements

CHAPTER 3

Evaluation of modeled changes in extreme precipitation in Europe and the Rhine basin[1]

Chapter Abstract

In this study, we investigate the change in multi-day precipitation extremes in late winter in Europe using observations and climate models. The objectives of the analysis are to determine if climate models can accurately reproduce observed trends and, if not, to find causes of the difference in trends.

Similar to earlier finding for mean precipitation trends and despite a lower signal to noise ratio, climate models fail to reproduce the increase in extremes in much of northern Europe: the model simulations do not cover the observed trend in large parts of this area. A dipole in the sea level pressure trend over continental Europe causes positive trends in extremes in northern Europe and negative trends in the Iberian Peninsula. Climate models have a much weaker pressure trend dipole and as a result a much weaker (extreme) precipitation response.

The inability of climate models to correctly simulate observed changes in atmospheric circulation is also primarily responsible for

the underestimation of trends in the Rhine basin. When adjusting for the circulation trend mismatch, the observed trend is well within the spread of the climate model simulations. Therefore, it is important that we improve our understanding of circulation changes, in particular related to the cause of the apparent mismatch between observed and modeled circulation trends over the past century.

3.1   Introduction

Estimates of future changes in extremes of multi-day precipitation sums are critical for estimates of future discharge extremes of large river basins and changes in frequency of major flooding events [*Kew et al.*, 2010]. A correct representation of past changes is an important (but not sufficient) condition to have confidence in projections for the future.

High discharge rates for the Rhine in the Netherlands usually occur in (late) winter [*Rijkswaterstaat Waterdienst*, 2012]. Evaporation rates in winter are low and soils are often saturated and sometimes frozen. Rainfall has the potential to melt large amounts of snow by bringing large amounts of thermal energy to the snowpack, increasing runoff [*Disse and Engel*, 2001]. Over the past century the average [*Disse and Engel*, 2001] and extreme [*Wang et al.*, 2005] discharge of the Rhine in winter increased. Model results project a further increase for the current century [e.g. *Hurkmans et al.*, 2010; *Lenderink et al.*, 2007; *Kew et al.*, 2010; *te Linde et al.*, 2010], mainly caused by an increase in precipitation [*van Pelt et al.*, 2012] and a shift of the snowmelt season from spring to winter [*Barnett et al.*, 2005].

The climate in Europe depends strongly on the atmospheric circulation. Western circulation brings moist air from the Atlantic to the continent [*van Ulden and van Oldenborgh*, 2006], leading to increasing precipitation over the continent. In an earlier paper we concluded that a misrepresentation of circulation changes in climate models is responsible for the underestimation of increase in winter precipitation in northwest Europe over the past century in climate models [*van Haren et al.*, 2013a]. Recent research finds that higher quantiles of daily precipitation correlate well with mean precipitation [*Benestad et al.*, 2012] and that the increase in mean winter extreme precipitation in Europe is similar across a range of

multi-day sums [*Kew et al.*, 2010]. The inability of climate models to capture the observed trend in atmospheric circulation could, through transport of moisture, also influence trends in extreme precipitation: particular circulation types may be more favorable for extreme precipitation events to occur.

In this paper we investigate whether the spread of climate models (which includes natural variability) covers the observed increase in extreme precipitation in Europe and the Rhine basin in late winter. We evaluate modeled trends in extreme precipitation, and try to find causes for the difference in trends. We only consider the uncertainty in trends of extreme precipitation. Estimates of trends in river discharge requires the coupling with a hydrological model of the catchment area and hydraulic models of the river and its main branches [e.g. *Lenderink et al.*, 2007], which is outside the scope of this study.

3.2 Data & methods

3.2.1 Study area

We study the extreme precipitation in Europe and the Rhine area (indicated by the area in figure 3.1a). The Rhine is the longest river in western Europe, originating in the Swiss Alps. From Switzerland it flows through the principality of Liechtenstein, Austria, Germany and France before it enters the Netherlands near Lobith, on the Dutch-German border. The main flow reaches the sea near Rotterdam, the Netherlands. The drainage area of the Rhine is approximately 185000 km^2.

Natural variability plays an important role in determining trends of extreme events. To give an impression of the magnitude of the inter-annual variability, we show in figure 3.1b the observed and modeled time-series (with accompanying trend estimates) of annual maxima January-March (JFM) 10-day running precipitation sums averaged over the Rhine basin. The modeled series is only shown for one climate model (EC-EARTH, 1 member). Strong inter-annual variability is found for both observed and modeled time-series, although with a larger (absolute) magnitude for the observed series.

In late winter precipitation in Europe is mainly caused by frontal systems from the Atlantic. The mean precipitation decreases from the coast and is highest on the west side of mountain ranges. The

latitude where most rain falls is determined by the zonal pressure difference, with a blocking high over northern Europe causing dry weather there and more rain in southern Europe. Conversely, a stronger westerly flow brings more rain to northern Europe and less to the Mediterranean area.

(a)   (b)
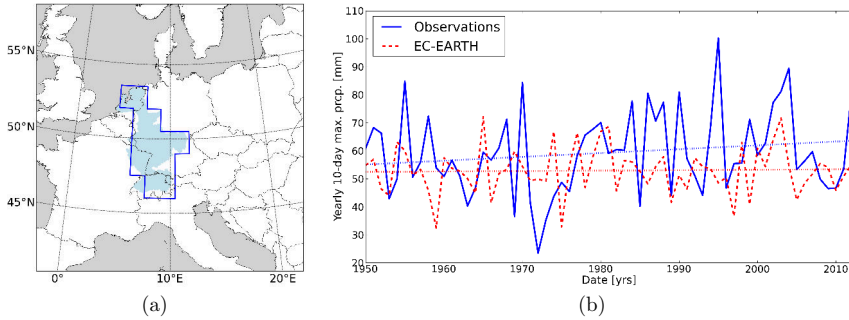
FIGURE 3.1: (a) Location and area of the Rhine basin within Europe. The light blue area indications the actual catchment area. The dark blue line represents the grid box approximation used in this study. (b) Time-series (with accompanying trend estimates) of JFM annual-maxima 10-day precipitation sums averaged over the Rhine basin [mm].

3.2.2   Analysis period

Trends are computed from the annual maximum series of the 10-day running precipitation sums (RX10day) for the northern hemisphere late winter (JFM) 1950-2012 period. Extreme 10-day precipitation sums are an important statistic for extreme peak flows for the Rhine river in the Netherlands [e.g. *Shabalova et al.*, 2003]. The choice for the late winter period is dictated by past discharge extremes of the river Rhine. More than 75% of winter annual discharge extremes [*Rijkswaterstaat Waterdienst*, 2012] at the Lobith station (near the Dutch–German border) since 1950 occurred in the second half of the winter (JFM), despite slightly more (multi-day) extreme precipitation events in the river basin occurring in the first half of the winter.

The JFM period happens to coincide with the season of strongest observed and simulated trends in atmospheric circulation in this region. The late European winter has seen a change in circulation regime over the past century, related to an eastward extension of

the belt of zonal winds [*Haarsma et al.*, 2013a; *Ulbrich et al.*, 2008], that is outside the range of natural variability of model results [e.g. *van Oldenborgh et al.*, 2009a; *van Haren et al.*, 2013a].

3.2.3 Datasets

We use daily precipitation data in this study. The multi-model ensemble used in this study is obtained from the Coupled Model Intercomparison Project Phase 5 [CMIP5, *Taylor et al.*, 2011]. The CMIP5 dataset consists of models at varying horizontal grid spacing, typically in the order of one hundred to a few hundreds of kilometers. For the period before 2005 we use the historic runs. For the period after 2005 we use the RCP4.5 experiment runs. We limit ourselves to use only historical runs that have a RCP4.5 extension. To not bias the results to models with more members available, we use only the first available member per model. The FGOALS-g2 model is omitted from this analysis due to inconsistencies between the daily and monthly precipitation fields. This brings the total number of models used in this study to 21 (EC-EARTH, HadGEM2-CC, HadGEM2-ES, CCSM4, GFDL-ESM2G, GISS-E2-R, MIROC-ESM-CHEM, NorESM1-M, BCC-CSM1-1, CNRM-CM5, GFDL-ESM2M, IPSL-CM5A-LR, MIROC5, MPI-ESM-LR, CSIRO-Mk3-6-0, CanESM2, IPSL-CM5A-MR, MIROC-ESM, MRI-CGCM3, IN-MCM4, ACCESS1-0). Different RCP scenarios are available, but for the short period after 2005 these are almost identical. All models are bilinearly interpolated on a regular 1.5 degree grid before analysis, resulting in 13 grid points for the Rhine area.

To evaluate the model results we use the state-of-the-art gridded high resolution (0.5°) precipitation fields of the European ENSEMBLES project version 7.0 [E-OBS, *Haylock et al.*, 2008]. The observations are averaged to the same regular 1.5 degree grid when compared directly with the model results.

For validation of our results we also use the high resolution (25 to 50 km resolution) multi-model ensemble of regional climate models (RCMs) provided by Research Theme 2b of the European ENSEMBLES project [RT2b, *van der Linden and Mitchell*, 2009]. The RCMs are forced at their lateral boundaries by results from global climate models (GCMs) from the Coupled Model Intercomparison Project Phase 3 [CMIP3, *Meehl et al.*, 2007]. There are no large differences between the results of CMIP3 and CMIP5 models over

Europe. The RCM ensemble consists of a total of 18 RCM/GCM combinations.

3.3   Methodology

3.3.1   Effect of circulation change

To investigate if the change in mean circulation characteristics affects the change in precipitation extremes, we fit a simple statistical model that isolates the linear effect of mean circulation anomalies [*van Ulden and van Oldenborgh*, 2006; *van Oldenborgh et al.*, 2009a; *van Haren et al.*, 2013a] to the anomalies of the annual maxima series of RX10day, $P'(x, y, t)$. This is done for each dataset separately. These effects include the influence of mean geostrophic wind anomalies $U_g(x, y, t)$, $V_g(x, y, t)$ and vorticity anomalies $G'_{vorticity}(x, y, t)$ and the remaining noise $\eta(x, y, t)$. The longitude and latitude of the grid box is indicated by (x, y), t indicates the time.

$$P'(x, y, t) = P'_{circ}(x, y, t) + P'_{residual}(x, y, t) \tag{3.1}$$

$$P'_{circ}(x, y, t) = B_W(x, y)U_g(x, y, t) + B_S(x, y)V_g(x, y, t) + \\ B_V(x, y)G'_{vorticity}(x, y, t) \tag{3.2}$$

$$P'_{residual}(x, y, t) = A(x, y)t + \eta(x, y, t) \tag{3.3}$$

The geostrophic wind anomalies and vorticity anomalies are computed from the monthly NCEP/NCAR Reanalysis sea-level pressure (SLP) dataset [NCEP/NCAR, *Kistler et al.*, 2001] when considering observed precipitation anomalies, but other SLP datasets (Twentieth Century Reanalysis [20C, *Compo et al.*, 2011], Trenberth Northern Hemisphere SLP [*Trenberth and Paolino*, 1980]) give similar results. Model SLP output is used in combination with modeled precipitation anomalies. The coefficients $B_W(x, y)$, $B_S(x, y)$, $B_V(x, y)$ and $A(x, y)$ are fitted over 1950-2012 for each 3 month winter period.

3.3.2   Trend definition

Our approach is to fit a non-stationary generalized extreme value (GEV) distribution to the annual maxima series of RX10day, as well as separately to the derived circulation and residual components.

The GEV distribution is described as [e.g. *Katz et al.*, 2002]

$$F(x; \mu, \sigma, \gamma) = \begin{cases} \exp\{-[1 + \gamma(x - \mu)/\sigma]^{-1/\gamma}\}, \\ \qquad \text{for } \{1 + \gamma(x - \mu)/\sigma > 0, \gamma \neq 0\} \\ \exp\{-\exp[-(x - \mu)/\sigma]\}, \text{for } \gamma = 0 \end{cases} \quad (3.4)$$

where μ, $\sigma > 0$, and γ are the location, scale and shape parameters, respectively. We adopted the homoscedastic model (constant variance) where the location parameter is described by

$$\mu(t) = \mu_0 + \mu_1 t \quad (3.5)$$

here μ_1 is a trend in the location parameter, and t is a covariate linear in time from 1950-2012. Whenever we refer to a trend in precipitation extremes in later sections we refer to the trend as estimated by the μ_1 parameter. The scale and shape parameters are constant in the homoscedastic model. Experiments allowing for a time-varying scale parameter produced similar trends in the location parameter.

The parameters are estimated by the maximum likelihood method because of its ability to estimate time-dependent covariates as recommended by *Katz et al.* [2002] and *Kharin and Zwiers* [2005].

3.3.3 Rank histograms

As an aggregated statistic for the performance of our model ensemble we compute rank histograms. A rank histogram is created by tallying the rank of the observation relative to values from the ensemble sorted from lowest to highest. If there are N ensemble members, there are N+1 ranks, including the two outer edges, the observation could fall. A *reliable* ensemble produces a flat histogram. If the model ensemble has a trend bias, a larger part of the area lies at one end of the ensemble and that edge of the histogram curves up.

To investigate whether there is a significant deviation from a reliable ensemble, i.e., whether it is unlikely to be a fluctuation in the distribution of model spread and natural variability, the strong correlation between neighboring grid points needs to be taken into account. We do this by including the correlation as represented by the models in the ensemble when constructing significance intervals. The significance intervals are constructed by considering each model

in turn to be the 'truth' [*Annan and Hargreaves*, 2010] and computing its rank histogram with respect to the other models. The 90% confidence interval is then given by the distance between the second lowest and the second highest ranked member for each bin (using a 1-sided test to only account for trend biases and assuming the outcomes of all members are equally likely).

3.4   Modeled versus observed trends

Precipitation extremes in late winter have increased in the northern half of Europe in the last 60 years. In figure 3.2 we show the observed (panel a) and modeled (panel b) trend in 10-day annual maxima (RX10day) for late winter between 1950–2012. Externally forced changes should appear in the mean trend of the model ensemble (figure 3.2b). If no trend is found here, the observed trend is either caused by natural variability or climate models fail to (correctly) represent processes that are important for precipitation. The figures show that the average modeled trend in northern Europe is much weaker than the observed trend. The trend bias in the models is significant in northern Europe: figure 3.2c shows that for a lot of grid points in this area the observed trend is larger than in any of the models (dark red color). A summary of this panel is given by the rank histogram in figure 3.2d (because of larger uncertainties in the observations in eastern Europe these are calculated over the area west of 20ºE), which shows that the underestimation of positive trends is significant at the 90% confidence interval: i.e. climate models likely underestimate natural variability or have common errors in processes that are important for precipitation. Another explanation could be that the quality of the observations is not good enough or the station network density is not high enough to compute reliable trends [*Haylock et al.*, 2008; *Hofstra et al.*, 2010]. However, the decorrelation scale of winter precipitation is larger than the inter-station distance in most of Europe (except in the far North). The relatively low horizontal grid spacing (1.5º) used when evaluating model results further reduces the influence of interpolation and station network density on the trends. A dedicated study to (extreme) precipitation trends in the Netherlands produces similar trends with a homogenized dataset [*Buishand et al.*, 2012], giving more confidence in the quality of the observations themselves.

The underestimation of the trend in extreme precipitation could originate from a number of possible causes: 1. The coarse resolution of global climate models may not be enough to describe extreme precipitation events, or may not provide enough detail on local conditions such as topography and coastlines that could affect modeled precipitation; 2. Climate models underestimate natural variability of extreme precipitation; 3. Underestimation in change of mean circulation characteristics.; 4. Model errors (unrelated to atmospheric circulation) present in both GCMs and RCMs; 5. Observational errors. We investigate the contribution of points 1–3 to the underestimation of trends in extreme precipitation. The contributions of points 4 and 5 are part of the remaining error budget.

To investigate if the trend bias is caused by the coarse resolution of GCMs we performed the same analysis with a multi-model ensemble of RCMs. We used the ensemble provided by Research Theme 2b of the European ENSEMBLES project, RT2b. The RCM ensemble has, with exception of details, similar trend biases as the ensemble composed of GCMs (not shown).

A second reason for the low reliability of climate models could be an underestimation of natural variability of extreme precipitation in climate models. Year-to-year natural variability is indeed underestimated in GCMs (standard error of the trend estimate for the models is smaller than for the observations), but this is not the case for RCMs (not shown). It is therefore unlikely that the trend bias is caused by an underestimation of natural variability on short timescales in the models. Underestimation of natural variability on multi-decadal or longer time scales could still be possible.

As discussed in section 3.3.1, particular circulation types may be more favorable for extreme precipitation events to occur. Using the statistical model defined by equations 3.1–3.3 we estimate atmospheric circulation induced precipitation changes. The observed/-modeled circulation dependent trend, within the linear approximation of equations 3.1–3.3, is given in figures 3.2e and 3.2f. The residual part of the trend that is not linearly dependent on circulation changes is given in panels i and j.

Seasonal mean circulation changes (figure 3.3a, the pattern is consistent over NCEP/NCAR, 20C and Trenberth) cause an increase in observed extreme precipitation in parts of central and northern Europe, as well as a decrease in much of southern Europe. The CMIP5 models also show a north-south dipole in the

pressure trends over continental Europe, although on average much weaker and more southeasterly displaced (and a trend to lower pressures over Greenland). Although, this pressure change also causes a (slightly displaced) north-south precipitation response, the response is too weak to show up in figure 3.2e. Figure 3.2g (with a summary in 3.2h) shows the fraction of the CMIP5 models with a circulation dependent trend larger than the observed circulation dependent trend. The observed circulation dependent trend caused by a change in geostrophic winds is larger than in any of the models for large parts of northern (increase in precipitation) and southern (decrease in precipitation) Europe. For northern Europe this shows up in an underestimation of the total trend by the models. The circulation dependent decrease in southern Europe is (partly) canceled out by an increase due to other factors. Inconsistencies in the underlying data provides low confidence in the results in the Balkan area. We did not find obvious problems in the Iberian Peninsula so we would have to assume that the (partial) cancellation is real in this area.

A possible explanation for the residual trend in the far north and in eastern Europe is a strong temperature increase in these regions. When the temperature increases, so does the water-holding capacity of the atmosphere, which in turn favors stronger rainfall events [*IPCC*, 2007]. An alternative explanation is that decreasing sea ice extent results in more open water, increasing evaporation.

3.5   Trend in the Rhine basin

We consider the trend in extreme 10-day precipitation over the Rhine basin (figure 3.1a). These trends are important for flood risk management in the Netherlands.

Figure 3.4a shows the observed and modeled trends in JFM RX10day as averaged over the Rhine basin area. The trend is calculated as the trend of the area average. The observed trend lies on the outer edge of the spread of modeled trends. We verified the results in an ensemble of regional climate models forced by global models (European ENSEMBLES RT2b), producing similar results (not shown).

A large part of the trend in this region is, within the linear approximation of a statistical decomposition, caused by a change
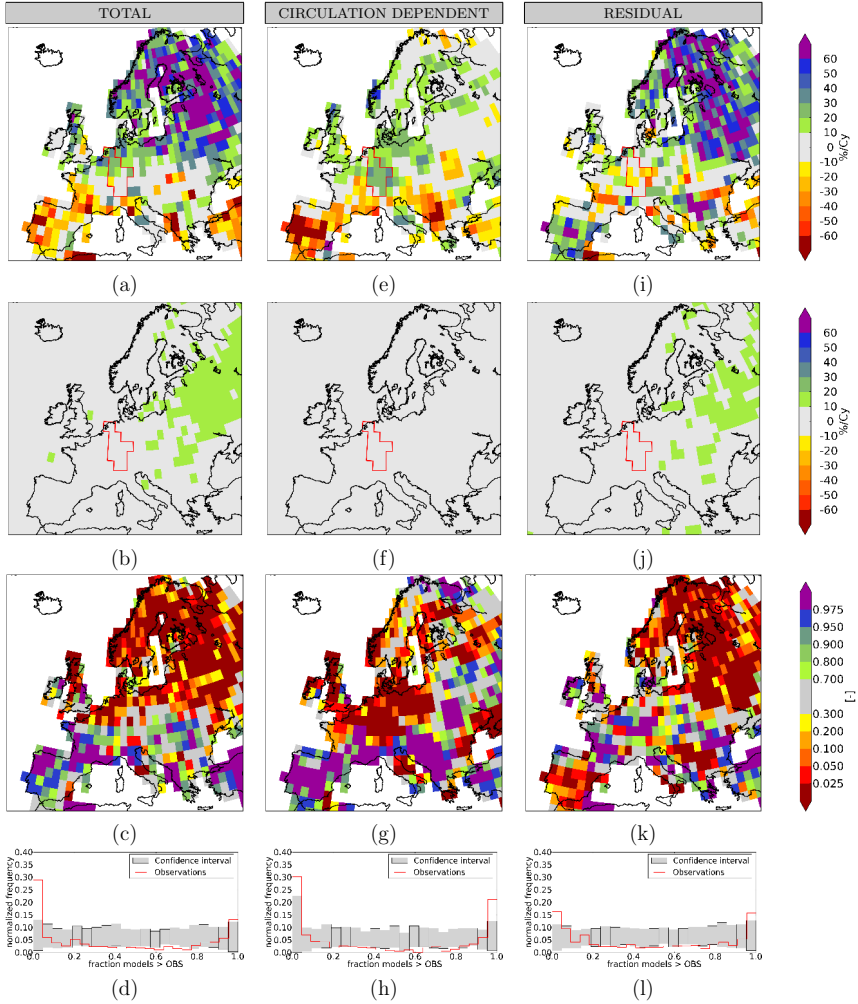
FIGURE 3.2: Comparison of observed and GCM RX10day precipitation trends of January–March for 1950-2012. (a) Relative trend in observed precipitation [%/century]. (b) Mean relative trend in the CMIP5 ensemble [%/century]. (c) Fraction of the CMIP5 ensemble with a trend larger than the observed one [-, non-linear scale]. (d) Rank histogram. (e-h) Same but for circulation dependent precipitation. (i-l) Residuals.

in circulation (figure 3.2). In a similar manner as before, we estimate the atmospheric circulation induced precipitation changes for the whole basin, where the averaged change in geostrophic wind anomalies over the basin area is used. We find that a large part
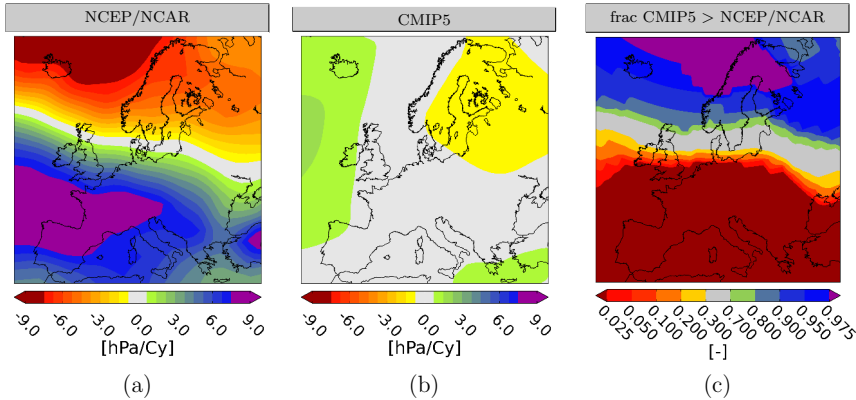
FIGURE 3.3: Observed (a) and modeled (b) trend in mean JFM sea-level pressure (1950-2012) [hPa/century]. (c) Fraction of models with a trend larger than observed [-, non-linear scale].

of the observed trend is linearly related to changes in mean atmospheric circulation. For the models the effect of circulation is much smaller. Adjusting for the circulation trend mismatch by only considering the residual component, the observed trend is well within the climate model ensemble (figure 3.4b).
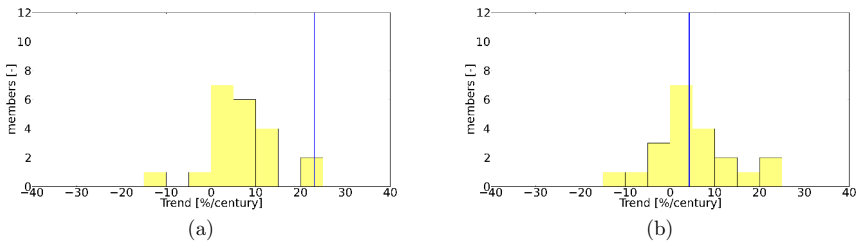
FIGURE 3.4: Observed modeled area average JFM RX10day trend for the Rhine basin (1950-2012). Total (a) and residual (b) trend for the Rhine basin. Observed trend is indicated by the blue line, models by the yellow bars.

3.6 Conclusions

Climate model based projections of future precipitation extremes are often used in projections of future river discharge extremes. Here, the trends in extreme precipitation in Europe and the Rhine river basin over the last 60 years are compared with observed trends.

A correct representation of past changes is an important (but not sufficient) condition to have confidence in projections for the future.

We find that climate models underestimate the trend in extreme precipitation in the northern half of Europe: the trend bias is significant in this area. Using a statistical decomposition we split the trend in a part that is linearly related to circulation change, and a residual part that is not linearly related to circulation change. Circulation changes have caused an increase in observed extreme precipitation in parts of mid and northern Europe, as well as a decrease over the Iberian Peninsula. Climate models underestimate the change in circulation over the past century and as a result have a much smaller (extreme) precipitation response.

Climate models are not capable of reproducing the observed trend in extremes for the Rhine basin. The underestimation is, within the linear approximation of a statistical decomposition and statistical uncertainties, caused by an underestimation of the change in mean circulation. The ensemble covers the observed trend when only the part of the trend not linearly related to mean circulation change is considered: the residual biases not linearly related to mean circulation changes are relatively small. Therefore, it is important that we improve our understanding of circulation changes, in particular related to the cause of the apparent mismatch between observed and modeled circulation trends over the past century [*Haarsma et al.*, 2013a].

Acknowledgements

Resolution dependence of European winter
precipitation in an atmospheric general circulation
model[1]

Chapter Abstract

In this study, we investigate the effect of GCM spatial resolution
on modeled winter precipitation over Europe. The objectives of
the analysis are to determine whether climate models have suffi-
cient spatial resolution to have an accurate representation of the
storm tracks that affect precipitation. We investigate if there is a
significant statistical difference in modeled precipitation between a
medium resolution ($\sim$112 km horizontal resolution) and a high res-
olution ($\sim$25 km horizontal resolution) version of a state-of-the-art
AGCM (EC-Earth), if either model resolution gives a better repre-
sentation of precipitation in the current climate, and what processes
are responsible for the differences in modeled precipitation.

   We find that the high resolution model gives a more accurate
representation of northern and central European winter precipita-
tion. The medium resolution model has a larger positive bias in
precipitation in most of the northern half of Europe. Storm tracks

are better simulated in the high resolution model, providing for a more accurate horizontal moisture transport and moisture convergence.

Using a decomposition of the precipitation difference between the medium- and high resolution model in a part related and a part unrelated to a difference in the distribution of vertical atmospheric velocity, we find that the smaller precipitation bias in central and northern Europe is largely unrelated to a difference in vertical velocity distribution. The smaller precipitation amount in these areas is in agreement with less moisture transport over this area in the high resolution model. We found that in areas with orography the change in vertical velocity distribution is more important.

4.1   Introduction

General circulation models (GCMs) attempt to simulate the Earth's climate. Often these models are used to isolate the drivers of climate change in response to natural and/or anthropogenic forcings. While some features are well represented in GCMs (e.g. global temperature), other aspects remain uncertain [*Flato et al.*, 2013]. One of these aspects is (regional) precipitation in Europe [*van Haren et al.*, 2013a, b]. A correct representation of precipitation in climate models is, among others, relevant for hydrological applications, such as flood risk management, navigation and energy production.

It remains to be seen whether the current generation of GCMs have sufficient spatial resolution to resolve the physical processes affecting climate [*Pope and Stratton*, 2002]. However, running high-resolution models is often expensive in terms of computing and data storage. *Demory et al.* [2013] found that an increase in horizontal resolution (N48 – N96 – N144 – N216 – N230 – N512) lead to a decrease in precipitation over the ocean and an increase over land in two atmospheric general circulation models (AGCMs) of the UK Met Office Hadley Centre. This changes the partitioning of moisture fluxes that contribute to precipitation over land from local to more non-local moisture sources with increasing resolution. *Hack et al.* [2006] found a robust systematic improvement in the large-scale dynamical circulation of the atmospheric component of the Community Climate System Model (CCSM, AGCM) by increasing the horizontal resolution (T42 – T85). *Berckmans et al.* [2013] found that

an increased horizontal resolution (N96 – N216) improved the accuracy of European blocking frequencies in the AGCMs studied. Several studies showed an improvement in storm track performance in higher resolution Coupled Model Intercomparison Project Phase 5 (CMIP5, coupled) GCMs [*Zappa et al.*, 2013; *Colle et al.*, 2013]. The storm track over the North Atlantic heavily influences the weather in Europe. *Jung et al.* [2012] found that increasing horizontal resolution from T159 to T511 in an AGCM improved the frequency of occurrence of Euro-Atlantic blocking, and the representation of extratropical cyclones in large parts of the Northern Hemisphere extratropics. Further increasing resolution to T1279 and T2047 yielded relatively small further changes. *Champion et al.* [2011] found an increase in ascending atmospheric motion, accompanied by an increase in precipitation extremes, within Northern Hemisphere extratropical cyclones, by increasing the resolution of the ECHAM5 global climate model (AGCM) from T213 to T319. *Willison et al.* [2013] found an enhanced positive feedback between cyclone intensification and latent heat release in the North Atlantic storm track at higher resolution (20 km, AGCM), resulting in a systematic increase in eddy intensity and a stronger storm track relative to the coarser simulations (120 km). The need for improved circulation statistics for regional downscaling over Europe was emphasized by *van Haren et al.* [2013a, b, coupled model study]. Regional climate models are often largely dependent on the storm tracks in the driving GCM because of their relatively small spatial domain. Biases in precipitation over Europe could be attributed for a large part to biases in the circulation in global climate models.

Previous studies have focused on one of the following points: (1) changes in the representation of the storm track or large-scale circulation with resolution [*Jung et al.*, 2012; *Willison et al.*, 2013; *Zappa et al.*, 2013; *Colle et al.*, 2013; *Hack et al.*, 2006]; (2) changes of precipitation within the stormtrack with resolution [*Champion et al.*, 2011]; (3) changes in blocking frequency with resolution [*Berckmans et al.*, 2013; *Jung et al.*, 2012]; (4) circulation dependence of precipitation [not resolution dependent, *van Haren et al.*, 2013a, b]; (5) effect of resolution on global average land/ocean precipitation partitioning [*Demory et al.*, 2013]. For different regions the impact of any of these, caused by a change in model resolution is different. Here we combine the results of these studies in an analysis of regional

precipitation over Europe. The objectives of the analysis are to determine whether climate models have sufficient spatial resolution to have an accurate representation of storm tracks affecting precipitation over Europe. We investigate if there is a significant statistical difference in modeled precipitation between a medium resolution and a high resolution ensemble of a state-of-the-art global AGCM, if either of the model resolutions gives a better representation of precipitation in the actual climate system, and what processes are responsible for the differences in modeled precipitation. AGCMs simplify the climate system by constraining it by observed boundary conditions (sea surface temperatures and sea ice cover) that: (1) make their results more comparable to observations and reanalyses; (2) allow for a better comparison between models; (3) make it easier to isolate atmospheric processes responsible for affecting the hydrological cycle in climate models with various resolutions [*Demory et al.*, 2013].

This paper is outlined as follows. In section 4.2 we define our study area, introduce the datasets used in this study and discuss the methodology. In section 4.3 we calculate the difference in precipitation and moisture convergence between the two model resolutions. In search for causes of the differences in modeled precipitation, we investigate differences in moisture transport and stormtracks in section 4.4. In section 4.5 we discuss the distribution of daily precipitation over our study area and try to link differences with differences in strength/frequency of atmospheric disturbances. Finally, some conclusions are drawn in section 4.6.

4.2   Data & methods

4.2.1   Data

The model data is from EC-Earth version 2.3, a state-of-the-art GCM developed by a consortium of European research institutions. The atmospheric component of the model is derived from the weather forecast model (Integrated Forecast System (IFS) cycle 31r1) of the European Centre for Medium-Range Weather Forecasts [*Hazeleger et al.*, 2010, ECMWF]. EC-Earth differs from the weather forecast model by a small number of changes in the physics parameterizations, applied to optimize the model for climate simulations

[*Hazeleger et al.*, 2012]: An improved description of the entrainment of environmental air in deep convecting plumes from IFS cycle 32r3 was used. Also the imhomogeneity scaling factor for shortwave cloud optical thickness has been reduced from 0.7 to 0.57 and an improved mass conservation correction scheme has been applied (the scheme from IFS cycle 33R2). The land surface component in IFS cycle 31r1 (TESSEL) was replaced by H-TESSEL, which uses an improved representation of hydrology, as in more recent cycles of IFS.

The experiment [*Haarsma et al.*, 2013b] consists of two sets of 5-year 6-member ensemble simulations from 2002-2006, resulting in 30 years of data for each set. The sets differ both in horizontal and vertical resolution. The model resolution of the medium resolution ensemble is T159L62 (∼112 km horizontal resolution, 62 vertical levels). The high-resolution ensemble is at T799L91 (∼25 km horizontal resolution, 91 vertical levels). The parameterizations packages of the high and medium resolution model runs are the same. Observed greenhouse gases and aerosol concentrations were used in the simulations. Also observed sea surface temperatures (SSTs) and sea-ice coverage were prescribed. The daily SSTs and sea ice data were taken from the daily optimum interpolation (OI) sea surface temperature (SST) analysis [*Reynolds et al.*, 2002] at 0.25 degree resolution and interpolated on the model grid. A 10 year spin-up run at medium resolution (T159) was made, followed by a 9 month (from January to October) spin-up run at the desired resolution. The 6 member ensemble was made by taking the atmospheric state of one of the first 6 days of October as initial state for each member. Thereafter, the model was run for another 3 months until 1 January before the data were used for the analysis. After this spin-up the spread in the atmospheric states was sufficient to treat the 6 runs as independent members. This computational very expensive experiment was done for multiple research questions. One of those was the impact of climate change on teleconnection responses to specific tropical SST patterns [*Haarsma et al.*, 2013b]. This motivated the larger ensemble approach of shorter runs. The research questions discussed in this paper could also be studied with a fewer longer runs.

The model data is verified against ERA-Interim [*Dee et al.*, 2011], a global atmospheric reanalysis produced by the ECMWF, extending back to 1979. We used the period 1982–2011 for the

ERA-Interim data. ERA-Interim has a T255L60 resolution ($\sim$80 km horizontal resolution, 60 vertical levels). Reanalysis data provide a multivariate, spatially homogeneous, and coherent record of the global atmospheric circulation. This reanalysis uses a single data assimilation system and is therefore not affected by changes in method. A sufficiently realistic model is able to extrapolate information from locally observed parameters to unobserved parameters at nearby locations, and it can also propagate this information forward in time. ERA-Interim uses a four-dimensional data assimilation system which allow the analyzed fields to evolve smoothly in time instead of with jumps at times of analyses, and this has a major advantage of largely eliminating the spinup problem of the hydrological cycle [*Trenberth et al.*, 2011]. In this way it is possible, for example, to obtain meaningful precipitation estimates from a reanalysis of temperature, humidity and wind observations [*Dee et al.*, 2011]. The forecast parameters (precipitation and evaporation) were calculated from averaging the accumulated values from the beginning of the forecast, initialized at 12 hours from 00 and 12 UTC, over the range of 12 hours.

Because precipitation in ERA-Interim is in fact calculated using short-range model forecast, a second evaluation of the simulated precipitation is performed using the state-of-the-art gridded high resolution (0.5º horizontal resolution) daily precipitation fields of the European ENSEMBLES project version 9.0 [*Haylock et al.*, 2008, E-OBS]. The dataset is based on meteorological station measurements and is designed to provide the best estimate of grid box averages to enable direct comparison with climate models. The same period is selected as for the ERA-Interim data (1982–2011). Figure 4.1 compares daily average November–April (NDJFMA) winter precipitation for ERA-Interim, E-OBS and two additional observational datasets: Climatic Research Unit (CRU) Time-Series (TS) 3.22 [*Jones, P.D. and Harris, I.*, 2014] and the dataset from the Global Precipitation Climatology Centre (GPCC) version 6 [*Becker et al.*, 2013]. All four datasets agree well over most of the European area for this period (figure 4.1e, exceptions are areas with orography), providing confidence in the representation of precipitation in ERA-Interim and E-OBS.

For storage limitations, the data was first averaged to daily means where applicable. To allow a fair comparison the data was then regridded on the T159 resolution of the medium resolution
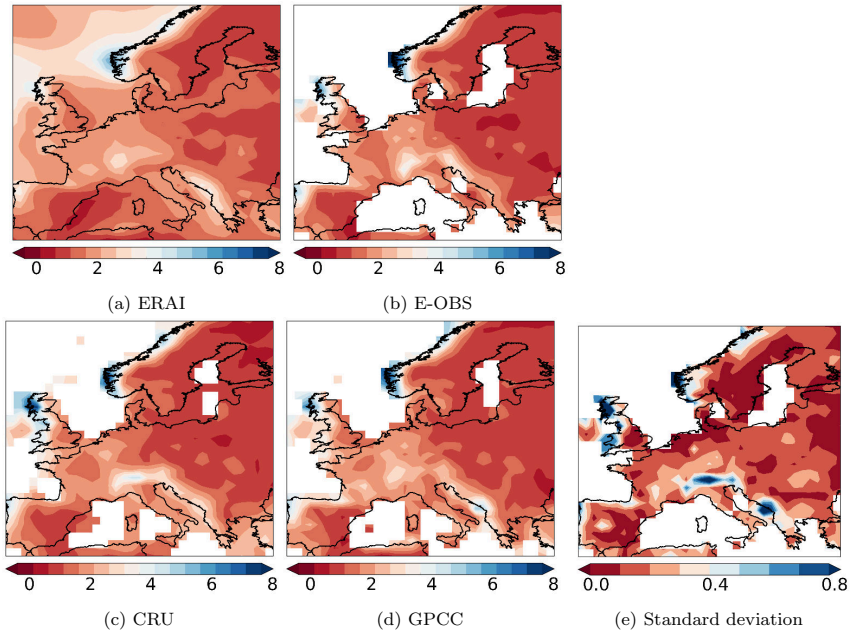
FIGURE 4.1: Comparison precipitation datasets for average winter (NDJFMA) precipitation for 1982–2011 [mm/day]. (a) ERA-Interim; (b) E-OBS; (c) CRU; (d) GPCC; (e) Standard deviation between panels (a–d).

ensemble. Regridding was done by means of second order conservative remapping [*Jones et al.*, 1999]. In conservative remapping, the flux on the new (destination) grid results in the same energy or water exchange as the flux on the old (source) grid. Second order conservative remapping is more accurate compared to first order conservative remapping, at the expense of computational demands. Note that we use a 30-year continuous period for the reanalysis and observations to verify the two sets of 5-year 6-member ensemble simulations. While this makes the influence of natural variability on the estimated quantities much better comparable, some differences between model results and observations may be due to different decadal variability due to different SSTs.

4.2.2 Study area

We focus in this study on European winter precipitation. In earlier studies we found that for this area and season, circulation driven

precipitation trends are not well represented in climate models [*van Haren et al.*, 2013a, b]. Increased spatial resolution in climate models may give a more accurate circulation and the associated precipitation. We discuss some results in more detail for a smaller area which is outlined in figure 4.2. This area consists of the Netherlands, Belgium, Luxembourg, Germany and part of France. It covers two major river basins (Meuse and Rhine) and no strong orography. Winter precipitation in this area is relevant for hydrological applications such as flood risk management, navigation and energy production. When we refer to the study area in later parts of this paper, we refer to this smaller area.
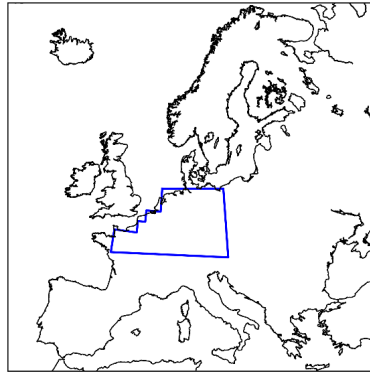
FIGURE 4.2: Outline of the study area.

4.2.3   Methods

4.2.3.1   Moisture convergence

Moisture convergence follows from the conservation of water vapor in the atmosphere [e.g. *Banacos and Schultz*, 2005]. Under the assumption that condensed water immediately precipitates out, moisture convergence is equal to the difference between evaporation (e) and precipitation (p),

$$\underbrace{\frac{\partial q}{\partial t}}_{\substack{\text{local rate of} \\ \text{change of q}}} + \underbrace{\nabla \cdot (q\mathbf{V})}_{\substack{\text{-horizontal moisture} \\ \text{flux convergence}}} + \underbrace{\frac{\partial}{\partial p}(qw)}_{\substack{\text{-vertical moisture} \\ \text{flux convergence}}} = \underbrace{e - p}_{\text{sources and sinks}}$$

$$(4.1)$$

where the vector $\mathbf{V}$ represent the horizontal wind components. Vertical integration between the surface and the top of the atmosphere yields

$$P - E = -\frac{1}{g} \int_0^{P_s} \frac{\partial q}{\partial t} \, dp - \frac{1}{g} \int_0^{P_s} \nabla \cdot (q\mathbf{V}) \, dp \qquad (4.2)$$

where g is the gravitational constant, and P and E are precipitation and evaporation, which follow from vertically integrating precipitation (p) and evaporation (e), respectively. The subscript s refers to surface quantities. Equation 4.2 can be simplified as [*Seager and Henderson*, 2013]

$$P - E = \underbrace{-\frac{1}{g}\nabla \cdot \int_0^{P_s} \mathbf{V}q \, dp}_{\text{moisture convergence}} - \underbrace{\frac{1}{g}\frac{\partial}{\partial t} \int_0^{P_s} q \, dp}_{\text{atmospheric water storage}} \qquad (4.3)$$

The 30-year averaged NDJFMA moisture convergence is related to P and E via

$$\overline{\langle P - E \rangle} = \overline{\left\langle -\frac{1}{g}\nabla \cdot \int_0^{P_s} \mathbf{V}q \, dp \right\rangle} - \overline{\left\langle \frac{1}{g}\frac{\partial}{\partial t} \int_0^{P_s} q \, dp \right\rangle} \qquad (4.4)$$

where the angles $\langle \rangle$ indicate a seasonal average and the overline indicates a 30-year average. We find that the last term on the right hand side of equation 4.4 is small compared to the other terms ($\mathcal{O}[10^{-4}]$) and is ignored. The difference in moisture convergence between medium- and high resolution model is finally written as

$$\Delta\overline{\langle P - E \rangle} = \Delta\overline{\left\langle -\frac{1}{g}\nabla \cdot \int_0^{P_s} \mathbf{V}q \, dp \right\rangle} \qquad (4.5)$$

While the (approximate) equality in equation 4.5 may be technically true, in reality this may not be the case due to [*Zahn and Allan*, 2013]: (1) Numerical issues, (2) the use of instantaneous velocity and humidity fields, whereas P and E are fluxes and non-instantaneous, and (3) limited vertical resolution of saved output fields (only atmospheric data at 850/700/500/300/200 hPa was saved) . Moreover, for reanalysis the moisture budget is generally not closed, which effectively adds another term to equation 4.5 [*Trenberth et al.*, 2011]. Because quantitative agreement may not be possible for these reasons, we will only look for qualitative agreement between the left and right side of equation 4.5.

Note that the integrations in the above equation, and further integrations in this study, are discretized before they are calculated.

4.2.3.2 Integrated vapor transport

Integrated vapor transport (IVT) is defined as

$$\text{IVT} = \sqrt{\left(g^{-1}\int_{850}^{200} \text{qu dp}\right)^2 + \left(g^{-1}\int_{850}^{200} \text{qv dp}\right)^2} \qquad (4.6)$$

with g the gravitational constant, q the specific humidity, p the atmospheric pressure, and u and v are the horizontal wind speed components. The integration takes place between 850 and 200 hPa (the lowest and highest vertical output level available).

4.2.3.3 Precipitation decomposition

The precipitation difference between the two models is decomposed using the ascending motion of the atmosphere into three different parts: a vertical velocity component, a non-vertical velocity component, and a co-variation term. The vertical velocity term indicates the precipitation response due to differences in strength/frequency of dynamic disturbances (change in distribution of w_{500}). The non-vertical velocity term indicates the difference in precipitation for a given w_{500}, which includes every influence that is not captured by changes of w_{500} (e.g. horizontal moisture transport). The last term in the equation arises from the correlation of the two effects. The decomposition is given by [*Bony et al.*, 2004]

$$\delta\overline{P} = \underbrace{\int_{-\infty}^{\infty} p_w \delta P_{r_w} dw}_{\text{non-vertical velocity}} + \underbrace{\int_{-\infty}^{\infty} P_{r_w}\delta p_w dw}_{\text{vertical velocity}} + \underbrace{\int_{-\infty}^{\infty} \delta p_w \delta P_{r_w} dw}_{\text{co-variation}} \quad (4.7)$$

where p_w is the probability distribution of w_{500} from the medium resolution model, P_{r_w} the precipitation for each w_{500} bin from the medium resolution model, and δ indicates the difference between the high and medium resolution model (T799-T159) for the accompanying term. The integration takes place over the whole range of vertical motions.

4.3 Comparison T159 and T799

4.3.1 Precipitation difference medium- and high resolution runs

The monthly averaged daily precipitation for our study area is shown in figure 4.3a for the two model ensembles, as well as ERA-Interim and E-OBS. We quantify the robustness of our results by bootstrapping [*Efron and Tibshirani*, 1993, bias-corrected accelerated (BC_a) method] the 30 years of data, assuming all years are independent. The error band in the figure represents the 95% confidence interval. The months May – October show in general better agreement between both the ensembles and ERA-Interim. During most of the winter months the average monthly precipitation in the ensembles deviates significantly from the quasi-observed reanalysis amounts. Although both model ensembles significantly overestimate the amount of winter precipitation compared to ERA-Interim, the bias in the high resolution model is much smaller. The difference in November – April (NDJFMA) winter precipitation between the medium and high resolution model is approximately 20%. E-OBS observed precipitation data agrees well with the quasi-observed ERA-Interim data, confirming the overestimation of the modeled precipitation. Similar results were obtained for daily extreme precipitation (figure 4.3b, 2 year return value estimated by fitting a generalized extreme value (GEV) distribution), although the signal is much more noisy.

4.3.2 P-E and moisture convergence

In order to explore the physical processes that can cause these differences we consider the average NDJFMA winter precipitation and evaporation in Europe in figure 4.4. The amount of winter precipitation is less in the high resolution model in much of northern Europe (exceptions are areas with orographic precipitation), with differences as large as 0.5 mm/day found in France, Netherlands, Belgium, Luxembourg, Germany, Czech and Poland (roughly equal to our smaller study area). Larger amounts of winter precipitation in the higher resolution model is found in in southern Europe, where also differences as large as 0.5 mm/day are found for much of Portugal, Spain and Italy. Areas with orographic precipitation have

(a) Average daily precipitation in the study area.

(b) 2 year return value maximum daily precipitation in the study area.
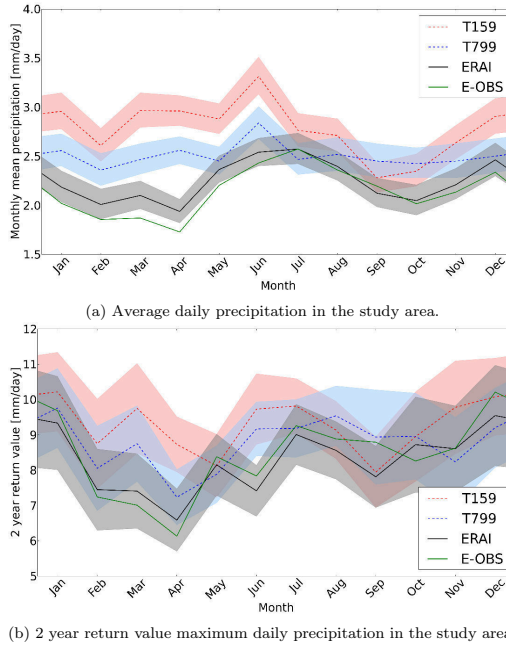
FIGURE 4.3: Average precipitation in the study area (a) and 2 year return value of maximum daily precipitation in the study area (b).

in general more precipitation (> 1 mm/day) in the high resolution model.

Over land we find only small differences in average NDJFMA evaporation between the two model resolutions. The most noteworthy difference is found in our study area, with less evaporation (0.2 mm/day) in the high resolution model. This could be related to the decrease in precipitation in the same area as described in the previous paragraph. In most of continental Europe, the difference in precipitation (figure 4.4c) is larger than the difference in evaporation between the two model resolutions (figure 4.4f).

In order to include the effect of circulation in our analysis of the differences we study the moisture convergence (see section 4.2.3.1). Calculations of the right hand side of equation 4.5 resulted in very noisy patterns, likely related to numerical issues and the limited number of vertical model output levels available. Alternatively, this term may also be computed as a line integral around a boundary using Gauss's theorem [e.g. *Zahn and Allan*, 2011]. Moisture convergence found from applying Gauss's theorem to our study area is
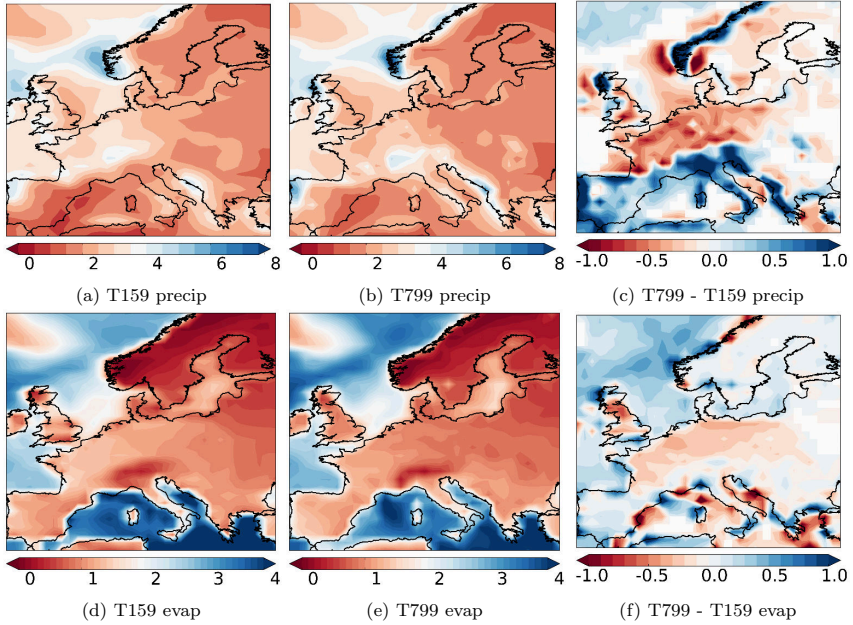
FIGURE 4.4: Average NDJFMA precipitation (a–b) and evaporation (d–e) for the medium- and high resolution model and the differences between the model resolutions (c,f) [mm day^{-1}]. Differences with p>0.05 (estimated with a two-sided *t*-test) have been masked.

given in figure 4.5b. The left hand side of the equation 4.5 is given by figure 4.5a. Both methods agree qualitatively that higher resolution model has less moisture convergence in the winter months for our smaller study area.

Figure 4.6 considers the moisture convergence as estimated from the left hand side of equation 4.5 for the larger European area. Panel 4.6c shows lower moisture convergence in much of the northern half of Europe in the high resolution model compared to the medium resolution model. Exceptions are areas with high orography in Scotland and Norway, where the high resolution model has higher and steeper mountains. In the southern half of Europe there is an increase in moisture convergence, between the medium to the high resolution model. Comparing figure 4.6c with the difference in average precipitation (figure 4.4c) and evaporation (figure 4.4f) in the two model resolutions in figure 4.4, we conclude that, over land,

(a) P–E
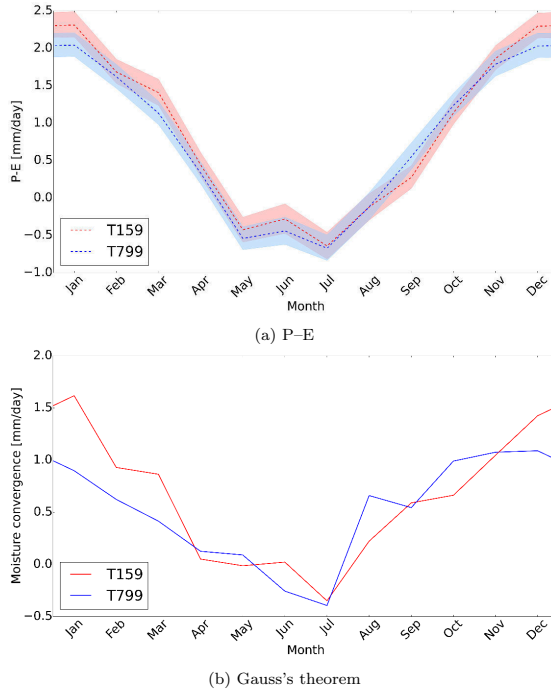
(b) Gauss's theorem

FIGURE 4.5: Moisture convergence for our study area [mm day^{-1}] computed using P–E (a) and Gauss's theorem (b).

precipitation is the dominant term in the left hand side of equation 4.5. Therefore, the results suggest that the difference in precipitation over Europe between the two models, that is, the dipole in figure 4.4c, is at least partly related to the convergence and advection of moisture. A comparison of the moisture convergence of the two models with ERA-Interim (figure 4.6a–b), shows a more accurate representation of moisture convergence in most of the central and northern part of continental Europe in the high resolution model. There is no clear improvement in the southern part of Europe, in fact, in highland areas the agreement with ERA-Interim is in general worse for the high resolution model. In other areas the magnitude of the bias is roughly the same, although the sign changes in some areas. The worse agreement in highland areas is likely related to the orography in ERA-Interim, which is more comparable with the orography in the medium resolution model than it is with the orography in the high resolution model. Figure 4.7 indeed shows that the precipitation bias in these areas is not larger

in the high resolution model when compared to actual observations (E-OBS).
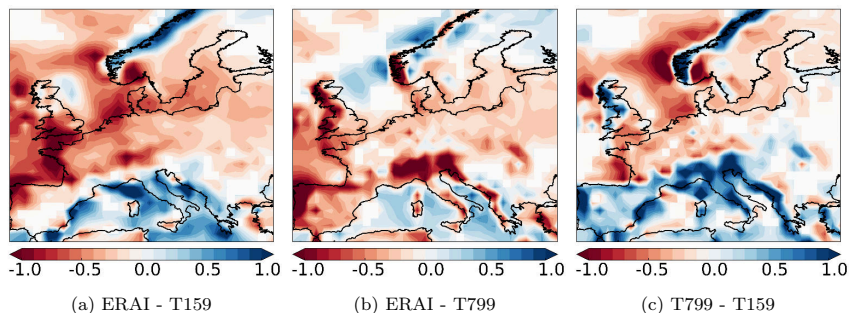
FIGURE 4.6: Difference average NDJFMA moisture convergence [mm day^{-1}]. Differences with p>0.05 (estimated with a two-sided t-test) have been masked.
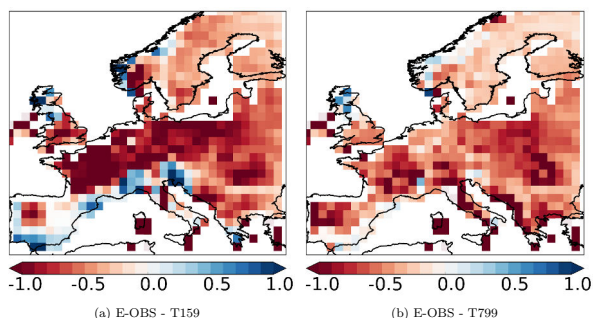
FIGURE 4.7: Average NDJFMA precipitation difference with E-OBS [mm day^{-1}]. Differences with p>0.05 (estimated with a two-sided t-test) have been masked.

4.4 Circulation

4.4.1 Moisture transport

In order to better understand the difference in moisture convergence between the medium- and high resolution model, we consider the individual quantities from the moisture convergence definition in figure 4.8: specific humidity in the left column, wind speed in the middle, and integrated water vapor transport (IVT, see section 4.2.3.2) at the right hand side of the figure.
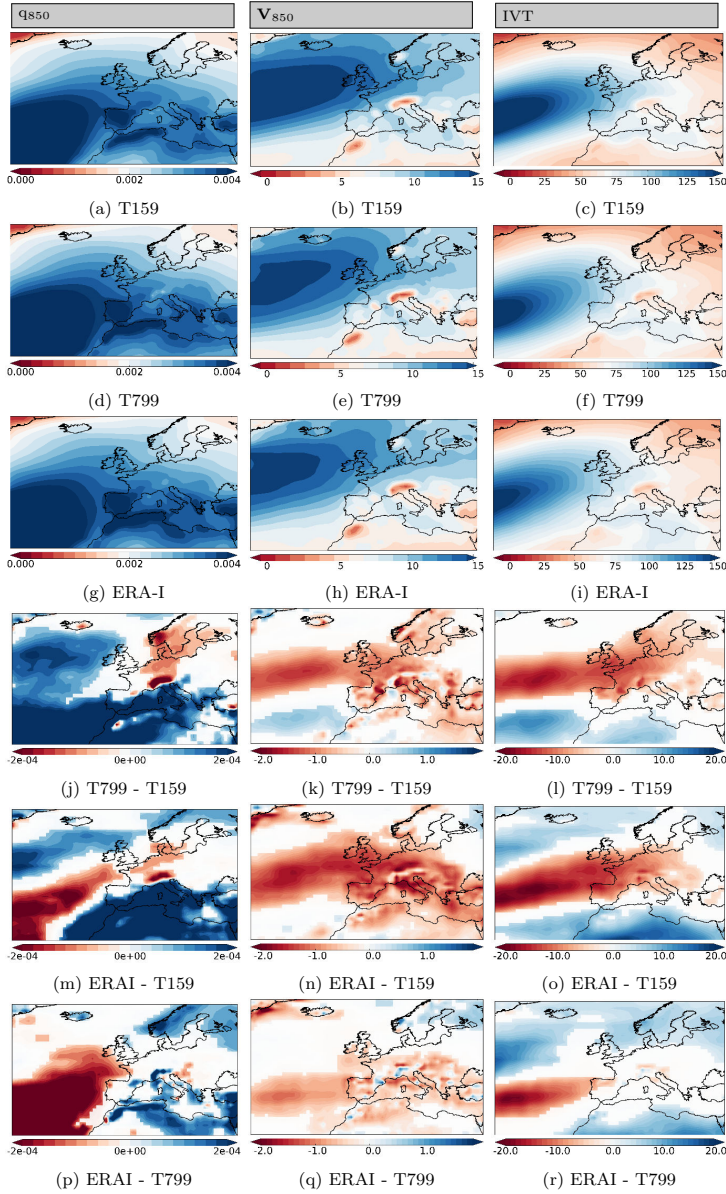
FIGURE 4.8: Left column: specific humidity at 850hPa [kg kg^{-1}]. Middle column: wind speed at 850hPa [m s^{-1}]. Right column: integrated water vapor transport [kg m^{-1} s^{-1}]. Differences with p>0.05 (estimated with a two-sided t-test) have been masked.

Specific humidity at 850 hPa is in the high resolution model on average lower in the northern half of continental Europe and higher in the southern half of continental Europe, compared to the medium resolution model (figure 4.8j). A similar difference pattern is found at 700 hPa, but, as moisture decreases with height, with somewhat lower values (not shown). Upon closer inspection of the vertical profile of the atmospheric moisture content in the models, we find that the difference in atmospheric moisture content between the high and medium resolution model in our study area is in the order of 5% (not shown), about 4 times smaller than the difference in average precipitation. This suggest that circulation differences play a large role.

The middle column of figure 4.8 shows that the average wind speed of the low level flow is too large in the medium resolution model compared to reanalysis data. The high resolution model is much closer to the reanalysis data. The combined effect of specific humidity and wind speed is less transport of moisture (IVT, right column figure 4.8) from the ocean to the western part of Europe at higher resolution. Figure 4.6 suggests that the extra moisture transported into our study area in the medium resolution model (partly) converges and rains out, thereby increasing precipitation. This is confirmed by considering only the zonal component of the moisture transport.

4.4.2   Storm track

The results shown in figure 4.8 suggest that the main differences are found over the Atlantic. This is the storm track region where extratropical cyclones form [*Blackmon*, 1976]. These storm track regions are associated with increased precipitation and winds and are subject to extreme weather events [e.g. *Graff and LaCasce*, 2012]. The weather in Europe is heavily influenced by the storm track over the North Atlantic: *Hawcroft et al.* [2012] estimate that over 70% of total winter precipitation in large parts of Europe is associated with the passage of an extratropical cyclone, and *Pfahl and Wernli* [2012] found a high percentage of precipitation extremes within the storm track region to be directly related to cyclones.

We calculate the storm track as the seasonal variance of 2-8 days bandpass filtered geopotential height at 500 hPa (Z500) [*Blackmon*, 1976], which is shown in figure 4.9. Note that the storm track definition does not discriminate between cyclones, anticyclones and

variability not related to geopotential minima. The storm track in the medium resolution model appears to be too zonal, which is a common problem in coarse resolution GCMs [*Chang et al.*, 2012; *Zappa et al.*, 2013]. The location of the storm track in the high resolution model is more realistic: fewer and/or less intense storms pass over central Europe. For our study area, the mean area averaged absolute bias of the storm track as shown in figure 4.9 improves with respect to ERA-Interim from 12.3 m^4s^{-4} in the medium resolution model (figure 4.9e) to 9.8 m^4s^{-4} in the high resolution model (figure 4.9f). In areas north and south of our study area in general larger improvements are found for the high resolution model.

(a) T159   (b) T799   (c) ERAI

(d) T799 - T159   (e) ERAI - T159   (f) ERAI - T799
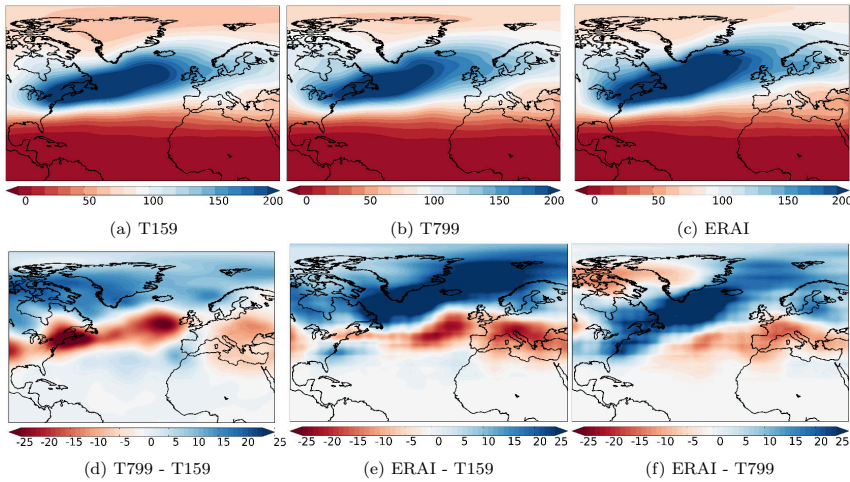
FIGURE 4.9: Storm track calculated as the variance of 2-8 days bandpass filtered Z500 [m^4s^{-4}].

The better representation of the storm track seems to be in agreement with *Zappa et al.* [2013]; *Colle et al.* [2013], who found that the performance of GCMs in representing North Atlantic cyclones was strongly dependent on model resolution: CMIP5 models performed better than CMIP3 models and higher resolution CMIP5 models performed better than lower resolution CMIP5 models. They found that higher resolution models had a more realistic representation of the North Atlantic storm track in terms of location, track density and intensity. The resolution used here for our high resolution model is not found in CMIP5. In fact, our medium resolution model is included in CMIP5 and is one of the highest

resolution models. *Colle et al.* [2013] showed that our medium resolution model was the best performing CMIP5 model in simulating western Atlantic extratropical cyclones in both track density and intensity, and *Zappa et al.* [2013] ranks it among the best performing CMIP5 models in simulating the storm track position, tilt, their number and their intensity. Figure 4.9 shows that increasing the resolution even further still improves the modeled storm track.

4.5   Precipitation decomposition

The results of the previous sections suggest that the high resolution model provides more accurate horizontal moisture transport and moisture convergence, caused partly by a lower humidity but mainly by a more realistic representation of the North Atlantic storm track. To look in more detail to the area-averaged precipitation in our study area, we consider the precipitation distribution in both models as well as ERA-Interim in figure 4.10. We find that both models underestimate the number of 'dry' days [0–1 mm]: 12% for the medium resolution model, 5% for the high resolution model. Both models overestimate the frequency of area averaged precipitation across the range of intensities larger than 2 mm/day. Similar to the frequency of 'dry' days, the bias with respect to ERA-Interim is smaller for the high resolution model.
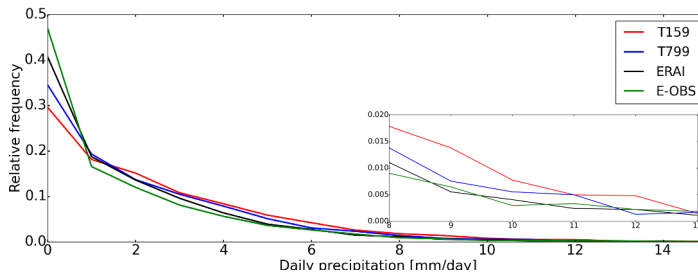
FIGURE 4.10: Probability distribution of daily NDJFMA precipitation averaged over the study area.

To understand these differences we consider the change in the strength and/or frequency of dynamic disturbances, and the associated change in precipitation, averaged over the study area, in figure 4.11. Similar to *Emori and Brown* [2005] we use daily mean 500 hPa

vertical velocity (w_{500}) as a proxy of the strength of dynamic disturbance. The change in distribution of w_{500} between the medium and high resolution model is shown on the left hand side of figure 4.11. Note that positive values of w_{500} represent upward motion here, unlike the usual definition of pressure velocity (ω_{500} scaled by -1). The figure shows an increase in extremes of w_{500} (both positive and negative), and a decrease of days with moderate vertical velocities when increasing the resolution from T159 to T799. The widening of the distribution is a general effect of the increase in horizontal resolution in the model and is also found in other areas of Europe (not shown).
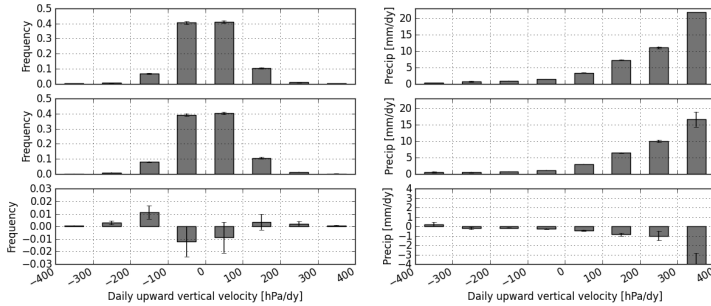
FIGURE 4.11: Probability distribution of w_{500} (left) and precipitation per w_{500} bin (right) averaged over the study area. Top: T159; Middle: T799; Bottom: T799-T159. The error bars are standard errors. On the left hand side of the figure these are represented by the standard error of Poisson counting ($\sqrt{n}/k$), the error bars on the right hands side are calculated assuming a normal distribution within each bin ($\sigma/\sqrt{n}$) (n:number of elements in a bin; k:total number of elements).

The increase in frequency of days with subsidence in the high resolution model is in agreement with the increase in number of dry days as was shown in figure 4.10. An increase in days with extreme precipitation associated with the increase in strong positive upward motion of the atmosphere is however not found. The latter is related to a decrease in precipitation in the high resolution model for the same upward motion (lower right panel of figure 4.11). Reduced horizontal moisture transport likely reduces the amount of available moisture to precipitate.

In order to confirm this, we decompose the precipitation difference between the two models using the ascending motion of the atmosphere into three different parts: a vertical velocity component, a non-vertical velocity component, and a co-variation term (see section 4.2.3.3). The distributions of the individual quantities are shown in figure 4.11 for the study area.

Figure 4.12 shows the spatial distribution of the three components in the precipitation decomposition. The non-vertical velocity component is responsible for much of the lower precipitation in the high resolution model in central and northern Europe, indicating that it is caused by less moisture available to precipitate . The decrease in precipitation in these areas is in agreement with reduced moisture transport over this area in the high resolution model (figure 4.8l).

The vertical velocity component is mainly positive along areas with high orography. Orography is much more pronounced in the high resolution model, resulting in increased precipitation and a change in w_{500} distribution. Increased storm track activity in the high resolution model (figure 4.9d) could also be a factor in the positive vertical velocity component in southern Spain and Scandinavia, where the difference in moisture transport between the two model resolutions is relatively small (figure 4.8l). The covariation term is small everywhere, i.e. there is low correlation between the change in precipitation due to changes in vertical velocity distribution and the change in precipitation unrelated to changes in vertical velocity distribution.

4.6 Conclusions

In this study we investigated if there is a significant statistical difference in modeled precipitation between a medium resolution and a high resolution state-of-the-art AGCM model, and if either of the model resolutions gives a better representation of precipitation in the actual climate system. The same AGCM was used for both model resolutions.

We found that the high resolution model gives a more accurate representation of northern and central European winter precipitation than the medium resolution model, both in the mean-state and in the extremes. The medium resolution model has a larger positive bias in precipitation in most of the northern half of Europe.

(a) total

(b) vertical velocity

(c) non-vertical velocity

(d) covariation
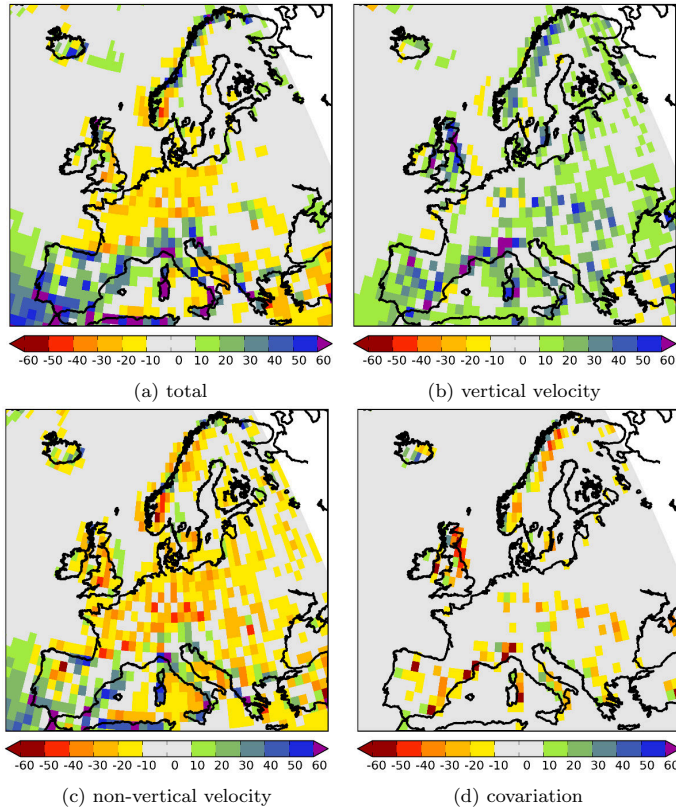
FIGURE 4.12: Decomposition of precipitation difference between the medium- and high-resolution model according to the method by [*Bony et al.*, 2004] [%]. Negative values indicate less precipitation in the high-resolution model.

In the southern half of Europe the magnitude of the precipitation bias is approximately the same, but the sign of the bias changes at some locations. We found a large difference in moisture transport and moisture convergence between the two model resolutions. In agreement with recent studies using multi-model ensembles we found that the performance of the model in representing the North Atlantic storm track was strongly dependent on model resolution: the high resolution model gives a more realistic representation.

A closer inspection of precipitation in the coastal region of mid-Europe reveals a higher frequency of dry days in the high resolution model, closer to the observed frequency. We found that this is related to a thickening of the tail in the downward motion regime

(subsidence) of the w_{500} distribution in the high resolution model. A thickening of the tail in the upward motion regime is not found to increase precipitation extremes. The latter is related to a decrease in precipitation for the same upward motion in the high resolution model.

Using a decomposition of the precipitation difference between the medium- and high resolution model in a part related (vertical velocity component) and unrelated (non-vertical velocity component) to a difference in the distribution of w_{500}, we found that the non-vertical velocity component is responsible for much of the smaller precipitation bias in central and northern Europe. The decease in precipitation in these areas is in agreement with reduced moisture transport over this area in the high resolution model. The difference in w_{500} distribution is only a minor factor in the difference in total precipitation over large parts of central and northern Europe. We found that the vertical velocity component is much more important along areas with high orography. Orography is much more profound in the high resolution model, resulting in increased precipitation and a change in w_{500} distribution.

These results are relevant for climate studies that assess present and future precipitation changes. In order to get climate information on the fine spatial scale that is required by decision makers, statistical downscaling or dynamical downscaling is often applied. Dynamical downscaling is done by embedding a high resolution regional climate model within a coarse resolution global model, allowing for a better representation of orographic and coastal effects, as well as more resolved model physics. Regional climate models however, are often largely dependent on the storm tracks in the driving GCM because of their relatively small spatial domain. Our findings show, assuming that sufficient temporal and vertical resolution data is saved to do a detailed moisture budget analysis, that our high resolution AGCM has a better representation of the North Atlantic storm track and therefore precipitation. This may be valid for other GCMs as well, showing the necessity to analyze other GCMs that may become available in the future with such high horizontal resolutions.

Acknowledgment

Circulation dependent future central European
summer drying[1]

Chapter Abstract

Climate model based projections suggest a drying of the central
European summer climate towards the end of the century. In this
study we investigate the influence of the spatial resolution of an
atmosphere-only climate model (EC-Earth) on the simulated sum-
mer drying in this area. High resolution models have a more real-
istic representation of circulation in the current climate and could
provide more confidence on future projections of circulation forced
drying.

We find that the high resolution model is characterized by a
stronger drying in spring and summer, mainly forced by circulation
changes. The initial spring drying intensifies the summer drying by
a positive soil moisture feedback.

The results are confirmed by finding analogs of the difference be-
tween the high and medium-resolution model circulation in the nat-
ural variability in another ensemble of climate model simulations.
In the current climate, these show the same precipitation difference
pattern resulting from the summer circulation difference. In the

---

[1]This chapter is a slightly modified version of: van Haren, R., R. Haarsma,
H. de Vries, G.J. van Oldenborgh, and W. Hazeleger, Circulation dependent
future central European summer drying, under review, 2014.

future climate the spring circulation also plays a key role. We conclude that the reduction of circulation biases due to increased resolution gives higher confidence in the strong drying trend projected for central Europe by the high-resolution version of the model.

5.1 Introduction

Summers are projected to become drier in central Europe due to anthropogenically forced climate change [*Polade et al.*, 2014]. This is accompanied by an enhanced increase in air temperatures [*Zampieri et al.*, 2009].

The mechanisms involved in future precipitation change can be divided in thermodynamic and dynamic mechanisms [*Polade et al.*, 2014]. Thermodynamic mechanisms include the consequences of the increase in atmospheric water vapor concentration and transport in a warmer climate. Dynamic mechanisms are related to changes in the atmospheric circulation: the descending Hadley cell branch and subtropical dry zones expand poleward and midlatitude westerlies adjust to a reduced equator-to-pole temperature gradient [*Polade et al.*, 2014] and other changes [e.g., *Bladé et al.*, 2012]. If a model is biased in its circulation characteristics, this has an impact on the quality of other simulated variables such as temperature and precipitation, not only in the mean state but also in the changes due to the radiative forcing [*van Ulden et al.*, 2007].

General circulation models (GCMs) often do not have the spatial resolution required to have an accurate representation of synoptic systems affecting precipitation [e.g., *van Haren et al.*, 2013a, b]. Different studies have shown that aspects of the simulated circulation improve with increasing spatial resolution [e.g. *Demory et al.*, 2013; *Hack et al.*, 2006; *Berckmans et al.*, 2013; *Zappa et al.*, 2013; *Colle et al.*, 2013; *Jung et al.*, 2012; *Champion et al.*, 2011; *Willison et al.*, 2013; *van Haren et al.*, 2014]. The need for improved circulation statistics for regional downscaling over Europe was emphasized by *van Haren et al.* [2013a, b]. Because of their small spatial domain, regional climate models strongly depend on the synoptic systems provided by the driving GCM: they can refine their features but not change the large-scale circulation.

Numerous studies have studied the simulated future European summer climate in climate models. Most of these studies focus on local feedbacks [e.g. *Seneviratne et al.*, 2013; *Teuling et al.*, 2013;

Mueller and Seneviratne, 2014; *Vidale et al.*, 2007; *Zampieri et al.*, 2009; *Haarsma et al.*, 2009], but some studies have shown that large scale circulation is also a relevant driver [e.g., *Rowell and Jones*, 2006; *Bladé et al.*, 2012]. In this study we investigate the influence of GCM spatial resolution on simulations of future central European summer drying, checking the hypothesis that increased resolution leads to a more realistic circulation and hence circulation-induced changes in precipitation. We then use analogs to determine to what extent the circulation changes affect the projected drying trend. If they are indeed a major factor and the high-resolution model is more realistic, this would increase our confidence in projections of summer drying in central Europe.

5.2 Data & study area

5.2.1 Data

The model used in this study is EC-Earth version 2.3 [*Hazeleger et al.*, 2012]. The atmospheric component of the model is derived from the weather forecast model (IFS cycle 31r1) of the European Centre for Medium-Range Weather Forecasts (ECMWF). The experiment consists of two 6-member ensembles of 5-year simulations members for both the current period (2002–2006) and the future period [2094–2098, RCP4.5 scenario, *Moss et al.*, 2010]. We used the data from the experiments done by *Haarsma et al.* [2013b]. The ensembles differ both in horizontal and vertical resolution. The high resolution model is at a T799L91 resolution (∼25 km horizontal resolution, 91 vertical levels), the medium resolution model is at a T159L62 resolution (∼112 km horizontal resolution, 62 vertical levels). Sea surface temperatures (SSTs) and sea-ice are prescribed for both the current and future period. For the current period these are from the Optimum Interpolation (OI) SST analysis [*Reynolds et al.*, 2002]. For the future period SSTs are computed by adding the ensemble mean SST change as simulated by the ECHAM5/MPI-OM model used in the ESSENCE project [*Sterl et al.*, 2008]. Future sea-ice coverage was computed by using a linear regression using the present SST and sea-ice cover fields [*Haarsma et al.*, 2013b].

For additional analysis to interpret the results we used data from an 8-member ensemble of coupled EC-Earth simulations in the RCP8.5 scenario. The coupled model is at a T159L62 resolution.

(a) Spring   (b) Summer
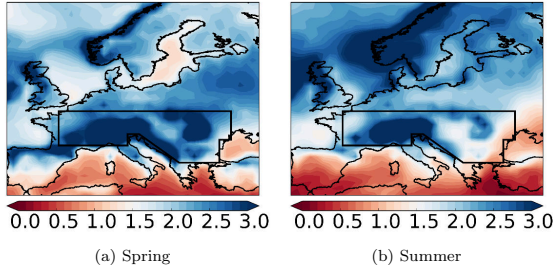
FIGURE 5.1: Mean precipitation in the current climate in the high resolution model (T799) for (a) late spring (April–June), and (b) late summer (July–September). The study area is outlined in black.

We used the period 1982–2011 to represent the current period, and 2070–2099 to represent the future period.

Precipitation is verified against ERA-Interim [*Dee et al.*, 2011], a global atmospheric reanalysis produced by the ECMWF, extending back to 1979. ERA-Interim has a T255L60 resolution (∼80 km horizontal resolution, 60 vertical levels). An additional evaluation of the simulated precipitation is performed using the precipitation fields of the European ENSEMBLES project version 9.0 [*Haylock et al.*, 2008, E-OBS, 0.5º horizontal resolution]. The dataset is based on meteorological station measurements and is designed to provide the best estimate of grid box averages to enable direct comparison with climate models. For both reanalysis and observations we used 1982–2011 to represent the current period.

All data was first regridded to the T159 grid of the medium resolution ensemble by means of second order conservative remapping [*Jones et al.*, 1999].

5.2.2 Study area

We focus in this study on the climate change signal in central European summer precipitation between the beginning and the end of the 21st century (figure 5.1). This area is wet in the current climate but is projected to show strong drying under climate change. Because preconditioning plays an important role we investigate both the season with most pronounced drying, late summer (July–September) and the preceding three months, late spring (April–June). For simplicity we refer to those periods as summer and spring.

5.3   Analysis and results

5.3.1   Mean climate and climate change signal in the study area

The seasonal cycle of modeled and observed precipitation averaged over the study area are shown in figure 5.2a for the current climate. In general, the model has a similar representation of the annual cycle at both resolutions, but significant differences occur for individual months. Considering the spring and summer seasons, the high resolution model simulates significantly less precipitation in May, and significantly more precipitation in August. Compared to ERA-Interim and E-OBS there is a very significant overestimation (∼20%) of average precipitation throughout most of the year, with the exception of late summer, July–September.

Panels 5.2b–d show the climate change signal for both the medium and high resolution model for precipitation, surface sensible heat flux and evaporation. Compared to the medium resolution model, the high resolution model simulates a slightly larger reduction of precipitation in spring (April–June, significant in the months April and June). In addition, the model simulates a much larger significant increase in evaporation in this period, resulting in drier soils at the beginning of summer. The much larger precipitation decrease in the high resolution model in summer (July–September, ~ -0.8 mm/day for the high resolution model versus ~ -0.5 mm/day for the medium resolution model) is accompanied by a decrease in evaporation and an increase in surface sensible heat flux, indicating drier soils. The high sensible heat flux produces a deeper, warmer and drier atmospheric boundary layer that tends to inhibit cloud formation. This positive land-atmosphere feedback intensifies the drying [e.g., *Alexander*, 2011; *Seneviratne et al.*, 2013; *Teuling et al.*, 2013; *Mueller and Seneviratne*, 2014].

Although the area-averaged precipitation in the current climate is similar in the high and medium resolution model (figure 5.2a), the models do differ in their circulation. The high resolution model has a more accurate representation of the atmospheric circulation in the current climate compared to ERA-Interim (figure 5.2e–h). The more accurate baseline provides more confidence in the simulated circulation response at this model resolution.

In order to better understand the larger drying due to anthropogenically forced climate change in the central European region in

(a) Precipitation [mm/day]

(b) Precipitation change [mm/day]

(c) Surface sensible heat flux change [kW m^{-2} s]

(d) Evaporation change [mm/day]

(e) Z500 bias AMJ
T159 − ERAI [m^{2}s^{-2}]

(f) Z500 bias AMJ
T799 − ERAI [m^{2}s^{-2}]

(g) Z500 bias JAS
T159 − ERAI [m^{2}s^{-2}]

(h) Z500 bias JAS
T799 − ERAI [m^{2}s^{-2}]
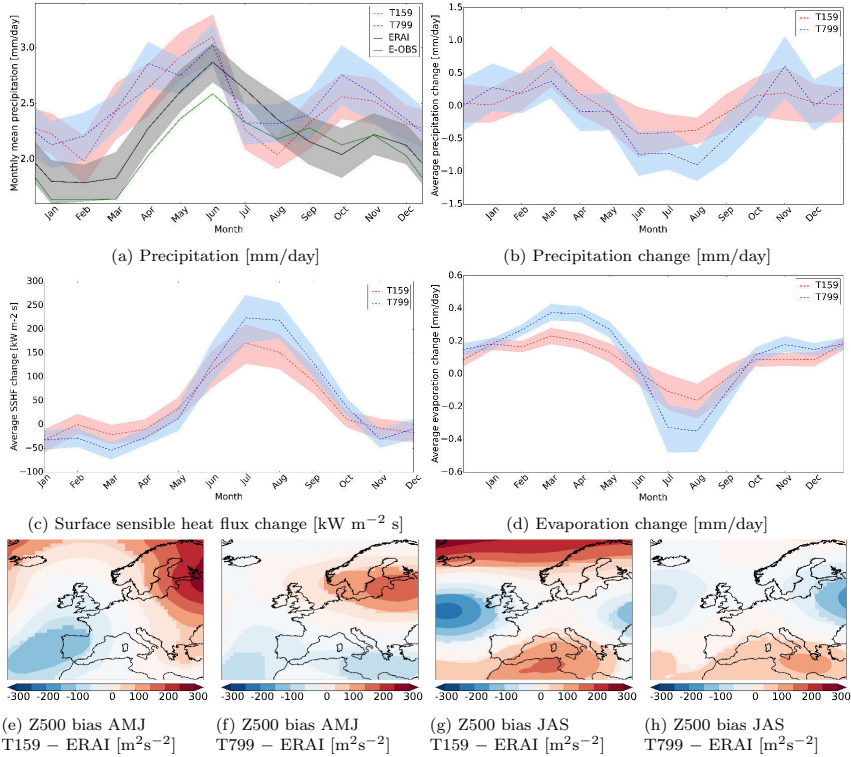
FIGURE 5.2: Annual cycle of precipitation averaged over the
study area (a). Climate change signals (difference between 2070–
2099 and 1982–2011) of precipitation (b), surface sensible heat
flux (c), and evaporation (d). Confidence intervals (90%) are
computed by bootstrapping [*Efron and Tibshirani*, 1993, bias-
corrected accelerated (BC$_a$) method] the 30 years of data, assum-
ing all years are independent. (e–h) Difference in geopotential
at 500 hPa (Z500) in the present climate between the EC-Earth
simulations and ERA-interim. Differences with p>0.1 (estimated
with a two-sided *t*-test) have been made lighter.

the high resolution model, we consider the differences in the climate change signal, for both spring and summer, in more detail in the next sections.

5.3.2 Dynamical driving mechanisms in spring

Figure 5.3 shows the climate change signal Δ_{high} for the high resolution model (figure 5.3a–e), as well as the difference in climate change signal between the high and medium resolution versions of the model $\Delta\Delta = \Delta_{\text{high}} - \Delta_{\text{medium}}$ for precipitation and related variables for the European region (panels 5.3f–j). The climate change signal in the geopotential at 500 hPa (Z500) is dominated by an increase over the Mediterranean area with an extension towards the British Isles, with the sea-level pressure (SLP) mainly showing the latter (figure 5.3b). The northern extension is absent in the medium-resolution model (figure 5.3g). It causes drying over the British Isles and central Europe north of the Alps due to increasing subsidence, decreasing convection and increasing surface solar radiation (figure 5.3e,j). This in turn results in an increase in evaporation and specific humidity (figure 5.3c–d,h–i).

(a) ΔPrecipitation (b) ΔZ500, ΔSLP (c) ΔEvaporation (d) ΔSpec. humidity (e) ΔSolar radiation

(f) $\Delta\Delta$Precipitation (g) $\Delta\Delta$Z500, $\Delta\Delta$SLP (h) $\Delta\Delta$Evaporation (i) $\Delta\Delta$Spec. humidity (j) $\Delta\Delta$Solar radiation
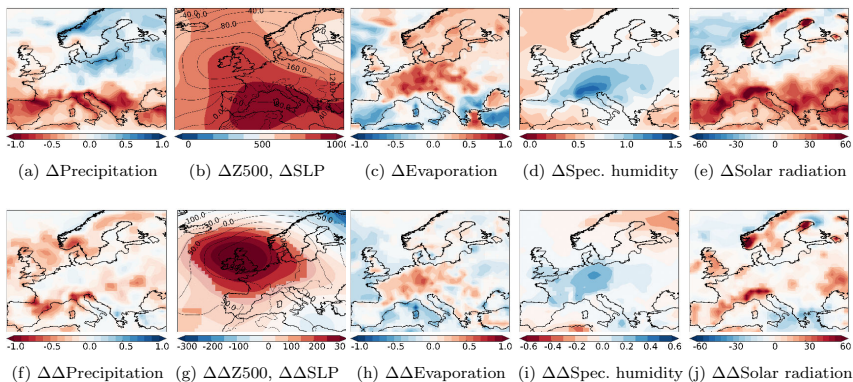
FIGURE 5.3: Top row: spring (April–June) climate change signal in the high resolution model for (a) precipitation [mm/day]; (b) geopotential at 500 hPa (shading, [m^2s^{-2}]) and mean sea level pressure (contour, [Pa]); (c) evaporation [mm/day]; (d) specific humidity [g/kg]; (e) net surface solar radiation [W m^{-2}]. Bottom row: (f–j) same but for the difference in climate change signal between the high and low resolution model $\Delta_{\text{high}} - \Delta_{\text{medium}}$. Differences with p>0.1 (estimated with a two-sided t-test) have been made lighter.

However, this does not explain the differences in precipitation in the southern part of our study area. The main change there is a larger decrease in precipitation in the high-resolution model on the south side of mountain ranges (figure 5.3f). This is due to a change in flow across these mountains, associated with the higher pressure over the British Isles, and higher mountains in the high-resolution version of the model. To estimate the relative contributions of these terms we computed the dependence of the precipitation P on the components ($\mathbf{G}$) of the geostrophic wind ($u = -(1/f_c\rho)d\,\mathrm{SLP}/dy$, $v = -(1/f_c\rho)d\,\mathrm{SLP}/dx$ and vorticity (ω)). The average dependence $dP/d\mathbf{G}$ times the difference in geostrophic wind change, $\Delta\Delta\mathbf{G}$ shows how much of the difference in precipitation change is due to the different circulation patterns between the high and medium resolution versions of the model. Conversely, the difference $\Delta dP/d\mathbf{G}$ times the average change in mean flow $\Delta\mathbf{G}$ shows the effect of the different orography. Both terms turn out to contribute about equally to the lower precipitation on the south side of the mountains (not shown).

The increased pressure over the British Isles and the higher mountains therefore cause less rain and more solar radiation and hence increased evaporation in central Europe in the high-resolution model, resulting in drier soils at the start of summer.

5.3.3   Climate change signal in July–September

The climate change signal for the high resolution model, as well as the difference in summer climate change signal between the high and medium resolution model, are shown in figure 5.4. Panel a shows the strong summer drying signal in central Europe. This is accompanied with a developing heat low over the Mediterranean [*Haarsma et al.*, 2009] and a pressure dipole between the British Isles and Greenland, the positive phase of the summer NAO [*Bladé et al.*, 2012]. Evaporation is projected to become lower in the future over the land areas of central and southern Europe due to drier soils and the increased pressure and lower relative humidity cause a large increase in solar radiation at the surface.

The high resolution model shows a much larger decrease in precipitation in central and southern Europe (figure 5.4a,f). The difference in climate change signal in geopotential at 500 hPa and mean sea level pressure is a high pressure area over central and southern Europe and a low pressure area over northern Europe (figure 5.4b,g).

(a) ΔPrecipitation (b) ΔZ500, ΔSLP (c) ΔEvaporation (d) ΔSpec. humidity (e) ΔSolar radiation

(f) ΔΔPrecipitation (g) ΔΔZ500, ΔΔSLP (h) ΔΔEvaporation (i) ΔΔSpec. humidity (j) ΔΔSolar radiation
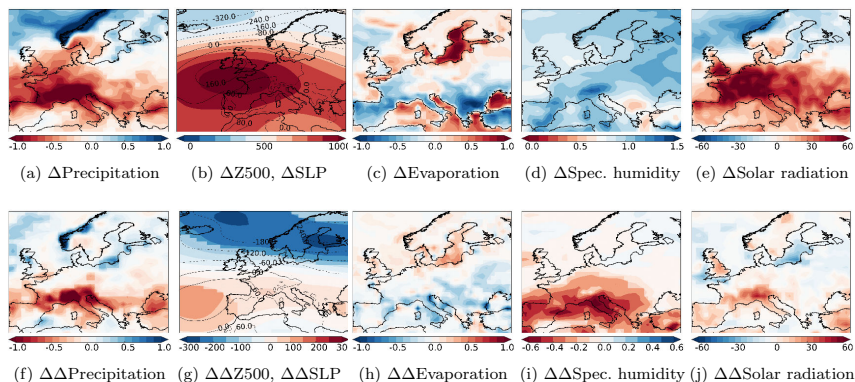
FIGURE 5.4: Climate change (2100–now) signal summer (July–September) for the high resolution model for (a) precipitation [mm/day]; (b) geopotential at 500 hPa (shading, $[m^2s^{-2}]$) and mean sea level pressure (contour, [Pa]); (c) evaporation [mm/day]; (d) specific humidity [g/kg]; (e) surface solar radiation [W m^{-2}]. (f–j) same but for the difference in climate change signal between the high and low resolution model $\Delta T799 - \Delta T159$. Differences with p>0.1 (estimated with a two-sided t-test) have been made lighter.

This results in an increase in zonal vapor transport mainly in the northern half of central Europe and a decrease over the Mediterranean. Furthermore, the areas of high pressure are associated with an increase in subsidence, thereby decreasing convection and increasing surface solar radiation (figure 5.4e,j). Drier soils in the high resolution model limit the rate of evaporation (figure 5.4c,h), thereby reducing specific humidity (figure 5.4d,i) and local recycling of moisture. Sensible heat flux and temperature increase (not shown).

5.3.4 Analogs in natural variability

In the previous sections we argued qualitatively that the circulation difference in the climate change signal between the high and medium resolution model (figures 5.3b and 5.4b) is an important driver for the stronger future summer drying in central and southern Europe in the high resolution model. In order to test this hypothesis, we extract analogs of this pressure difference (at mean sea level) in the natural variability of a coupled model (figure 5.5). We assume that the difference in circulation response also shows up as natural

variability in the coupled model. This enables us to isolate the effect of circulation on precipitation differences. If these are similar to the modeled differences between the two resolutions, the circulation changes are a major driver.
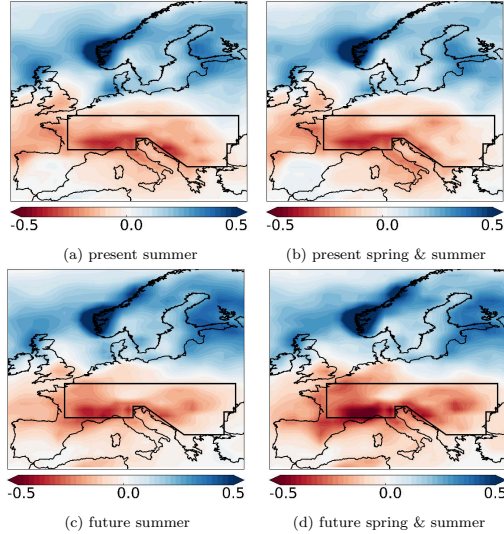
FIGURE 5.5: Analogs in natural variability of the circulation driven climate change signal [mm/day]. (a) Analogs based on MSL pattern summer (fig 5.4g) in the current climate; (b) Analogs based on MSL pattern in summer (fig 5.4g) and spring (fig 5.3g); (c–d) Same but for the future climate.

To replicate the climate change signal, we make random combinations in the available 240 years of model data (e.g. [member 4, year 20] with [member 7, year 2]), both for the current climate and the future climate. For each climate, this results in a total of 57360 possible combinations. Pressure differences are computed for each of these combinations. To find analogs of the difference in pressure climate change signal between the high and model resolution model (contours in figures 5.3g and 5.4g), we compare this pattern to the extracted pressure differences in the coupled model. The best matching patterns are found by minimizing the area-weighted Euclidean distances between the (anomalized) pressure fields.

The effect of the difference in summer circulation change (5.4g) is computed from the closest matching 5000 combinations to this pattern. The additional effect of a drier spring caused by the difference in spring circulation change (5.3g) is computed from the

closest 500 matching combinations to this pattern in the pool of 5000 matching summer patterns.

Compared to the average summer precipitation in the coupled model, the analogs based only on summer circulation result in a decrease in precipitation over central Europe and the Mediterranean area, and an increase north of it (figures 5.5a,b). This precipitation response is in agreement with the difference in precipitation change between the high and medium resolution model (figure 5.4a). The analogs based on both spring and summer circulation (figures 5.5c,d) yield a similar pattern, but is intensified (from -0.16 to -0.22 mm/day) in the future climate (area-averaged difference between figures 5.5c and 5.5d for our study area is significant at p<0.05, estimated with a two-sided *t*-test). The results confirm that circulation differences in the high-resolution model compared to the medium resolution model in both spring and summer are important drivers for the stronger summer drying in central and southern Europe. We note that the improvement in summer circulation could also help seasonal predictions in this area.

5.4   Conclusion

Future drying over mid-latitude continents is often assessed using climate model simulations. Here we investigate the influence of AGCM resolution on the simulated summer drying over the central European region by comparing the results of a medium (T159) and a high resolution version of the same AGCM (T799). The simulated circulation in the current climate in the high resolution model is more realistic, providing more confidence in the simulated circulation change at this model resolution.

We find that the high resolution model simulates a larger drying in spring, resulting in drier soils at the beginning of summer. The larger spring drying in the high resolution model is caused by two factors. The projected circulation change over the European area differs and the mountains in central Europe are resolved better.

The initial drying in spring is intensified in summer by a positive soil moisture feedback and a dipole structure in the pressure difference in climate change pattern between the high and medium resolution model. The dipole structure is one of high pressure over central and southern Europe, and low pressure over northern Europe, causing a decrease of moisture transport over southern Europe

and an increase in subsidence over central and southern Europe, thereby reducing precipitation in this area.

The hypothesis that the circulation difference in the climate change signal between the medium and the high resolution model is an important driver for the difference in projected change in precipitation has been tested by finding analogs in the natural variability of a coupled model. The results confirm that circulation differences in both spring and summer are important drivers for the larger summer drying in central and southern Europe in the high resolution model. Preconditioning in spring yields a stronger drying in summer. These results show that the improvements in the global circulation that are the result of increased resolution have a large influence on the local climate change projections in central Europe. Due to the smaller bias in the current climate we have more confidence in the strong drying trend of the high-resolution version of the model.

CHAPTER **6**

Synthesis

6.1 Overview of the research presented in this thesis

The research presented in this thesis was aimed at understanding the changes and the simulation of precipitation in Europe. In the introduction this was divided in three parts. The division is repeated in this section, after which in the following section the results for each of the parts are discussed. The subjects that were studied are:

- **Evaluation of 20th century European precipitation trends**
  In chapter 2 an evaluation of European summer and winter precipitation trends over the past century was performed. Chapter 3 discussed the performance of climate models in simulating trends in extreme winter precipitation over the Rhine river basin.

- **Effect of GCM spatial resolution on simulated western European winter precipitation in the current climate**
  Chapter 4 investigated the effect of GCM spatial resolution on simulated western European winter precipitation in the current climate.

- **Effect of GCM spatial resolution on simulated future summer drying in central and southern Europe**
  Chapter 5 investigated the influence of GCM spatial resolution on simulations of future central European summer drying.

6.2   Evaluation of 20th century European precipitation trends

6.2.1   Research questions

In chapters 2 and 3 an evaluation of 20th century European precipitation trends was performed. In these chapters the following two research questions were addressed:

Q1 Can the current generation climate models realistically represent observed trends over the past century?

Q2 What are the underlying physical mechanisms responsible for biases in simulated trends?

6.2.2   Results & answers research questions

Clear precipitation trends have been observed in Europe over the past century. In winter, precipitation has increased in north-western Europe ($\sim 10 - 20\%$ over the past century). In summer, there has been an increase along many coasts in the same area ($\sim 5 - 10\%$ over the past century). Over the second half of the past century precipitation also decreased in southern Europe in winter (chapter 2). Since 1950, the trend in winter extreme precipitation shows a similar north-south structure as the trend in mean winter precipitation: increase in the northern half of Europe and a decrease in the southern half of Europe (chapter 3).

Key result 1 An investigation of trends in (extreme) precipitation in multi-model ensembles including both global and regional climate models shows that these models fail to reproduce the observed trends over (parts of) the past century: • Climate models are found to significantly underestimate the observed trend to increased winter precipitation in northern Europe and parts of western Europe; • In addition, climate

models also underestimate the winter drying trends in southern Europe in the second half of the past century; • In summer, climate models were found to underestimate wetting trends along coastal regions of western Europe.

In chapter 2 the precipitation trends over the past century in two large multi-model ensembles, including both global and regional models, were compared to observed trends in precipitation. It was investigated whether the spread of the model ensemble (which includes natural variability and model uncertainty) covers the observed trend.

The results in chapter 2 show that a multi-model GCM ensemble significantly underestimates the trend to increased precipitation over the past century (1901–2009) in northern Europe and parts of western Europe, both in winter and in summer. In these regions, the trend in the observations does not fall within the spread of the multi-model ensemble. As an aggregated statistic a Talagrand diagram or rank histogram was computed over the land area of Europe, confirming that the bias in reproducing wetting trends is significant. The same analysis was repeated for two shorter periods (1951 –2009 and 1960–2000) in the second half of the past century using a multi-model GCM forced RCM (RCM/GCM) ensemble. These time periods are considerably shorter compared to the period used for the GCM evaluation because the RCM/GCM data was only available for the period after 1950. As a result the observed trends, and trend mismatches with a model ensemble, are harder to detect against the background of natural variability. Nevertheless, the RCM/GCM ensemble showed large significant biases in producing wetting trends in northern Europe and drying trends in southern Europe in winter in the second half of the past century. The underestimation of precipitation trends in the RCM/GCM ensemble in summer was found to be mainly limited to coastal regions of western Europe.

In chapter 3 a similar comparison was made, but for the trend in 10-day annual maxima (RX10day) for late winter over the last 60 years. The results found were in agreement with the results found for mean winter precipitation trends, despite the lower signal to noise ratio for the extremes. Climate models fail to reproduce the increase in extremes in much of northern Europe: the model

simulations do not cover the observed trend in large parts of this area.

> **Key result 2** A misrepresentation of large scale atmospheric circulation changes in climate models is responsible for the underestimation of winter precipitation trends in Europe over the past century. In summer a misrepresentation of SST trends is found to be responsible for the underestimation of summer precipitation trends along the coastal regions of western Europe.

One possible reason for the low reliability of the models would be that they underestimate the natural variability of precipitation and therefore uncertainty in the trend. The results in chapter 2 show that natural variability is indeed underestimated in GCMs, but is overestimated in RCM/GCMs. It is therefore unlikely that the underestimation of precipitation trends is largely caused by a misrepresentation of natural variability in the models. Other possible causes for the trend biases are that they are caused by RCM boundary conditions, large scale atmospheric circulation and stratification, and sea surface temperatures (SSTs), or local model errors present in both RCMs and GCMs.

Changes in SST and large scale atmospheric circulation influence regional and local precipitation through convergence, evaporation and transport of moisture. To investigate the influence of these boundary conditions a comparison was made between the results of the RCM/GCM ensemble and the results of a multi-model ERA-40 forced RCM (RCM/ERA40) ensemble with more realistic boundary conditions. The RCM/ERA40 ensemble was found to reproduce the observed precipitation trends much better. The observed trends were found to be largely compatible with the range of uncertainties spanned by the ensemble, indicating that the boundary conditions of RCMs are responsible for large parts of the trend biases.

To investigate the effects of trends in the atmospheric circulation a statistical model that isolates the linear effect of circulation anomalies was adopted from *van Ulden and van Oldenborgh* [2006]; *van Oldenborgh et al.* [2009a]. The underestimation of precipitation trends in GCM forced RCM ensembles in the summer half year is mainly limited to the coastal regions and is, within the linear approximation of a statistical decomposition, largely caused by

SST trend biases in the boundary conditions. The underestimation of precipitation trends in the winter half year that were found in both northern and southern Europe are, under the same assumption of linearity, for a large part caused by circulation trend biases as present in the GCMs.

> **Key result 3** The inability of climate models to correctly simulate observed changes in atmospheric circulation is primarily responsible for the underestimation of trends in winter precipitation extremes in the Rhine basin.

Particular circulation types may be more favorable for extreme precipitation events to occur. To investigate if the change in mean circulation affects the change in precipitation extremes, a slightly adapted version of the statistical model was implemented in chapter 3. The results showed that the underestimation is, within the linear approximation of a statistical decomposition and statistical uncertainties, caused by an underestimation of the change in mean circulation.

6.2.3   Discussion

In this section additional discussion is provided for some of the choices made in the analysis and the results presented.

Trend definition. Precipitation trends were computed using the common definition of a trend in the analysis presented here, linear regression of precipitation against time. Previous studies have shown that the magnitude of regional climate changes increases quasi-linearly with changes in the global mean temperature [*Räisänen*, 2007; *Alexander and Arblaster*, 2009], a definition adopted in e.g. *van Oldenborgh et al.* [2009a]. Although the latter definition may physically be better justified, it did not significantly increase the signal-to-noise ratio, nor did it affect any of the conclusions. The former, more common, approach was therefore adopted in this analysis.

Analysis period. The length of the time period used in different parts of the analysis was restricted by the length of the available data sets. A shorter length of the analysis period makes

it harder to detect trend mismatches between the observations and model ensemble against the background of natural variability. Nevertheless, modeled atmospheric circulation and SST trends over the past century were found to be significantly different from the observed ones, even on shorter time scales. For SST there may be a connection with the well-known ocean circulation biases in low-resolution ocean models, for atmospheric circulation there may be connection with the resolution of the atmospheric component of climate models as well (chapters 4 and 5).

Another possibility is that the trend mismatches are caused by an underestimation of natural variability. Although it was shown that climate models do not underestimate natural variability on short timescales, underestimation of natural variability on multi-decadal or longer timescales could still be possible. Because it is not clear (yet) whether the trend biases in SST and large scale circulation are due to greenhouse warming, their importance for future climate projections need to be determined. Therefore, a quantitative understanding of the causes of these trends is needed so that climate model based projections of future climate can be corrected for these trend biases.

Observations. It is well known that observations are affected by many sources of error. Errors stem from sources of uncertainty in the observational data and their analysis, from measurement, recording and representativity errors to data quality, homogeneity and interpolation errors [*Haylock et al.*, 2008]. *Haylock et al.* [2008] claim that the typical interpolation error is much larger than the expected magnitude of other sources of uncertainty. Considerable trend differences between the observational datasets over Greece, Finland, the former Soviet Union and the Iberian peninsula (both seasons) and France and the Scandinavian peninsula (winter half year) were found, making it difficult to evaluate the model results in some instances. Differences on smaller spatial scales were found in many other areas. For these regions the trend mismatches were only considered significant if the model trend biases were larger than the difference between the different observational datasets.

Models. The multi-model ensembles used in the analysis consist of a limited number of independent models [*Masson and Knutti*, 2011; *Knutti et al.*, 2013]. In the first place because these ensembles are ensembles of opportunity, depending on funding, computational resources and interest of individual research organizations. Additionally, parameterizations, and in case of RCMs also boundary conditions, are shared among different GCMs. As a result these models are not completely independent. Another aspect of the same problem is that the models are not designed to span the full range of behavior or uncertainty that is known to exist [*Tebaldi and Knutti*, 2007]. Therefore, the range spanned by multi-model ensembles is to some extent arbitrary.

An alternative approach consists of exploring modeling uncertainties systematically within a single GCM, referred to as the perturbed physics ensemble (PPE) method [e.g. *Murphy et al.*, 2004; *Stainforth et al.*, 2005; *Collins et al.*, 2006; *Murphy et al.*, 2007]. In the PPE approach a single model structure is used and perturbations are introduced to the physical parameterization schemes in the model [*Collins et al.*, 2006]. This allows to determine which parameters are the main drivers of uncertainty across the ensemble. A disadvantage of this approach is that the estimated uncertainty depends on the underlying model and may be too narrow [*IPCC*, 2013, chapter 9].

A third approach is to study model uncertainty is using stochastic parameterizations. *Palmer* [2001] suggests that some of the remaining errors in weather and climate prediction models may have their origin in the neglect of subgrid-scale variability, and that such variability should be parameterized by non-local dynamically based stochastic parametrization schemes. An ensemble generated by repeating a stochastic forecast gives an indication of the uncertainty in the forecast due to the parametrization process.

Statistical model. RCMs are constrained by lateral boundaries, and it is therefore relatively straightforward to prescribe large scale atmospheric circulation. Also SSTs are commonly prescribed in RCM simulations. This property is used to compare the results of GCM forced RCM ensemble with the results of a similar set of RCMs forced by quasi-observed (reanalysis)

boundary conditions. This allows for a separation between errors in lateral boundary conditions and internal model errors [*Hudson and Jones*, 2002]. Trend biases that exist in both RCM ensembles are ascribed to model errors, whereas trend biases only found in the GCM driven RCM ensemble are ascribed to errors in the boundary conditions. The RCM ensemble forced by reanalysis data was found to have a much more realistic precipitation trend.

A statistical model was used to extract the effect of changes in large scale atmospheric circulation on the trends in precipitation in the reanalysis forced RCM ensemble. The statistical model assumes that this effect is linear. Any non-linear effects circulation changes might have on precipitation is therefore neglected and could bias the results. The remaining part of the trend differences between the two RCM ensembles is, within the linear approximation of a statistical decomposition, caused by changes in other boundary conditions. For summer, large SST trend biases are likely responsible for the underestimation of summer precipitation trends along the coastal region of western Europe. Changes in other boundary conditions, such as stratification or humidity, may also be responsible for setting precipitation trends. Additionally, the effect of circulation trend biases and SST trend biases are likely not independent. To extract the exact individual (independent) contributions of all boundary conditions would require setting up a new experiment, which was beyond the scope of this analysis.

6.3 Effect of GCM spatial resolution on simulated western European winter precipitation in current climate

6.3.1 Research question

In chapter 4 the effect of GCM spatial resolution on simulated western European winter precipitation in current climate was analyzed using an AGCM at two model resolutions. In this chapter the following research question was answered:

Q3 Do climate models have sufficient spatial resolution to accurately represent synoptic systems that are associated with European winter precipitation?

6.3.2 Results & answer research question

> **Key result 4** The high resolution model gives a more accurate representation of northern and central European winter precipitation than the medium resolution model, both in the mean state and in the extremes. The medium resolution model has a larger positive bias in precipitation in most of the northern half of Europe.

In chapter 4 the effect of spatial resolution on modeled precipitation over Europe was investigated using one AGCM at the same two model resolutions as in the previous chapter. The results showed that the high resolution model gives a more accurate representation of northern and central European winter precipitation than the medium resolution model, both in the mean state and in the extremes. The medium resolution model has a larger positive bias in precipitation in most of the northern half of Europe. In the southern half of Europe the magnitude of the precipitation bias is approximately the same, but the sign of the bias changes at some locations

A closer inspection of precipitation in the coastal region of mid-Europe revealed a higher frequency of dry days in the high resolution model, closer to the observed frequency. It was found that this is related to a thickening of the tail in the downward motion regime (subsidence) of the w_{500} distribution in the high resolution model. A thickening of the tail in the upward motion regime was not found to increase precipitation extremes. The latter is caused by a decrease in precipitation for the same upward motion in the high resolution model.

> **Key result 5** Large scale circulation is better simulated in the high resolution model, providing for a more accurate horizontal moisture transport and precipitation.

A comparison of the moisture convergence of the two models with ERA-Interim, showed a more accurate representation of moisture convergence in most of the central and northern part of continental Europe in the high resolution model. No clear improvement in the representation of moisture convergence in the southern part of Europe was found. In order to better understand the difference in moisture convergence between the medium- and high resolution model, the moisture transport was considered. The results showed that there is less transport of moisture from the ocean to the western part of Europe at higher resolution.

The main differences in atmospheric moisture transport were found over the Atlantic. This is the storm track region where extra-tropical cyclones form [*Blackmon*, 1976]. These storm track regions are associated with increased precipitation and winds and are subject to extreme weather events [e.g. *Graff and LaCasce*, 2012]. In agreement with several other studies [e.g. *Jung et al.*, 2012; *Willison et al.*, 2013; *Zappa et al.*, 2013; *Colle et al.*, 2013], the performance of the model in representing the North Atlantic storm track was found to be strongly dependent on model resolution: the high resolution model has a more realistic representation.

> **Key result 6** The smaller precipitation bias in central and northern Europe is largely unrelated to a difference in vertical velocity distribution.

The increase in frequency of days with subsidence in the high resolution model was found to be related to the increase in number of dry days as expected. An increase in days with extreme precipitation associated with the increase in strong positive upward motion of the atmosphere was however not found. The latter is related to a decrease in precipitation in the high resolution model for the same upward motion. Reduced horizontal moisture transport likely reduces the amount of available moisture to precipitate.

In order to confirm this, the precipitation difference between the two models was decomposed using the ascending motion of the atmosphere into three different parts: a vertical velocity component, a non-vertical velocity component, and a co-variation term. The non-vertical velocity component was found to be responsible for much of the lower precipitation in the high resolution model in central and northern Europe. The decrease in precipitation in these

areas is in agreement with reduced moisture transport over this area in the high resolution model.

The vertical velocity component was found to be mainly positive along areas with high orography. Orography is much more pronounced in the high resolution model, resulting in increased precipitation and a change in w_{500} distribution. Increased storm track activity in the high resolution model could also be a factor in the positive vertical velocity component in southern Spain and Scandinavia, where the difference in moisture transport between the two model resolutions is relatively small. The covariation term was found to be small everywhere.

6.3.3 Discussion

In this section additional discussion is provided for some of the choices made in the analysis and the results presented.

Uncoupled. AGCMs simplify the climate system by constraining it by observed boundary conditions (sea surface temperatures and sea ice cover) that: (1) make their results more comparable to observations and reanalysis compared to coupled models with ocean and sea ice modules; (2) allow for a better comparison between models; (3) make it easier to isolate atmospheric processes responsible for affecting the hydrological cycle in climate models with various resolutions [*Demory et al.*, 2013]. Nevertheless, the use of an uncoupled model model also introduces additional problems: the amplitude of the atmospheric variability is considerably reduced and the air-sea heat fluxes are of the reverse sign to those observed [*Bretherton and Battisti*, 2000].

Single model. Running high-resolution models is expensive in terms of computing cost and data storage, and is therefore often not possible on climatic time scales. The results presented are valid for a single AGCM (EC-Earth), but may be valid for other GCMs as well, showing the necessity to analyze other GCMs that may become available in the future with such high horizontal resolutions.

Saved output levels. Output levels were saved only at 5 vertical levels (850/700/500/300/200hPa). An important part of the

lower atmosphere is therefore absent. Most moisture transport takes place in the lower part of the atmosphere. By omitting the lower part of the atmosphere, an important part of this moisture transport is missed and accurate budgets could therefore not be calculated. Nevertheless, the results were found to be consistent and of the same order of magnitude with moisture convergence calculated from precipitation and evaporation, providing confidence that the sign and spatial structure of the difference in moisture transport between the high and medium resolution model results are correct.

Natural variability. A 30-year continuous period for the observations was used to verify two sets of 5-year 6-member ensemble simulations. This makes the influence of natural variability on the estimated quantities much better comparable, compared to using a short 5-year overlapping period to verify the model ensemble simulations. Differences between model results and observations may be due to different characteristics of decadal variability due to different SSTs, and due to the chaotic nature of the atmosphere in the climate system. A test using only the five overlapping years for the observations yields, despite the added influence of natural variability, a similar precipitation bias over western Europe (not shown).

6.4 Effect of GCM spatial resolution on simulated future summer drying in central and southern Europe

6.4.1 Research question

In chapter 5 the effect of GCM spatial resolution on simulated future drying in central and southern Europe was analyzed using an AGCM at two model resolutions. In this chapter the following research question was answered:

Q4 Does the increased AGCM spatial resolution change the future climate change projected circulation forced summer drying over central and southern European?

Q5 Is there a link between resolution dependent projected future spring circulation change, drying of the soil in spring, and soil moisture feedback in summer?

6.4.2 Results & answer research questions

> **Key result 7** Although the area-averaged precipitation in the current climate is similar in the high and medium resolution model, the models do differ in their circulation. The high resolution model has a more accurate representation of the atmospheric circulation in the current climate compared to ERA-Interim. The more accurate baseline, as a result of a better representation of physics in the high resolution model, provides more confidence in the simulated circulation response at this model resolution.

In chapter 5 the effect of GCM spatial resolution on simulated future summer drying in central and southern Europe was analyzed using an AGCM at the same two model resolutions as in the previous chapter. The results showed that the model has, in general, a similar representation of the seasonal cycle at both resolutions, but significant differences occur for individual months. Considering the spring and summer seasons, the high resolution model simulates significantly less precipitation in May, and significantly more precipitation in August. Compared to ERA-Interim and E-OBS there is a very significant overestimation (~20%) of average precipitation throughout most of the year, with the exception of late summer, July–September.

Although the area-averaged precipitation in the current climate is similar in the high and medium resolution model, the models do differ in their circulation. The high resolution model has a more accurate representation of the atmospheric circulation in the current climate compared to ERA-Interim. The more accurate baseline, as a result of a better representation of physics in the high resolution model, provides more confidence in the simulated circulation response at this model resolution.

Key result 8 The high resolution model is characterized by a stronger (partly) large scale circulation forced future drying in spring, resulting in drier soils at the beginning of summer. In an already drier future climate, the initial drying in spring is intensified in summer by a positive soil moisture feedback and differences in the pressure climate change pattern between the high and medium resolution model.

The results in chapter 5 showed that the high resolution model simulates a larger drying in spring, resulting in drier soils at the beginning of summer. The larger spring drying in the high resolution model is caused by two factors. The projected circulation change over the European area differs and the mountains in central Europe are resolved better.

In an already drier future climate, the initial drying in spring is intensified in summer by a positive soil moisture feedback in the future climate, and differences in the pressure climate change pattern between the high and medium resolution model. The difference in pressure climate change pattern is one of high pressure over central and southern Europe, and low pressure over northern Europe. This causes a decrease of moisture transport over southern Europe and an increase in subsidence over central and southern Europe, thereby reducing precipitation in this area.

The hypothesis that the circulation difference in the climate change signal between the medium and the high resolution model is an important driver for the difference in projected change in precipitation was tested by finding analogs in the natural variability of a coupled model. The results confirmed the hypothesis.

6.4.3   Discussion

Because the model experiments used to answer the research questions in this section are the same as the experiments used in the previous section, the discussion provided in section 6.2.2.3 is valid here as well. Additionally, the unavailability of saved model output for soil moisture is discussed here.

Soil moisture. A limitation of the study performed in chapter 5 is that the model output for soil moisture was not saved. A

larger drying of the soil in the high resolution model was detected by comparing the difference in climate change signals of evaporation and surface sensible heat flux between the two model resolutions. It was however not possible to quantify the drying and study the effect of soil drying in more detail.

6.5 Outlook

The research presented in this thesis was aimed to understanding the changes and the simulation of precipitation in Europe. A correct representation of simulated (trends in) European precipitation is important to have confidence in projections of future changes therein. These projections are relevant for different hydrological applications. Among others, simulated changes of summer drying are often accompanied by an enhanced increase in air temperatures [*Zampieri et al.*, 2009]. This can be expected to have large impacts on society and ecosystems, affecting, for example, water resources, agriculture and fire risk [*Rowell*, 2009]. Projections of changes in extreme precipitation are critical for estimates of future discharge extremes of large river basins, and changes in frequency of major flooding events [e.g. *Kew et al.*, 2010].

The analysis performed in this thesis showed that circulation driven winter precipitation climatology and trends over Europe are in general not well represented in the current generation of climate models. This holds for the seasonal mean (chapter 2) and for extreme events (chapter 3). Circulation (trends) often showed large biases, as well as the associated precipitation (trends). A high resolution AGCM (EC-Earth) was found to improve the representation of circulation driven winter precipitation in the current climate (chapter 4). For summer, SST trend biases are likely an important cause for the underestimation of the trend to increased precipitation along the coastal region of western Europe (chapter 2). The cause of the large trends in observed atmospheric circulation and summer SST relative to the modeled trends is not known. For SST there may be a connection with the well-known ocean circulation biases in low-resolution ocean models, for atmospheric circulation there may be connection with the resolution of the atmospheric component of climate models as well (chapters 4 and 5).

These results have implications for projections of future climate change and climate adaptation. Because it is not clear (yet) whether

the trend biases in SST and large scale circulation are due to greenhouse warming, or due to an underestimation of natural variability on multi-decadal or longer timescales, their importance for future climate projections needs to be determined. Therefore, a quantitative understanding of the causes of these trends is needed so that climate model based projections of future climate can be corrected for these trend biases.

For future research, additional work should be focused on expanding the work done in the latter part of the thesis, where the effect of climate model resolution on the representation of precipitation was analyzed. In the first place the analysis should be extended to other models to see if other models have a similar behavior compared to EC-Earth. An ensemble of high resolution models, such as the proposed HighResMIP for CMIP6, could be compared to for instance CMIP5 results to extract the effect of resolution on circulation driven precipitation (trends). In addition, an analysis of 20th century precipitation trends should be performed using an ensemble of high resolution models, similar to the analysis performed in the first part of the thesis. Do high resolutions models objectively perform better when considering observed trends and should we therefore have more confidence in them for future projections? Depending on the time-frame that such a high-resolution multi-model ensemble could be realized, the EC-Earth ensemble used in the second part of the analysis could be extended to validate the results in a larger ensemble. If such an extension would take place it is important that the variables that are relevant for circulation-driven precipitation are saved for more output levels lower in the atmosphere, so that a more accurate analysis can be performed.

To conclude, climate models have become an important tool to study the Earth's climate system over the past few decades. Industry and society increasingly rely on the outcome of these studies: information on climate and future climate change is used in decision making and climate adaptation. Uncertainty in climate projections plays an important role in, for example, the chosen adaptation strategy and its design. What the best adaptation strategy is, is very context dependent and depends for example on the types of uncertainty that dominate, the time horizons that need to be taken into account, the robustness of the strategy to a range of climate change scenarios, and the flexibility of the chosen adaptation strategy. In order for decision makers to be able to choose the right

adaptation strategy, the uncertainty in climate change projections should be studied in great detail. Understanding what makes the projections of two models agree or disagree, evaluating models on key processes, developing metrics that demonstrably relate to projections, and searching for emerging constraints in the system on the basis of observations may be ways forward [*Knutti et al.*, 2010]. In emerging constraints, relationships are derived between currently observable quantities and the GCM response to changes in forcing [*Caldwell et al.*, 2014; *Xie et al.*, 2014]. With this technique, statistical relationships between future and historical model runs in multi-model ensembles are exploited to make more constrained projections [*Bracegirdle and Stephenson*, 2013].

Dankwoord

Het dankwoord is misschien wel het hoofdstuk van je proefschrift dat het meest gelezen wordt. Helaas beginnen de meeste dankwoorden van een proefschrift met een weinig originele clichézin zoals 'dit proefschrift heeft niet tot stand kunnen komen zonder de hulp van anderen'. Natuurlijk is dat zo, maar een dankwoord geeft je juist de gelegenheid om tenminste één hoofdstuk in je proefschrift op te nemen dat fijn is om te lezen. Moet het dan echt vol staan met al die clichés? Het antwoord is "ja", om de simpele reden dat het ook vaak gewoon zo is. Ook ik ontkom er dus niet aan: Bij deze wil ik iedereen bedanken die een bijdrage heeft geleverd aan de voltooiing van mijn proefschrift.

Nu sta ik niet echt bekend om iemand die lang van stof is, dus misschien zou ik het wel gewoon bij die ene zin moeten laten. Toch wil ik nog enkele mensen persoonlijk noemen in dit dankwoord, er is per slot van rekening nog wat ruimte over in dit proefschrift.

Allereerst wil ik Wilco, Geert-Jan en Rein bedanken voor de begeleiding en goede adviezen die ik tijdens mijn promotietijd van jullie heb gekregen. Ook wil ik alle co-auteurs bedanken voor de bijdrage aan de wetenschappelijke artikelen waar dit proefschrift op gebaseerd is. Camiel, bedankt voor het leiden van de discussiegroep over *model development*. PhD's en postdocs, bedankt voor de discussies over statistiek en het samen doorploegen van het literaire werk van 'Storch en Zwiers'. Daarnaast wil ik al mijn collega's op het KNMI bedanken. Ik vond het een gezellige tijd, en waar nodig kon ik altijd aankloppen voor hulp. Bedankt!

De leden van de commissie, Dr. E. Hawkins, Prof.dr. B.J.J.M. van den Hurk, Prof.dr. R. Uijlenhoet en Dr. R. Vautard, ik wil jullie van harte bedankten voor de moeite die jullie genomen hebben bij het beoordelen van dit proefschrift.

Als afsluiting wil ik nog enkele personen bedanken die niet direct een bijdrage hebben geleverd aan de wetenschappelijke inhoud van dit proefschrift, maar die wel heel belangrijk zijn geweest in de totstandkoming van dit proefschrift.

Mijn familie en schoonfamilie wil ik bedanken voor alle interesse in mijn onderzoek. Hoewel jullie misschien niet altijd snapten wat ik deed waardeer ik het zeer dat jullie altijd interesse toonden. Pa, ma, bedankt dat jullie me altijd gesteund hebben. Mede door jullie heb ik dit kunnen bereiken, dus dit proefschrift is ook een beetje

van jullie. Sebastiaan, als grote broer heb je mij wegwijs gemaakt in het leven. Hoewel je vaak in het buitenland bent, ben je nog altijd een grote inspiratie als ik je weer zie!

Tot slot wil ik me graag nog richten tot mijn lieve vrouw. Bijou, het is niet te beschrijven wat je voor me betekent. Je staat altijd voor me klaar en sleept me er ook in moeilijke tijden doorheen. Bedankt voor alle steun en liefde die je me hebt gegeven tijdens het onderzoek! Het is altijd fijn om weer thuis te komen. Zonder jou zou het afronden van mijn proefschrift een stuk zwaarder zijn geweest.

References

Jones, P.D. and Harris, I., CRU TS3.22: Climatic Research Unit (CRU) Time-Series (TS) Version 3.22 of High Resolution Gridded Data of Month-by-month Variation in Climate (Jan. 1901- Dec. 2013), doi: 10.5285/18BE23F8-D252-482D-8AF9-5D6A2D40990C, 2014.

Abbaspour, K. C., M. Faramarzi, S. S. Ghasemi, and H. Yang, Assessing the impact of climate change on water resources in Iran, *Water Resour. Res.*, *45*(10), W10,434+, doi:10.1029/2008wr007615, 2009.

Alexander, L., Climate science: Extreme heat rooted in dry soils, *Nature Geoscience*, *4*, 12–13, doi:10.1038/ngeo1045, 2011.

Alexander, L. V., and J. M. Arblaster, Assessing trends in observed and modelled climate extremes over Australia in relation to future projections, *International Journal of Climatology*, *29*(3), 417–435, doi:10.1002/joc.1730, 2009.

Annan, J., and J. Hargreaves, Reliability of the CMIP3 ensemble, *Geophys. Res. Lett.*, doi:10.1029/2009GL041994, 2010.

Arrhenius, S., On the influence of carbonic acid in the air upon the temperature of the ground, *Phil. Mag.*, *41*, 237–276, 1896.

Ashfaq, M., C. Skinner, and N. Diffenbaugh, Influence of SST biases on future climate change projections, *Climate Dynamics*, pp. 1–17, 10.1007/s00382-010-0875-2, 2010.

Banacos, P. C., and D. M. Schultz, The use of moisture flux convergence in forecasting convective initiation: historical and operational perspectives, *Weather and Forecasting*, *20*, 351–366, doi: 10.1175/WAF858.1, 2005.

Barnett, T. P., J. C. Adams, and D. P. Lettenmeier, Potential impacts of a warming climate on water availability in snow-dominated regions, *Nature*, *438*, 2005.

Becker, A., P. Finger, A. Meyer-Christoffer, B. Rudolf, K. Schamm, U. Schneider, and M. Ziese, A description of the global land-surface precipitation data products of the global precipitation climatology centre with sample applications including centennial (trend) analysis from 1901present, *Earth System Science Data*, *5*(1), 71–99, doi:10.5194/essd-5-71-2013, 2013.

Benestad, R., D. Nychka, and L. Mearns, Specification of wet-day daily rainfall quantiles from the mean value, *Tellus Series A-dynamic Meteorology and Oceanography*, doi:10.3402/tellusa. v64i0.14981, 2012.

Berckmans, J., T. Woollings, M.-E. Demory, P.-L. Vidale, and M. Roberts, Atmospheric blocking in a high resolution climate model: influences of mean state, orography and eddy forcing, *Atmospheric Science Letters*, *14*(1), 34–40, doi:10.1002/asl2.412, 2013.

Bhend, J., and H. von Storch, Consistency of observed winter precipitation trends in northern Europe with regional climate change projections, *Clim. Dynam.*, *31*, 17–28, doi:10.1007/ s00382-007-0335-9, 2008.

Bjerknes, V., Weather forecasting as a problem in mechanics and physics, 1954.

Blackmon, M. L., A climatological spectral study of the 500 mb geopotential height of the northern hemisphere, *J. Atmos. Sci.*, *33*(8), 1607–1623, doi:10.1175/1520-0469(1976)033\ %3C1607:acssot\%3E2.0.co;2, 1976.

Bladé, I., B. Liebmann, D. Fortuny, and G. van Oldenborgh, Observed and simulated impacts of the summer NAO in

Europe: implications for projected drying in the Mediterranean region, *Climate Dynamics*, *39*(3-4), 709–727, doi:10.1007/s00382-011-1195-x, 2012.

Bony, S., J.-L. Dufresne, H. Le Treut, J.-J. Morcrette, and C. Senior, On dynamic and thermodynamic components of cloud changes, *Climate Dynamics*, *22*(2-3), 71–86, doi:10.1007/s00382-003-0369-6, 2004.

Bracegirdle, T. J., and D. B. Stephenson, On the robustness of emergent constraints used in multimodel climate change projections of Arctic warming, *J. Climate*, *26*(2), 669–678, doi:10.1175/jcli-d-12-00537.1, 2013.

Bretherton, C. S., and D. S. Battisti, An interpretation of the results from atmospheric general circulation models forced by the time history of the observed sea surface temperature distribution, *Geophysical Research Letters*, *27*(6), 767–770, doi:10.1029/1999GL010910, 2000.

Buishand, T. A., G. De Martino, J. Spreeuw, and T. Brandsma, Homogeneity of precipitation series in the Netherlands and their trends in the past century, *Int. J. Climatology*, 2012.

Caldwell, P. M., C. S. Bretherton, M. D. Zelinka, S. A. Klein, B. D. Santer, and B. M. Sanderson, Statistical significance of climate sensitivity predictors obtained by data mining, *Geophysical Research Letters*, *41*(5), 1803–1808, doi:10.1002/2014GL059205, 2014.

Champion, A. J., K. I. Hodges, L. O. Bengtsson, N. S. Keenlyside, and M. Esch, Impact of increasing resolution and a warmer climate on extreme weather from northern hemisphere extratropical cyclones, *Tellus A*, *63*(5), 893–906, doi:10.1111/j.1600-0870.2011.00538.x, 2011.

Chang, E. K. M., Y. Guo, and X. Xia, CMIP5 multimodel ensemble projection of storm track change under global warming, *Journal of Geophysical Research: Atmospheres*, *117*(D23), doi:10.1029/2012JD018578, 2012.

Christensen, J. H., and O. B. Christensen, A summary of the PRUDENCE model projectionsof changes in European climate

by the end of the century, *Climatic Change*, *81*, 7–30, doi: 10.1007/s10584-006-9210-7, 2007.

Colle, B. A., Z. Zhang, K. A. Lombardo, E. Chang, P. Liu, and M. Zhang, Historical evaluation and future prediction of eastern North American and western Atlantic extratropical cyclones in the CMIP5 models during the cool season, *Journal of Climate*, *26*(18), 6882–6903, doi:10.1175/jcli-d-12-00498.1, 2013.

Collins, M., B. Booth, G. Harris, J. Murphy, D. Sexton, and M. Webb, Towards quantifying uncertainty in transient climate change, *Climate Dynamics*, *27*(2-3), 127–147, doi:10.1007/s00382-006-0121-0, 2006.

Compo, G. P., et al., The twentieth century reanalysis project, *Quarterly Journal of the Royal Meteorological Society*, *137*(654), 1–28, doi:10.1002/qj.776, 2011.

Cox, P., and D. Stephenson, A changing climate for prediction, *Science*, *317*(5835), 207–208, doi:10.1126/science.1145956, 2007.

Dai, A., Precipitation characteristics in eighteen coupled climate models, *J. Climate*, *19*(18), 4605–4630, doi:10.1175/jcli3884.1, 2006.

Dee, D. P., et al., The ERA-Interim reanalysis: configuration and performance of the data assimilation system, *Quarterly Journal of the Royal Meteorological Society*, *137*(656), 553–597, doi:10.1002/qj.828, 2011.

Demory, M.-E., P. Vidale, M. Roberts, P. Berrisford, J. Strachan, R. Schiemann, and M. Mizielinski, The role of horizontal resolution in simulating drivers of the global hydrological cycle, *Climate Dynamics*, pp. 1–25, doi:10.1007/s00382-013-1924-4, 2013.

Déqué, M., et al., An intercomparison of regional climate simulations for Europe: assessing uncertainties in model projections, *Climatic Change*, *81*(0), 53–70, doi:10.1007/s10584-006-9228-x, 2007.

Disse, M., and H. Engel, Flood events in the Rhine basin: Genesis, influences and mitigation, *Natural Hazards*, *23*, 271–290, doi:10.1023/A:1011142402374, 2001.

Eden, J. M., and M. Widmann, Downscaling of GCM-simulated precipitation using model output statistics, *J. Climate*, *27*(1), 312–324, doi:10.1175/jcli-d-13-00063.1, 2013.

Edwards, P., General circulation model development, in *A brief history of atmospheric general circulation modeling*, edited by D. Randall, pp. 67–90, Academic Press, 2000.

Edwards, P., *A vast machine*, Cambride MA:MIT Press, 2010.

Edwards, P. N., History of climate modeling, *WIREs Clim Change*, *2*(1), 128–139, doi:10.1002/wcc.95, 2011.

Efron, B., and R. J. Tibshirani, *An Introduction to the Bootstrap*, Chapman & Hall, New York, 1993.

Emori, S., and S. J. Brown, Dynamic and thermodynamic changes in mean and extreme precipitation under changed climate, *Geophysical Research Letters*, *32*(17), doi:10.1029/2005GL023272, 2005.

Feser, F., B. Rockel, H. von Storch, J. Winterfeldt, and M. Zahn, Regional climate models add value to global model data: A review and selected examples, *Bull. Amer. Meteor. Soc.*, *92*(9), 1181–1192, doi:10.1175/2011bams3061.1, 2011.

Flato, G., et al., *Evaluation of climate models. In Climate Change 2013: The Physical Science Basis. Contribution of Working Group I to the Fifth Assessment Report of the Intergovernmental Panel on Climate Change.*, 741–882 pp., Cambridge University Press, 2013.

Fourier, J.-B. J., On the temperatures of the terrestrial sphere and interplanetary space, 1827.

Giorgi, F., and L. O. Mearns, Calculation of average, uncertainty range, and reliability of regional climate changes from aogcm simulations via the reliability ensemble averaging (rea) method, *Journal of Climate*, *15*(10), 1141–1158, doi:10.1175/1520-0442(2002) 015⟨1141:COAURA⟩2.0.CO;2, 2002.

Goosse, H., P. Barriat, W. Lefebvre, M. Loutre, and V. Zunz, Introduction to climate dynamics and climate modeling, 2014.

Graff, L. S., and J. H. LaCasce, Changes in the extratropical storm tracks in response to changes in SST in an AGCM, *J. Climate*, *25*(6), 1854–1870, doi:10.1175/jcli-d-11-00174.1, 2012.

Greve, P., B. Orlowsky, B. Mueller, J. Sheffield, M. Reichstein, and S. I. Seneviratne, Global assessment of trends in wetting and drying over land, *Nature Geosci*, *7*(10), 716–721, doi:10.1038/ngeo2247, 2014.

Grønøs, S., *Vilhelm Bjerknes' vision for scientific weather prediction*, pp. 357–366, American Geophysical Union, doi:10.1029/158GM22, 2013.

Haarsma, R., F. Selten, and G. van Oldenborgh, Anthropogenic changes of the thermal and zonal flow structure over Western Europe and Eastern North Atlantic in CMIP3 and CMIP5 models, submitted, 2013a.

Haarsma, R. J., F. M. Selten, B. J. J. M. van den Hurk, W. Hazeleger, and X. Wang, Dry mediterranean soils due to greenhouse warming bring easterly winds over summertime central europe, *Geophys. Res. Lett.*, *36*, L04,705, doi:10.1029/2008GL036617, 2009.

Haarsma, R. J., W. Hazeleger, C. Severijns, H. de Vries, A. Sterl, R. Bintanja, G. J. van Oldenborgh, and H. W. van den Brink, More hurricanes to hit western Europe due to global warming, *Geophysical Research Letters*, *40*(9), 1783–1788, doi:10.1002/grl.50360, 2013b.

Hack, J. J., J. M. Caron, G. Danabasoglu, K. W. Oleson, C. Bitz, and J. E. Truesdale, CCSM-CAM3 climate simulation sensitivity to changes in horizontal resolution, *J. Climate*, *19*(11), 2267–2289, doi:10.1175/jcli3764.1, 2006.

Hawcroft, M. K., L. C. Shaffrey, K. I. Hodges, and H. F. Dacre, How much northern hemisphere precipitation is associated with extratropical cyclones?, *Geophysical Research Letters*, *39*(24), doi:10.1029/2012GL053866, 2012.

Hawkins, E., and R. Sutton, The potential to narrow uncertainty in projections of regional precipitation change, *Climate Dynamics*, *37*, 407–418, doi:10.1007/s00382-010-0810-6, 2011.

Hawkins, E., and R. T. Sutton, The potential to narrow uncertainty in regional climate predictions, *Bulletin of the American Meteorological Society*, *90*, 1095–1107, doi:10.1175/2009BAMS2607.1, 2009.

Haylock, M. R., N. Hofstra, A. M. G. K. Tank, E. J. Klok, P. D. Jones, and M. New, A European daily high-resolution gridded data set of surface temperature and precipitation for 1950-2006, *Journal of Geophysical Research*, *113*(D20), D20,119+, doi:10. 1029/2008JD010201, 2008.

Hazeleger, W., et al., EC-Earth a seamless earth-system prediction approach in action, *Bulletin of the American Meteorological Society*, *91*(10), 1357–1363, doi:DOI10.1175/2010BAMS2877.1, 2010.

Hazeleger, W., et al., Ec-earth v2.2: description and validation of a new seamless earth system prediction model, *Climate Dynamics*, *39*(11), 2611–2629, doi:10.1007/s00382-011-1228-5, 2012.

Hegerl, G., and F. Zwiers, Use of models in detection and attribution of climate change, *Wiley Interdisciplinary Reviews: Climate Change*, doi:10.1002/wcc.121, 2011.

Ho, C. K., D. B. Stephenson, M. Collins, C. A. T. Ferro, and S. J. Brown, Calibration strategies: A source of additional uncertainty in climate change projections, *Bull. Amer. Meteor. Soc.*, *93*(1), 21–26, doi:10.1175/2011bams3110.1, 2011.

Hofstra, N., M. New, and C. McSweeney, The influence of interpolation and station network density on the distributions and trends of climate variables in gridded daily data, *Climate Dynamics*, *35*(5), 841–858, doi:10.1007/s00382-009-0698-1, 2010.

Hudson, D., and R. Jones, Regional climate model simulations of present-day and future climates of Southern Africa, *Technical note 39*, Hadley Centre for Climate Prediction and Research, 2002.

Hulme, M., On the origin of the greenhouse effect: John tyndall's 1859 interrogation of nature, *Weather*, *64*(5), 121–123, doi:10. 1002/wea.386, 2009.

Hundecha, Y., and A. Bárdossy, Trends in daily precipitation and temperature extremes across western germany in the second half

of the 20th century, *International Journal of Climatology*, *25*(9), 1189–1202, doi:10.1002/joc.1182, 2005.

Hurkmans, R., W. Terink, R. Uijlenhoet, P. Torfs, D. Jacob, and P. A. Troch, Changes in streamflow dynamics in the Rhine basin under three high-resolution regional climate scenarios, *J. Climate*, *23*(3), 679–699, doi:10.1175/2009JCLI3066.1, 2010.

IPCC, *Climate Change 2007 - The Physical Science Basis: Working Group I Contribution to the Fourth Assessment Report of the IPCC*, Cambridge University Press, Cambridge, UK and New York, NY, USA, 2007.

IPCC, *Climate Change 2013 - The Physical Science Basis: Working Group I Contribution to the Fifth Assessment Report of the IPCC*, Cambridge University Press, Cambridge, doi:10.1017/cbo9781107415324, 2013.

Jones, P. D., E. B. Horton, C. K. Folland, M. Hulme, D. E. Parker, and T. A. Basnett, The use of indices to identify changes in climatic extremes, *Climatic Change*, *42*, 131–149, 1999.

Jung, T., et al., High-resolution global climate simulations with the ECMWF Model in Project Athena: Experimental design, model climate, and seasonal forecast skill, *J. Climate*, *25*(9), 3155–3172, doi:10.1175/jcli-d-11-00265.1, 2012.

Katz, R. W., M. B. Parlange, and P. Naveau, Statistics of extremes in hydrology, *Advances in Water Resources*, *25*(8-12), 1287–1304, doi:10.1016/S0309-1708(02)00056-8, 2002.

Kew, S. F., F. M. Selten, G. Lenderink, and W. Hazeleger, Robust assessment of future changes in extreme precipitation over the Rhine basin using a GCM, *Hydrology and Earth System Sciences Discussions*, *7*(6), 9043–9066, doi:10.5194/hessd-7-9043-2010, 2010.

Kharin, V., and F. Zwiers, Estimating extremes in transient climate change simulations, *Journal of Climate*, *18*(8), 1156–1173, 2005.

Kistler, R., et al., The NCEP-NCAR 50-year reanalysis: Monthly means CD-ROM and documentation, *Bulletin of the American Meteorological Society*, *82*(2), 247–267, 2001.

Kjellström, E., and K. Ruosteenoja, Present-day and future precipitation in the Baltic Sea region as simulated in a suite of regional climate models, *Climatic Change*, *81*(0), 281–291, doi: 10.1007/s10584-006-9219-y, 2007.

Knutti, R., Should we believe model predictions of future climate change?, *Philosophical Transactions of the Royal Society A: Mathematical, Physical and Engineering Sciences*, *366*(1885), 4647–4664, doi:10.1098/rsta.2008.0169, 2008.

Knutti, R., R. Furrer, C. Tebaldi, J. Cermak, and G. A. Meehl, Challenges in Combining Projections from Multiple Climate Models, *J. Climate*, *23*(10), 2739–2758, doi:10.1175/2009jcli3361.1, 2009.

Knutti, R., R. Furrer, C. Tebaldi, J. Cermak, and G. A. Meehl, Challenges in combining projections from multiple climate models, *J. Climate*, *23*(10), 2739–2758, doi:10.1175/2009jcli3361.1, 2010.

Knutti, R., D. Masson, and A. Gettelman, Climate model genealogy: Generation CMIP5 and how we got there, *Geophysical Research Letters*, *40*(6), 1194–1199, doi:10.1002/grl.50256, 2013.

Lenderink, G., A. Buishand, and W. van Deursen, Estimates of future discharges of the river Rhine using two scenario methodologies: direct versus delta approach, *Hydrology and Earth System Sciences*, *11*(3), 1145–1159, doi:10.5194/hess-11-1145-2007, 2007.

Lenderink, G., E. van Meijgaard, and F. Selten, Intense coastal rainfall in the Netherlands in response to high sea surface temperatures: analysis of the event of August 2006 from the perspective of a changing climate., *Clim. Dyn.*, *32*, 19–33., 2009.

Lynch, P., *The emergence of scientific weather forecasting*, Cambridge University Press, 2014.

Manabe, S., The dependence of atmospheric temperature on the concentration of carbon dioxide, in *Global Effects of Environmental Pollution*, edited by S. Singer, pp. 25–29, Springer Netherlands, doi:10.1007/978-94-010-3290-2_4, 1970.

Manabe, S., Estimates of future change of climate due to the increase of carbon dioxide, in *Man's impact on the climate*, edited by W. Matthews, W. Kellog, and G. Robinson, pp. 250–264, MIT Press, 1971.

Manabe, S., and K. Bryan, Climate calculations with a combined ocean-atmosphere model, *J. Atmos. Sci.*, *26*(4), 786–789, doi:10.1175/1520-0469(1969)026\%3C0786:ccwaco\%3E2.0.co;2, 1969.

Manabe, S., and R. J. Stouffer, Multiple-century response of a coupled ocean-atmosphere model to an increase of atmospheric carbon dioxide, *J. Climate*, *7*(1), 5–23, doi:10.1175/1520-0442(1994)007\%3C0005:mcroac\%3E2.0.co;2, 1994.

Masson, D., and R. Knutti, Climate model genealogy, *Geophysical Research Letters*, *38*(8), doi:10.1029/2011GL046864, 2011.

McGuffie, K. and Henderson-Sellers, A., *The climate modelling prime*, Wiley Blackwell, 2014.

Meehl, G. A., C. Covey, T. L. Delworth, M. Latif, B. McAvaney, J. F. B. Mitchell, R. J. Stouffer, and K. E. Taylor, The WCRP CMIP3 multimodel dataset: A new era in climate change research, *Bulletin of the American Meteorological Society*, *88*, 1383–1394, doi:10.1175/BAMS-88-9-1383, 2007.

Mitchell, T. D., and P. D. Jones, An improved method of constructing a database of monthly climate observations and associated high resolution grids, *Int. J. Climatol.*, *25*, 693–712, doi:10.1002/joc.1181, 2005.

Moss, R. H., et al., The next generation of scenarios for climate change research and assessment, *Nature*, *463*(7282), 747–756, doi:10.1038/nature08823, 2010.

Mueller, B., and S. I. Seneviratne, Systematic land climate and evapotranspiration biases in CMIP5 simulations, *Geophysical Research Letters*, *41*(1), 128–134, doi:10.1002/2013GL058055, 2014.

Murphy, J., An evaluation of statistical and dynamical techniques for downscaling local climate, *J. Climate*, *12*(8), 2256–2284, doi:10.1175/1520-0442(1999)012\%3C2256:aeosad\%3E2.0.co;2, 1999.

Murphy, J. M., D. M. H. Sexton, D. N. Barnett, G. S. Jones, M. J. Webb, M. Collins, and D. A. Stainforth, Quantification of modelling uncertainties in a large ensemble of climate change simulations, *Nature*, *430*, 768–772, 2004.

Murphy, J. M., B. B. B. Booth, M. Collins, G. R. Harris, D. Sexton, and M. Webb, A methodology for probabilistic predictions of regional climate change from perturbed physics ensembles, *Phil. Trans. R. Soc. A*, *365*, 1993–2028, doi:10.1098/rsta.2007.2077, 2007.

Murphy, J. M., et al., UK Climate Projections Science Report: Climate change projections, *Tech. rep.*, Met Office Hadley Centre, Exeter, UK, 2009.

Osborn, T. J., Simulating the winter North Atlantic Oscillation: the roles of internal variability and greenhouse gas forcing, *Clim. Dynam.*, *22*, 605–623, doi:10.1007/s00382-004-0405-1, 2004.

Osborn, T. J., D. Conway, M. Hulme, J. M. Gregory, and P. D. Jones, Air flow influences on local climate: observed and simulated mean relationships for the United Kingdom, *Climate Research*, *13*(3), 173–191, doi:10.3354/cr013173, 1999.

Palmer, T. N., A nonlinear dynamical perspective on model error: A proposal for non-local stochastic-dynamic parametrization in weather and climate prediction models, *Q.J.R. Meteorol. Soc.*, *127*(572), 279–304, doi:10.1002/qj.49712757202, 2001.

Pfahl, S., and H. Wernli, Quantifying the relevance of cyclones for precipitation extremes, *J. Climate*, *25*, 6770–6780, doi:10.1175/JCLI-D-11-00705.1, 2012.

Polade, S. D., D. W. Pierce, D. R. Cayan, A. Gershunov, and M. D. Dettinger, The key role of dry days in changing regional climate and precipitation regimes, *Sci. Rep.*, *4*, doi:10.1038/srep04364, 2014.

Pope, V., and R. Stratton, The processes governing horizontal resolution sensitivity in a climate model, *Climate Dynamics*, *19*(3-4), 211–236, doi:10.1007/s00382-001-0222-8, 2002.

Räisänen, J., How reliable are climate models?, *Tellus A*, *59*(1), 2–29, doi:10.1111/j.1600-0870.2006.00211.x, 2007.

Reynolds, R. W., N. A. Rayner, T. M. Smith, D. C. Stokes, and W. Wang, An improved in situ and satellite SST analysis for climate, *J. Climate*, *15*, 1609–1625, doi:10.1175/1520-0442(2002) 015$\langle$1609:AIISAS$\rangle$2.0.CO;2, 2002.

Richardson, L., Weather prediction by numerical process, 1922.

Rijkswaterstaat Waterdienst, Droogtestudie Lobith, 2012.

Rowell, D. P., The impact of Mediterranean SSTs on the Sahelian rainfall season, *Journal of Climate*, *16*(5), 849–862, 2003.

Rowell, D. P., Projected midlatitude continental summer drying: North America versus Europe, *Journal of Climate*, *22*, doi:10.1175/2008JCLI2713.1, 2009.

Rowell, D. P., and R. G. Jones, Causes and uncertainty of future summer drying over Europe, *Clim. Dyn.*, *27*, 281–299, 2006.

Rummukainen, M., S. Bergstrom, G. Persson, J. Rodhe, and M. Tjernstrom, The Swedish regional climate modelling programme, SWECLIM: a review, *Ambio*, *33*(4-5), 176–82, 2004.

Schneider, U., T. Fuchs, A. Meyer-Christoffer, and B. Rudolf, Global precipitation analysis products of the GPCC, *Tech. rep.*, Global Precipitation Climatology Centre (GPCC), Deutscher Wetterdienst, Offenbach, Germany, 2010.

Seager, R., and N. Henderson, Diagnostic computation of moisture budgets in the ERA-Interim Reanalysis with reference to analysis of CMIP-archived atmospheric model data, *J. Climate*, doi:10.1175/jcli-d-13-00018.1, 2013.

Seneviratne, S. I., et al., Impact of soil moisture-climate feedbacks on CMIP5 projections: First results from the GLACE-CMIP5 experiment, *Geophysical Research Letters*, *40*(19), 5212–5217, doi:10.1002/grl.50956, 2013.

Shabalova, V., W. van Deursen, and T. Buishand, Assessing future discharge of the river rhine using regional climate model integrations and a hydrological model, *Climate Research*, *23*, 233–246, 2003.

Stainforth, D. A., et al., Uncertainty in predictions of the climate response to rising levels of greenhouse gases, *Nature*, *433*(7024), 403–406, doi:10.1038/nature03301, 2005.

Sterl, A., et al., When can we expect extremely high surface temperatures?, *Geophys. Res. Lett.*, *35*, L14,703, doi:10.1029/ 2008GL034071, 2008.

Taylor, K. E., R. J. Stouffer, and G. A. Meehl, An Overview of CMIP5 and the Experiment Design, *Bull. Amer. Meteor. Soc.*, *93*(4), 485–498, doi:10.1175/BAMS-D-11-00094.1, 2011.

te Linde, A. H., J. C. J. H. Aerts, A. M. R. Bakker, and J. C. J. Kwadijk, Simulating low-probability peak discharges for the Rhine basin using resampled climate modeling data, *Water Resources Research*, *46*(3), W03,512+, doi:10.1029/2009WR007707, 2010.

Tebaldi, C., and R. Knutti, The use of the multi-model ensemble in probabilistic climate projections, *Philosophical Transactions of the Royal Society A: Mathematical, Physical and Engineering Sciences*, *365*(1857), 2053–2075, doi:10.1098/rsta.2007.2076, 2007.

Tebaldi, C., R. L. Smith, D. Nychka, and L. O. Mearns, Quantifying uncertainty in projections of regional climate change: A bayesian approach to the analysis of multimodel ensembles, *Journal of Climate*, *18*, 1524–1540, doi:10.1175\%2FJCLI3363.1, 2005.

Teuling, A. J., et al., Evapotranspiration amplifies European summer drought, *Geophysical Research Letters*, *40*(10), 2071–2075, doi:10.1002/grl.50495, 2013.

Trenberth, K., *Climate system modeling*, Cambridge University Press, 1992.

Trenberth, K. E., and D. A. Paolino, The Northern Hemisphere sea level pressure data set: Trends, errors, and discontinuities, *Mon. Wea. Rev.*, *108*, 855–872, doi:10.1175/1520-0493(1980) 108$\langle$$0855:TNHSLP$\rangle$$2.0.CO;2, 1980.

Trenberth, K. E., J. T. Fasullo, and J. Mackaro, Atmospheric moisture transports from ocean to land and global energy flows in reanalyses, *J. Climate*, *24*(18), 49074924, doi:10.1175/ 2011JCLI4171.1, 2011.

Turnpenny, J. R., J. F. Crossley, M. Hulme, and T. J. Osborn, Air flow influences on local climate: comparison of a regional climate model with observations over the United Kingdom, *Climate Research*, *20*, 189–202, doi:10.3354/cr020189, 2002.

Ulbrich, U., J. Pinto, H. Kupfer, G. Leckebusch, T. Spangehl, and M. Reyers, Changing northern hemisphere storm tracks in an ensemble of IPCC climate change simulations, *Journal of Climate*, *21*, 1669–+, doi:10.1175/2007JCLI1992.1, 2008.

van der Linden, P., and J. F. B. Mitchell (Eds.), *ENSEMBLES: Climate Change and its Impacts: Summary of research and results from the ENSEMBLES project*, 160pp. pp., Met Office Hadley Centre, Fitzroy Road, Exeter EX1 3PB, UK, 2009.

van der Schrier, G., and J. Barkmeijer, North American 1818–1824 drought and 1825-1840 pluvial and their possible relation to the atmospheric circulation, *Journal of Geophysical Research*, *112*(D13), D13,102+, doi:10.1029/2007JD008429, 2007.

van Haren, R., G. J. van Oldenborgh, G. Lenderink, M. Collins, and W. Hazeleger, SST and circulation trend biases cause an underestimation of European precipitation trends, *Climate Dynamics*, *40*, 1–20, doi:10.1007/s00382-012-1401-5, 2013a.

van Haren, R., G. J. van Oldenborgh, G. Lenderink, and W. Hazeleger, Evaluation of modeled changes in extreme precipitation in Europe and the Rhine basin, *Environmental Research Letters*, *8*(1), 014,053, doi:10.1088/1748-9326/8/1/014053, 2013b.

van Haren, R., R. Haarsma, G. van Oldenborgh, and W. Hazeleger, Resolution dependence of European precipitation in a state-of-the-art atmospheric general circulation model, under review, 2014.

van Oldenborgh, G. J., and A. P. van Ulden, On the relationship between global warming, local warming in the Netherlands and changes in circulation in the 20th century, *Int. J. Climatol.*, *23*, 1711–1724, doi:10.1002/joc.966, 2003.

van Oldenborgh, G. J., S. S. Drijfhout, A. P. van Ulden, R. Haarsma, C. Sterl, A. Severijns, W. Hazeleger, and H. A.

Dijkstra, Western Europe is warming much faster than expected, *Clim. Past.*, *5*, 1–12, doi:10.5194/cp-5-1-2009, 2009a.

van Oldenborgh, G. J., L. A. te Raa, H. A. Dijkstra, and S. Y. Philip, Frequency- or amplitude-dependent effects of the atlantic meridional overturning on the tropical pacific ocean, *Ocean Science*, *5*(3), 293–301, doi:10.5194/os-5-293-2009, 2009b.

van Pelt, S. C., J. J. Beersma, T. A. Buishand, B. J. J. M. van den Hurk, and P. Kabat, Future changes in extreme precipitation in the rhine basin based on global and regional climate model simulations, *Hydrology and Earth System Sciences*, *16*(12), 4517–4530, doi:10.5194/hess-16-4517-2012, 2012.

van Ulden, A. P., and G. J. van Oldenborgh, Large-scale atmospheric circulation biases and changes in global climate model simulations and their importance for climate change in Central Europe, *Atmos. Chem. Phys.*, *6*, 863–881, doi:10.5194/acp-6-863-2006, 2006.

van Ulden, A. P., G. Lenderink, B. van den Hurk, and E. Van Meijgaard, Circulation statistics and climate change in central Europe: PRUDENCE simulations and observations, *Climatic Change*, *81*, 179–192, 2007.

Vidale, P., D. Lthi, R. Wegmann, and C. Schr, European summer climate variability in a heterogeneous multi-model ensemble, *Climatic Change*, *81*(1), 209–232, doi:10.1007/s10584-006-9218-z, 2007.

Wang, W., P. van Gelder, and J. Vrijling, in *Proceedings of the IWA International Conference on Water Economics, Statistics, and Finance, Rethymno, Greece, 8-10 July 2005*, pp. 481–490, 2005.

Weart, S., The development of general circulation models of climate, *Studies in History and Philosophy of Science Part B: Studies in History and Philosophy of Modern Physics*, *41*(3), 208–217, doi:10.1016/j.shpsb.2010.06.002, 2010.

Wentz, F. J., L. Ricciardulli, K. Hilburn, and C. Mears, How much more rain will global warming bring?, *Science*, *317*(5835), 233–235, doi:10.1126/science.1140746, 2007.

Willison, J., W. A. Robinson, and G. M. Lackmann, The importance of resolving mesoscale latent heating in the north atlantic storm track, *J. Atmos. Sci.*, *70*, 22342250, doi:10.1175/JAS-D-12-0226.1, 2013.

Xie, S. P., et al., Towards predictive understanding of regional climate change: Issues and opportunities for progress, submitted, 2014.

Xu, Z., and Z.-L. Yang, An improved dynamical downscaling method with GCM bias corrections and its validation with 30 years of climate simulations, *J. Climate*, *25*(18), 6271–6286, doi:10.1175/jcli-d-12-00005.1, 2012.

Zahn, M., and R. P. Allan, Changes in water vapor transports of the ascending branch of the tropical circulation, *Journal of Geophysical Research: Atmospheres*, *116*(D18), n/a–n/a, doi:10.1029/2011JD016206, 2011.

Zahn, M., and R. P. Allan, Quantifying present and projected future atmospheric moisture transports onto land, *Water Resources Research*, *49*(11), 7266–7277, doi:10.1002/2012WR013209, 2013.

Zampieri, M., F. DAndrea, R. Vautard, P. Ciais, N. de Noblet-Ducoudr, and P. Yiou, Hot European summers and the role of soil moisture in the propagation of Mediterranean drought, *Journal of climate*, *22*, 4747–4758, doi:10.1175/2009JCLI2568.1, 2009.

Zappa, G., L. C. Shaffrey, and K. I. Hodges, The ability of CMIP5 models to simulate North Atlantic extratropical cyclones, *J. Climate*, *26*(15), 5379–5396, doi:10.1175/jcli-d-12-00501.1, 2013.

Zhang, X., F. W. Zwiers, G. C. Hegerl, F. H. Lambert, N. P. Gillett, S. Solomon, P. A. Stott, and T. Nozawa, Detection of human influence on twentieth-century precipitation trends, *Nature*, *448*, 461–465, doi:10.1038/nature06025, 2007.

Netherlands Research School for the
Socio-Economic and Natural Sciences of the Environment

D I P L O M A

For specialised PhD training

The Netherlands Research School for the
Socio-Economic and Natural Sciences of the Environment
(SENSE) declares that

Ronald van Haren

born on 18 February 1983 in 's-Hertogenbosch, The Netherlands

has successfully fulfilled all requirements of the
Educational Programme of SENSE.

Wageningen, 15 December 2014

the Chairman of the SENSE board

Prof. dr. Huub Rijnaarts

the SENSE Director of Education

Dr. Ad van Dommelen

The SENSE Research School has been accredited by the Royal Netherlands Academy of Arts and Sciences (KNAW)

K O N I N K L I J K E   N E D E R L A N D S E
A K A D E M I E   V A N   W E T E N S C H A P P E N

The SENSE Research School declares that **Mr Ronald van Haren** has successfully fulfilled all requirements of the Educational PhD Programme of SENSE with a work load of 32.5 EC, including the following activities:

SENSE PhD Courses

o   Environmental Research in Context (2012)
o   Research in Context Activity: Writing popular article 'Neerslagverandering in Europa tot nu toe groter dan verwacht', published in H2O (2012)
o   Autumn school: 'Dealing with uncertainties in research for climate adaptation' (2012)

Other PhD and Advanced MSc Courses

o   Alpine Summer School: 'Regional Climate Dynamics in the Mediterranean and beyond: An Earth System perspective', Italy (2011)

Management and Didactic Skills Training

o   Initiate PhD and post-doc discussion group on 'Statistics' at KNMI (2011-2012)
o   Initiate PhD discussion group on 'Model development' at KNMI (2013)

Oral Presentations

o   Assessment of uncertainties in regional climate change. Annual meeting theme 6 KfC High–quality Climate Projections, 2 February 2012, De Bilt, The Netherlands
o   Resolution dependence of European precipitation in a state-of-the-art atmospheric general circulation model. International Conference Deltas in Times of Climate Change II, 24-26 September 2014, Rotterdam, The Netherlands

SENSE Coordinator PhD Education

Dr. ing. Monique Gulickx